KASDI MERBAH UNIVERSITY - OUARGLA -

**FACULTY OF HYDRCARBONS AND RENEWABLE ENERGIES
AND EARTH AND UNIVERSE SCIENCES**

Department of Earth and Universe Sciences

FINAL DISSERTATION

With a view to obtaining a Master's degree in

Petroleum Geology

Geophysical, sedimentary and petrophysical evaluation of the Ri and Ra Cambrian reservoirs in the El Gassi region (southeast Algeria)

Presented by:

SAYEH CHAHRAZED

BOUHNIK TAHANI

ASSAL YAMINA

Defended publicly: /06/2024

Jury members:

President:	……………………………………	MCA Univ.	- Ouargla
Supervisor:	Fellah Lahcene	MCA Univ.	- Ouargla
Co-supervisor:	Merad Mohamed Zakaria	PhD. St. Univ.	- Ouargla
Examiner:	……………………………………	MCA Univ.	- Ouargla

Academic year: 2023/2024

Acknowledgements

I would first like to express my deep gratitude to my dissertation supervisor, Fellah Lahcene, for his supervision, his patience and his trust throughout this research work. His valuable advice, expertise and unwavering support were invaluable and contributed greatly to the success of this project.

I would like to thank of professionals met, for agreeing to be interviewed as part of this study Mr.Djoudi Adbelhalim and Alizoui Omar. Their feedback enriched this work, allowed me to question, and reorient my memory problem.

Finally, I would like to thank all the people who, directly or indirectly, contributed to the production of this dissertation.

Whether through enriching discussions, advice or simply by their presence, their contribution was valuable.

Dedication

I dedicate this journal to myself as a constant reminder of the importance of dedication and perseverance in achieving my dreams and goals. Let us continue to grow and evolve, always striving for the best.

To my dear parents, thank you for your boundless love and continuous support. You are the epitome of warmth and inspiration in my life, and my happiness lies in seeing you proud of me always.

To my beloved siblings, I send you this journal as a symbol of my deep affection and appreciation for our strong bond. We are a team that supports each other, sharing dreams and challenges together.

To my dear childhood friends Hayat, Zoubeida, those beautiful memories with you remain engraved in my heart. I hope you continue to be a part of my life, and we stay connected always.

To Supervisor Mr. Lahcene Fellah, thank you for your valuable guidance and unwavering support. I hold you in high esteem and respect.

To my wonderful colleagues in this journal, Assal Yamina and Sayah Chahrazed, I dedicate this journal to you as a symbol of our great collaboration and the friendship that unites us. We are part of one team striving together for success and excellence.

Tahani

Dedication

I tend to dedicate this modest end-of-studies project:

I mainly dedicate this thesis to myself because of its major role in my journey towards achieving this accomplishment and the insistence on overcoming challenges with confidence.

To my dear parents who taught me the alphabet of life. To my reason for being, my dear Mother Zahra Naoui, my only source of joy, will and courage. May God protect her and make her enjoy good health for her prayer and supplication.

To my dear father Brahim   expressing my pride for his many sacrifices

To my two dear sisters "Safa" and "Hana" for their invaluable support

To my dear Brothers Abd Ennour Oussam, Achref and Hamada with his Marie" for their encouragement, their comfort and their relevant support.

May God protect them all from all evil and reserve for them the life they dream of.

I dedicate it to my entire family, my uncles and aunts, in particular my cousins Taher Naoui and Kamal Naoui, for whom I express my most devoted love and respect.

To my dear and kind friend Chahinez   for her cordial love and moral support. She will remain eternally engraved in my memory.

To my dear friend Moussa (Zize) , whom I love with all my heart because he wears the word "friend" well and who shared with me the worst and the best moments.

To my dear Binômes Tahani and Yamina For his kindness and his sympathies.

To all those who are dear to me, I say: I love you with all my heart for life.

Chahrazed Sayah

Dedication

Dedicate this thesis first to myself for the big role in my journey towards completing this achievement and the determination to overcome challenges with confidence.

I would like to congratulate everyone who supported me from family and friends, especially my friends in this thesis, Chahrazed Sayah and BouhnikTahani, and for every word of encouragement and every moment of support, and that this work will be the beginning of more achievements and achievements in the futureI.

.

Yamina

Table of contents

List of Figures

List of tables

General Introduction

Algeria is considered one of the leading countries in the oil and gas industry, possessing vast natural resources of petroleum and natural gas. Additionally, it holds a prominent position in the sector due to numerous petroleum fields undergoing continuous exploration and exploitation efforts.

Among the regions rich in natural resources in Algeria, the Gassi area in the southeast stands out for its specialization in oil and gas.

On the other hand, the Gassi el Agreb region is recognized as one of Algeria's prominent petroleum sites, housing significant oil and gas reservoirs. The Ri and Ra reservoirs, formed during the Cambrian period, are notable geological features in this area due to their unique petrophysical and geophysical properties that positively impact their ability to efficiently store and extract oil and gas.

This memorandum aims to explore and analyze the petrophysical and geophysical characteristics of the Ri and Ra reservoirs in the Gassi el Agreb region. The study will employ a range of methods and technologies; including laboratory studies, field surveys, and geophysical data analysis, to understand how these characteristics influence the reservoirs' capacity for oil and gas storage and enhance their extraction efficiency.

Consequently, understanding these characteristics is expected to improve the exploration and exploitation processes of the Ri and Ra reservoirs in the Gassi el Agreb region, thereby boosting Algeria's economic potential in the oil and gas sector.

Chapter one:

Regional and local geology of the Gassi el Agreb field

Chapter One:
Regional and Local Geology of the Gassi El Agreb Field

Introduction

Given the significance of oil and gas, and their by-products, to the Algerian national economy, it is necessary to briefly examine the history of this product since its discovery in Algeria. It is also necessary to discuss the various national and multinational companies that have contributed to the exploration and production of this material. Furthermore, it is important to acknowledge the significance of Hassi Messaoud. It is noteworthy that the Hassi Messaoud region (Hassi Messaoud field) is regarded as the largest oil field in Algeria. Hassi Messaoud is situated in the western portion of the Saharan Platform.

This chapter will examine the geological and tectonic features that have enabled the Hassi Messaoud field (HMD) to become a significant oil-producing region.

Exploration History of Paleozoic Petroleum Systems in North Africa and Algeria

This passage details the exploration history of Paleozoic petroleum systems in North Africa, focusing on Algeria.

Pre-Discovery Period (Up to 1953):

- After World War II, France established organizations to secure oil supplies from its colonies.
- SNREPAL, formed in Algeria, focused on exploring Tertiary and Mesozoic rocks, leading to the modest Oued Gueterine discovery (1949).[1-3]
- By 1949, a vast Paleozoic basin was identified south of the Saharan Atlas [1, 2, 4].

Discovery Period (1953-1956):

- Exploration intensified with various companies acquiring permits.
- Dozens of exploration wells were drilled, resulting in 12 discoveries with significant reserves (27.6 billion barrels of oil equivalent) [1, 3, 5].
- Key discoveries included:
  - Djebel Berga (1953): First discovery by CREPS group, a gas accumulation in Devonian sandstone.

- Edjeleh (1956): Major oil and gas find in Devonian and Carboniferous reservoirs by CREPS.
- Hassi Messaoud (1956): Huge oil accumulation in Cambrian sandstone, discovered by SNREPAL-CFP (A) group, becoming a cornerstone of Algerian oil industry.
- Hassi R'Mel (1956): Major gas discovery by SNREPAL [1, 6, 7]..

Boom Period (1957-1964):

- Algerian War of Independence did not disrupt exploration.
- Extensive exploration efforts with various techniques (mapping, seismic surveys) led to high success rates (29%).
- Major discoveries in the Illizi Basin:
  - Essameid tin discovery (1957)
  - El Adeb Larache, In Amenas North, Zarzaitine, and others (1957-1961)
- Discoveries along the Hassi Touareg and El Biod Highs, including Gassi-Touil (1961) and Rhourde gas fields (1962).
- Exploration success in the Ahnet and Gourara basins with gas discoveries like Err Bazzene (1955) and Tineldjane (1957) [1, 6, 7].
- Exploration began in Libya (1957) with discoveries in the Hamra Basin, but focus shifted to Cretaceous and Tertiary plays later.

This period established North Africa, particularly Algeria, as a major producer of oil and gas from Paleozoic petroleum systems.

Geographical location of the Hassi Messaoud field

The Hassi Messaoud field is situated in a geographically advantageous location. It is considered one of the world's largest deposits and forms part of a complex of structures in the northern part of the Triassic province and of the Paleozoic oil fields. Its location is 800 km southeast of Algiers, 350 km from the Tunisian border, and 80 km east of Ouargla (Figure 2). The Hassi Messaoud field has a surface area of 2,000 km^2 and an average altitude of 142 m. It is bounded to the northwest by the Ouargla, Guellala, and Haoud-Berkaoui deposits; to the southwest by the El-Gassi, Zotti, and El-Agreb deposits; to the southeast by the Rourde-El-Baguel and Mesdar deposits; and to the east by the Berkine deposit.

The Lambert Sud Algérie coordinates are as follows:

790,000 to 840,000 East

110,000 to 150,000 North

In geographical coordinates:

North by latitude 32 15° - West by longitude 5 40

South by latitude 31 30° - East by longitude 6 35°
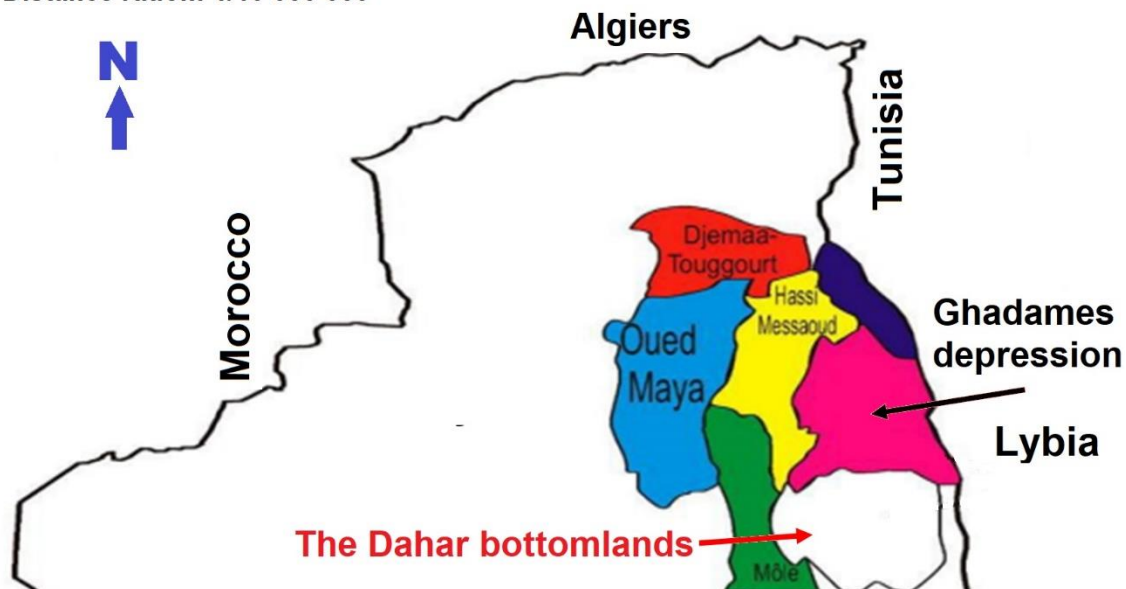
Fig.1: Geographical situation of Hassi Messaoud region [9].

Geological context of the Hassi Messaoud field
Geological overview of the Hassi Messaoud region

The Hassi Messaoud region, located in the heart of the Algerian Sahara, is renowned for its prolific oil fields. These fields primarily tap into hydrocarbon reserves trapped within Cambrian-age rock formations. Notable discoveries include El Agreb, Zotti, El Gassi, Rhourde El Baguel, and Mesdar. The crown jewel, however, is the super-giant Hassi Messaoud field itself, encompassing a vast dome-shaped area exceeding 1,600 square kilometers (Figure 1.9).

Reservoir Rocks

Cambrian deposits, dominated by sandstones and quartzites, are the most well-understood and prolific reservoirs in the region. These formations are designated as Cambrian Ri and Ra.

Ordovician Potential

Underlying the Cambrian reservoirs lies the Ordovician horizon, characterized by Hamra quartzites. This layer was partially eroded during a geological period known as the Hercynian Orogeny. Interestingly, the remaining Hamra quartzites fringing the Hassi Messaoud dome (known as the Hassi Messaoud ring) hold significant oil potential. Recent exploration efforts have yielded promising discoveries in this zone, including HGA, HTF, and HDZ.

The Hassi Messaoud field occupies the central part of the Triassic province, due to its surface area and its reserves it is the largest oil deposit in Algeria. From a geological point of view, this field is limited by [4,9]:

The Oued Maya depression to the west.

By the Mole of Amguid El Biod to the south.

By the Djamaa-Touggourt structure to the North.

Via the Dahar shoals, Rhourd El Baguel and the Eastern Ghadames depression.
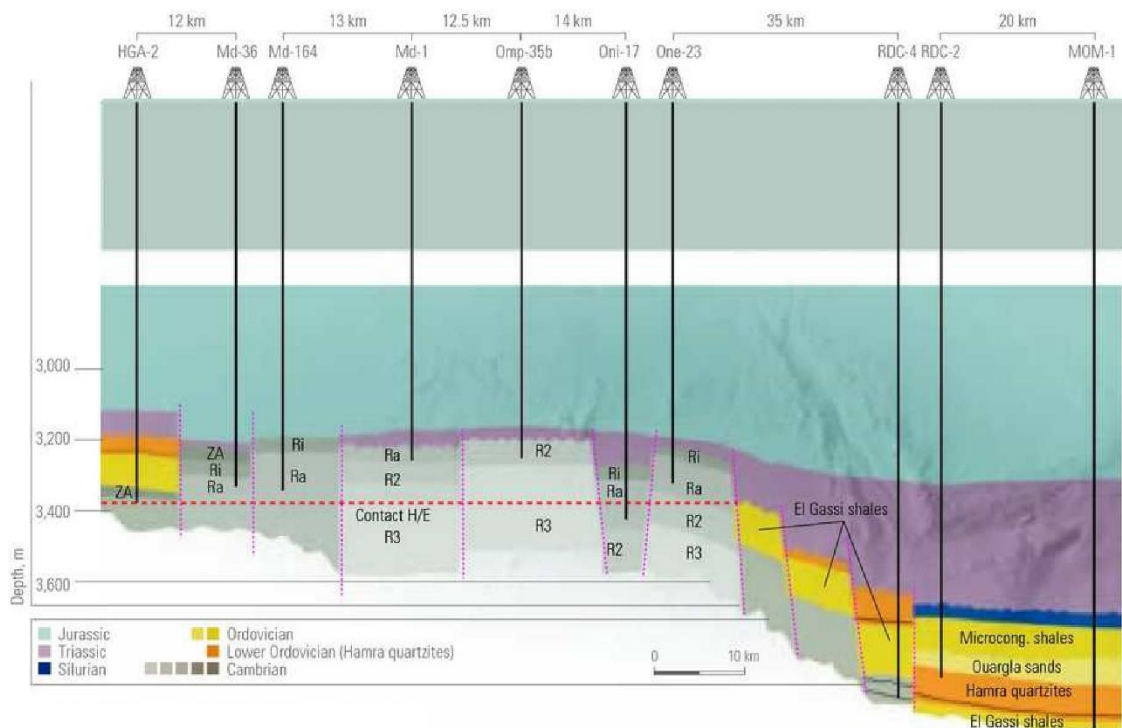
Fig.2: Cross-section of the Hassi Messaoud oil field area [4, 10].

Lithostratigraphic description

Stratigraphy

The stratigraphic series of the Hassi Messaoud field rests on the granitic basement at approximately

4393 m thick. This series is incomplete; it is marked by the absence of the Silurian, Devonian, Carboniferous and Permian. The Hercynian unconformity appears more accentuated in the center of the structure, where the clay-sandstone and salt deposits of the Triassic rest directly on the Cambrian. Moving towards the periphery, this discordance truncate more and more recent Ordovician terms (Beicip. Franlab, 1979) [2].

Based on the geological work carried out on the Hassi Messaoud field, the Hassi Messaoud stratigraphic series is summarized as follows:

Geologically, the Hassi Messaoud field comprises a succession of formations from bottom to top (Figs. 4 and 5):

1.1.1. Bedrock

Encountered at a depth of around 4,000 m. The basement consists mainly of pink porphyroid granites.

1.1.2 Infra-Cambrian

Represents the oldest geological unit at a thickness of 4092 m, and rests on the basement. It is composed of red clays.

1.1.3. Paleozoic

Resting on the so-called "Pan-African unconformity", the Paleozoic is composed of:

1.1.3.1. Cambrian (av. depth. 590 m)

Forming the main reservoir of the Hassi Messaoud field, the Cambrian is essentially sandstone. The following litho-zones can be distinguished from bottom to top [6] :

- Litho ozone R3 (av. depth. 370 m): resting on the Infra-Cambrian, it is composed of medium- to coarse-grained sandstones, mainly feldspathic and micaceous, which are ma classes, with cement of a clayey nature. In the R3 zone, permeability is lower (I md and sometimes zero).

- Litho zone R2 (av. depth. 100 m): medium to coarse isometric quartzite and greasy quartzite sandstones, with clayey cement. Interlayered siltstones may be present. Stratification is often oblique. Porosity increases while permeability remains unchanged.

- Litho zone Ra (av. depth. 125 m): representing the reservoir, the Ra is composed of medium to coarse-grained an isometric quartzite sandstone, with silico-clay cement. The sedimentary structures are represented by oblique, intersecting bedding; the upper part of the litho zone encloses Tigillites. Permeability ranges from 60 to over 100md and porosity varies. The Ra is eroded in the central part of the Hassi Messaoud field.

- Litho zone Ri (Cambro-Ordovician) (av. depth. 42 m): corresponds to the isometric reservoir, which is composed of quartzite sandstones with clayey and siliceous cement, very rich in Tigillites. Its porosity is low on average, a few tens of md, and the porosity is different [11].

1.1.3.2. Ordovician (Av. depth. 180 m)

It comprises, in ascending order, the following parts:

Alternation zone (Av. depth. 20 m): mainly black clay alternating with isometric quartzite beds of medium to fine sandstone El-Gassi clay (Av. depth. 50 m): green to black shaly clay. Note the presence of graptolites, indicative of a marine depositional environment El Atchane sandstones (Av. depth. 12 m to 25 m): these are fine to very fine-grained sandstones. Gray-beige to gray-dark in color, with clayey or glauconitic cement. Hamra quartzites (Av. depth. 12 m to 75 m): fine-grained quartzite sandstones, sometimes with clay intercalation.

1.1.4. Mesozoic

1.1.4.1. Triassic

Resting in the center on the Ordovician and on the Cambrian on the flanks of the structure, the Triassic is represented by the following succession:

- Eruptive Triassic (Av. depth. 0 to 92 m): eruptive flows with sandstone levels. Approximately located between the Hercynian unconformity and the clay-sandstone Triassic wall, and rarely localized in the Ra.
- Sandstone Triassic (Av. depth. 35 m): accompanied by eruptive flows. It represents the first filling of the Paleozoic relief.
- Clay Triassic (Av. depth. 113 m): brown, red or variegated dolomitic or silty clays with intercalations of salt beds. The following main logs can be seen here:
- G10: very characteristic regional marker (clay bench) corresponds to the top of the Triassic clay.
- G20: seismic marker (end of frank clays).
- G35: marks the last influence of salt, and the appearance of dirty clay banks.
- G40: appearance of the first sandstone lens.
- G50: marker corresponds to the top of the Triassic sandstone.
- The Saliferous Triassic (Av. depth. 340 m): these are massive salt beds with anhydritic intercalations at the top and beds of slightly silty and dolomitic clay. It is subdivided into three horizons:
- The Saliferous Triassic (TS3): averaging 200 m in thickness. It alternates moderately hard clays with massive salt levels.
- The Saliferous Triassic (TS2): with an average thickness of 189m, it represents a succession of soft gray-brown clays, with beds of massive salt.
- The Saliferous Triassic (TS1): With a thickness of 46 m, this level is formed by a soft, dolomitic clay, interspersed with anhydrite beds.

1.1.4.2. Jurassic

Deposits in the Jurassic range range from lagoonal and marine facies at the base to clayey-sandstone facies with limestone intercalations towards the top. More precisely, we find the following litho-stratigraphic succession:

- Le Lias (Av. depth. 300 m): from bottom to top:
- LD3 (Av. depth. 30 m): grey marl with dolomite layers
- LS2 (Av. depth. 60 m): Massive, white, translucent salt with clay-salt intercalations.
- LD2 (Av. depth. 55m): Massive, microcrystalline dolomites with a few marly layers containing water. Chloride-calcic.
- LS1 (Av. depth. 90 m): Banks of salts and clays with white anhydrite layers.
- LD1 (Av. depth. 65 m): Grey, hard dolomite, white anhydrite with occasional silty clays.

Ere/Sy	ETAGES			LITHO	Ep(m)	DESCRIPTION
CZ	NEO	MIO PLIOCENE			239	SABLE, CALCAIRE
		EOCENE			122	CALCAIRE
MESOZOIQUE	CRETACE	SENONIEN	CARBONATE		107	CALCAIRE, DOLOMIE, , ANHYDRITE
			ANHYDRITIQUE		209	ANHYDRITE, MARNE, DOLOMIE
			SALIFERE		149	SEL MASSIF
		TURONIEN			112	CALCAIRE
		CENOMANIEN			147	MARNE, CALCAIRE, DOLOMIE
		ALBIEN			362	GRES, ARGILE
		APTIEN			24	DOLOMIE
		BARREMIEN			276	ARGILE, SABLE
		NEOCOMIEN			182	DOLOMIE, MARNE, ARGILE
	JURASSIQUE	MALM			226	ARGILE, MARNE, CALCAIRE
		DOGG	ARGILEUX		107	ARGILE, MARNE
			LAGUNAIRE		211	ANHYDRITE, DOLOMIE
		LIAS	LD1		66	DOLOMIE, ANHYDRITE, ARGILE
			LS1		90	SEL, ANHYDRITE
			LD2		55	DOLOMIE, MARNE
			LS2		58	SEL MASSIF
			LD3		31	DOLOMIE, MARNE
	TRIAS	SALIF	TS1		46	ANHYDRITE, ARGILE
			TS2		189	SEL, ARGILE, ANHYDRITE
			TS3		202	SEL MASSIF
		ARGILEUX			113	ARGILE
		GRESEUX			0 à35	GRES, ARGILE
		ERUPTIF			0 à 92	ANDESITE
PALEOZOIQUE	ORDOVICI	Quartzites de Hamra			75	Grès très fins
		Grès d 'El-Atchane			25	Grès fins glauconieux
		Argiles d 'El-Gassi			50	Argile verte ou noire
		Zones des Alternances			18	Alternances grès et argiles
	CAMBRIEN	R Isométriques			42	GRES Isométriques, Silts
		R anisométriques			125	GRES Anisométriques, Silts
		R2			100	GRES Grossiers, Argile
		R3			370	GRES Grossiers, Argiles
PROTERO ZOIQUE		Infra Cambrien			45	GRES Argileux rouge
		SOCLE				Granite porphyroïde rose

Fig.3: Lithostratigraphic column of the Hassi Messaoud field [9].

- Le Dogger (Av. depth. 320 m): includes the following two levels:
- Clayey (Av. depth. 105 m): Silty clays, dolomitic marls with fine sandstone layers.
- Angular (Av. depth. 210 m): Anhydrite, clayey dolomite, marl.
- Le Malm (Av. depth. 226 m): clayey and marly deposits with carbonate interlayers (limestone and dolomite), with some traces of anhydrite.

1.1.4.3. Cretaceous

In this region, the sedimentary series consists of:

- Neocomian (Av. depth. 182 m)
- These are sandstones with clayey layers, changing towards the top to clays with numerous limestone and dolomite intercalations.
- Barremian (Av. depth. 280 m): fine- to medium-grained sandstones with carbonate admitting levels of sandstone clays and dolomites.
- Aptian (Av. depth. 25 m): Represented by two crystalline dolomite beds framing a clay level.
- Albian (Av. depth. 350 m): fine-grained sandstones and sands with intercalations of silty clays.
- Cenomanian (Av. depth. 145 m): alternating anhydrites, clays, grey marls and dolomites.
- Turonian (Av. depth. 95 m): carbonate formations with alternating clayey limestone, dolomitic limestone and chalky limestone.
- The Senonian: this corresponds to the following two levels:
- Sen. Carbonate (Av. depth. 92 m): dolomitic limestone with fine anhydrite layers.
- Sen. Anhydritic (Av. depth. 219 m): composed of white, crystalline anhydrite, medium-hard dolomite, marl and clay-dolomitic limestone.
- Saliferous (140 m): massive salt with traces of anhydrite [11].

1.1.5. Cenozoic

With an average thickness of 360 m, the Cenozoic deposits consist of dolomitic limestone of Eocene age with an average thickness of 122 m and sands attributed to the Mio-Pliocene with a thickness of 240 m.

- Ra lower: A coarse lower zone.
- Ra middle: a median fine zone
- Upper Ra: an upper coarse zone.

The base of the Ra is distinguished by the development of three drains:

- D1 (R170 - R200): coarse sandstones with dominant, well-marked, oblique-arched stratifications, often with a micro-conglometric base.

Silurian — Lower — Wenlock Liandovery — Radioactive shales (50 m)

Hercynian unconformity
TOC middle: 6-8%

Ordovician — Upper — Ashgill — M'abKratta dalle (25 m)
Microconglomeratic shales (65 m)

Caradocian — Oued Saret sands (60 m)

Taconic unconformity

Lower — Llandeilian — Azzel shales (25 m)
Llanvirnian — Ouargla sands (50 m)
Arenigian — Hamra quartzites (75 m)

HGA-1: 500 bopd
HGA-2: 2,000 bopd
HGA-4: 1,450 bopd

Atchane sands (20 m)
Tremadocian — El Gasssi shales (85 m)

Cambrian — Alternance zone (25 m)

Md-28: 1,150 bopd

Ri unit (50 m)

Hassi Messaoud
El Agreb
Zotti
El Gassi
Rhourde El Baguel
Messdar
Oil field

Ra unit (120 m)

HGA-1: 2,000 bopd
HGA-3: 1,750 bopd
3,800 bopd
OL-2: 5,000 bopd

R2 unit + R3 unit (300 m)

Legend:
- Primary source rock
- Possible source rock
- Primary reservoir
- Secondary reservoir
- Sandstones
- Shales
- Eruptive rocks

Fig.4 Paleozoic section of the Hassi Messaoud oil field area. [4]

- ID (R150 -R170): marking the gradual transition between D1 and D2, this level is the thinnest and most frequent. It is represented by silty levels, with the presence of Tigillites.

- D2 (R140-R150): Coarse but well-graded sandstone with dominant oblique tabular stratifications forming mega-ridges, with occasional intercalations of silt levels. This lower part of the Ra contains the best reservoir levels.

This part of the Ra is recognized by the fact that it contains the best reservoir levels. The progressive extension of erosion zones can be seen towards the central zone of the field.

- D3: (R130-R140): represents the median fine zone (lower granulometry). Its main characteristic is the abundance of silty interbeds and fine sandstones with very strong bioturbations (Tigillites in particular).

- D4: (R100-R130): This corresponds to the upper coarse zone. These are sandstones with frequent oblique tabular stratification forming mega-ripples.

- D5: This is a marine-type depositional environment characterized by a high lateral continuity of siltstones. It is made up of finer, higher-grade materials than Ra.
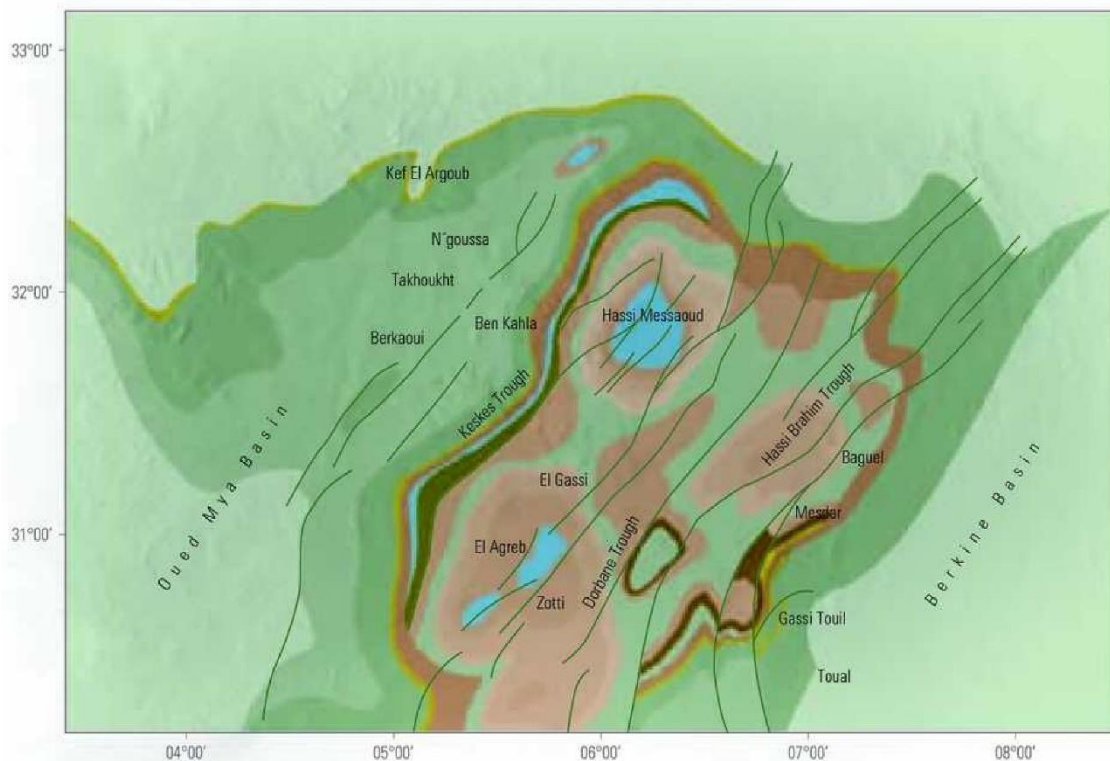
Fig.5: Cutaway view of the Mesozoic of the Hassi Messaoud field and neighboring zones [4].

4. Petrography of the reservoirs

The microscopic study demonstrated that the various Cambrian levels exhibit similar petrographic constituents, albeit with varying proportions. The primary constituents, as outlined by Yahiaoui (2010) [12], are as follows:

- Quartz: This is the predominant constituent, comprising an average of 75% of the rock. The grains are typically rounded to sub-angular, with the contact between the grains exhibiting a concave-convex configuration.

- Rock fragments: These are very common in the Ra. They are linked to coarse zones and include fragments of quartzites and tectonic breccia's.

- Micas: The frequency of micas does not exceed 2%. They are more frequent in salty pasts and most often represented by muscovite or biotite. They are presented in the tank in the form of authigenic cement, which seals the cracks and their surroundings. It should be noted that the main carbonate fraction is siderite, and calcite degeminates.

- Cements and matrices: They are subdivided as follows:
  Secondary silica: it is essentially in the form of a cement for nourishing quartz grains. It is more widespread in Ra than in R2.

- Clays are very prevalent in the lower levels of the Cambrian. Clay cement is represented by two fractions: a detrital fraction, which appears to be composed largely of illite, and an authigenic fraction, which is kaolinite.

4. Reservoir description

The reservoir consists of three zones: The set of geophysical techniques used in the borehole to measure physical parameters such as resistivity and density, known as logging, provides information with fine resolution.

Interpretation of the log allows us to establish hypotheses about the nature and structure of the rocks and their contents, thus enabling us to subdivide the field.

At the start of its reconnaissance, the Hassi Messaoud field was subdivided into four zones according to the nature of the sandstones: Ri, Ra, R2 and R3.

- Ri or D5 zone: isometric sandstone zone, usually very compact (R 70 -R 90).
- Ra zone: composed of 3 litho zones.
- Upper coarse zone: D4 (R100 to R130).
- The middle fine zone: D3 (R130 to R140).

- The lower coarse zone: includes D2 (R140 to R150), ID (R150 to R170), D1 (R170 to R190) and the ZPG passage zone (R190 to R200).

- R2 zone: Quartzite sandstone zone, more clayey, rare presence of reservoir qualities in its upper part (R200-R300).

- R3 zone: very coarse to micro conglomeratic zone, very clayey, with no oil potential (R300-R400).

Fig. 6: Hassi Messaoud Cambrian drain division. [13, 14]

Geodynamic Evolution of the Hassi Messaoud Field

The Hassi Messaoud field is defined as a vast flattened anticlinal dome. The reservoir is susceptible to two distinct types of geological accidents.

The subsurface geology is characterized by the presence of sub-meridian faults running in a north-north-east-south-south-west orientation, as well as perpendicular faults running in a north-west-south-east direction. These observations highlight the presence of Horst and Graben tectonic features.

Additionally, fractures without discharges have had a significant impact on reservoir fracturing.

1.2 Structuring the Hassi-Messaoud Field

The tectonic phases responsible for the evolution of the field can be summarized as follows:

- The Pan-African phase is the first tectonic phase to be considered.
- The Early Neo-Caledonian phase is also a significant period in the evolution of the Hassi-Messaoud field.
- The Caledonian phase is also a significant period in the evolution of the Hassi-Messaoud field.
- The Hercynian phase is also a significant period in the evolution of the Hassi-Messaoud field.

1.2.1. Post-Triassic Structuring

The structural closure, which is found in an interval (50-100m), has weak effects and is therefore divided into two phases:

- The Austrian phase is the subsequent phase.
- The Atlasic phase is next in line.

1.2.2. The current structure, which is 300 meters in length, is situated between the edges and the top of the deposit.

1.2.3. Hercynian paleo valleys

The Hassi Messaoud field contains six (6) paleo valleys, which are distinguished by a thicker Triassic fill and an eruptive series at the base.
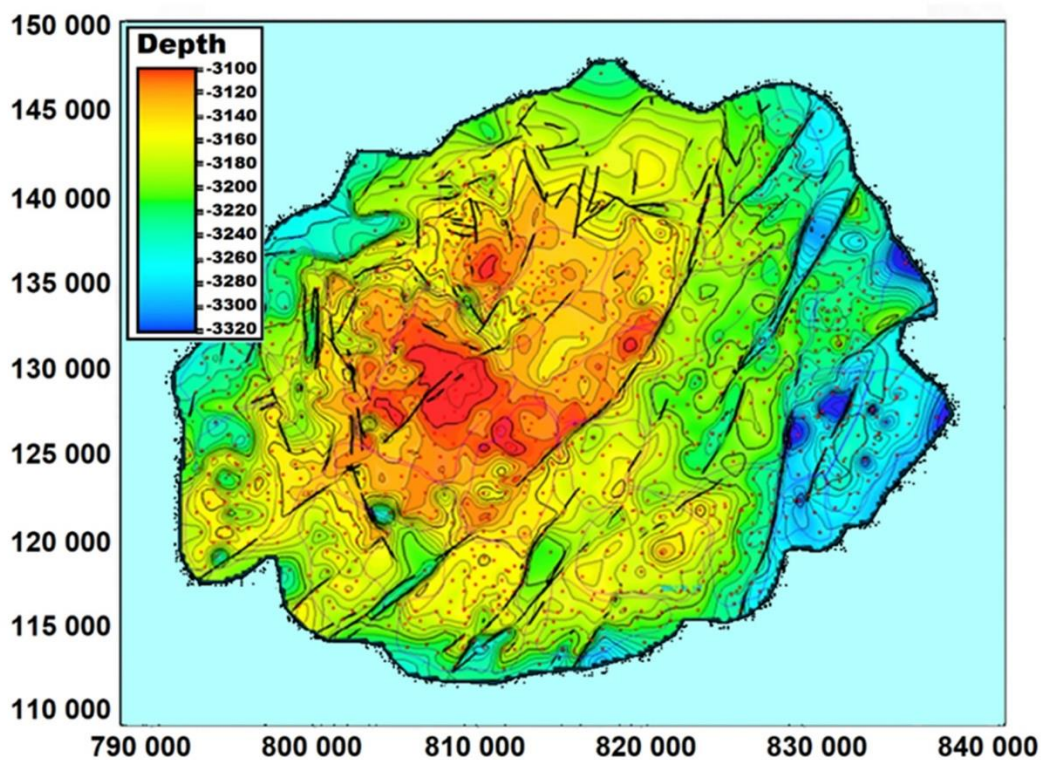
Fig. 7: Isobathic map at the Hercynian unconformity showing the faulted tectonic structure of the Hassi Messaoud field [15].

Information on the El-Gassi, Zotti and El-Agreb fields

Geographical location of the El-Gassi, Zotti and El-Agreb fields

The El-Gassi, Zotti, and El-Agreb (GEA) fields are situated in the southwest locality of Hassi Messaoud, approximately 120 km from Hassi Messaoud and 950 km from central Algiers, at an altitude of 190 m above sea level (Sonahess, 2007) [10]. The area is bounded by:

- The 4° and 6° East-West meridians.
- The 30° and 32° North-South parallels.

The region comprises three distinct deposits.

- El Gassi, with an area of 207 km², is divided into two main entities: The Gassi-North and Gassi-Core deposits.
- Zotti, with an area of 77 km².
- The area of El-Agreb is 162 km².
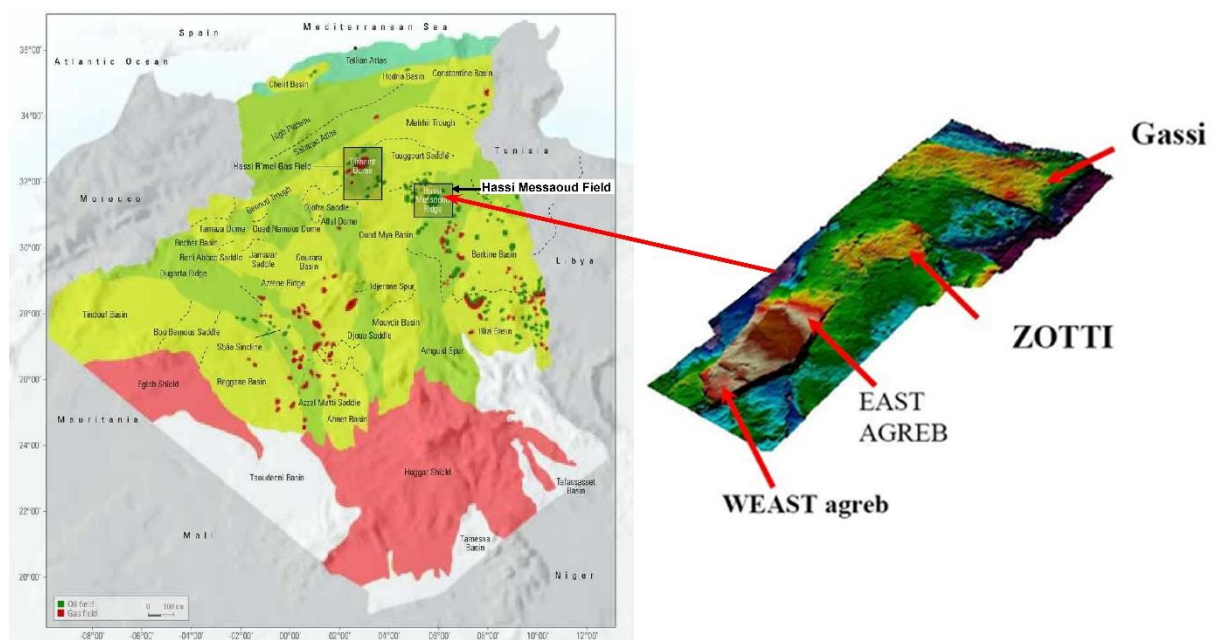
Fig. 8: Geographical situation of El-Gassi, Zotti and El-Agreb field [4]

Structural overview

The Gassi El-Agreb structure is a large double-slope anticline. The structural style of this trend is dominated by a northwest-southeast orientation and reverse sub vertical faults, which are characteristic of a strike-slip tectonic regime. It is a well-established phenomenon that faults, by their very nature, tend to strongly fragment the reservoir into compartments. This is exemplified by the Hassi-Messaoud deposit. The structure appears to have been affected by a

regional NE-trending structural tilt, which also created large residual oil zones below the current oil-water interface.

A pronounced structural saddle separates the main structure of El-Gassi from a structural slope that plunges towards the north-west part of the operating permit, as evidenced by the ARNE1 well. A minor trend of normal faults, oriented NW–SE, was delineated through seismic and drilling data. These faults appear to be permeable, as the reservoir, pressures on either side of them are balanced. The extent, nature, and distribution of these faults and other accidents will be more clearly defined by 3D seismic and its interpretation (Sonahess, 2007) [10]. A number of key events, which are as follows, has defined the structural evolution of the Gassi El-Agreb region, from pre-Cambrian times:

- The Precambrian (Pan-African) event established the dominant structural orientations. The Caledonian event at the beginning of the Paleozoic reactivated these orientations.

- The Late Paleozoic (Hercynian) event saw the reactivation of pan-African orientations, accompanied by widespread uplift and peneplanation. The duration of subaerial exposure was approximately 180 million years.

- The mid-Cretaceous event (Austrian) represents a further major reactivation of Hercynian and earlier structures. The earlier Tertiary event (Alpine) also involved other reactivations and significant lateral movement on major faults subject to strike-slip movement.
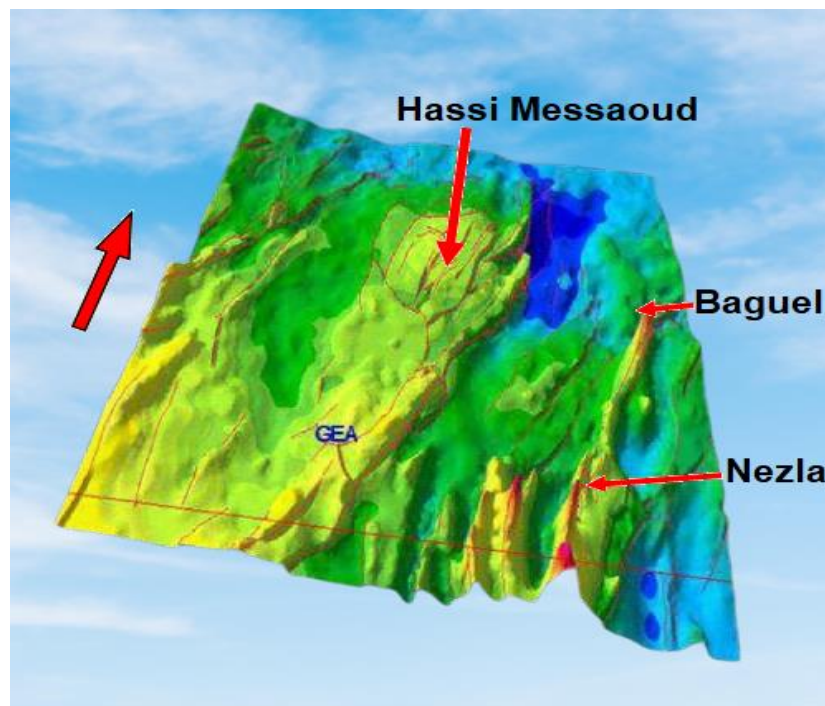
Fig. 9: Block diagram of lineaments in the El-Gassi/ Hassi Messaoud area [10].

2. 3. 2. Tectonics of the Gassi El-Agreb Field

It is not necessary to possess knowledge and an understanding of the different orogenic phenomena and phases that have been responsible for the architectural configuration of a region in order to comprehend the tectonic history of that region. This is according to Sonahess (2007) [10]. The orogenic phases that have affected the region are as follows:

The Early Caledonian phase is defined as follows: This is related to the late Cambrian structuring, with erosion and the establishment of faults following a SW-NE direction.

Compressive movements that commenced at the end of the Cambrian period and resulted in the formation of structures exhibiting low amplitude characterize the subsequent Major Caledonian phase [10].

The Major Hercynian phase is the following phase in the orogenic sequence. This phase is likely responsible for the current NE-SW direction of structuring. It began in the Upper Devonian and lasted until the end of the Primary. The area is characterized by the absence of sediments of Silurian, Devonian, Carboniferous, and Permian age, as well as the upper part of the Ordovician, across the entire surface of the Amguid El-Biod-Hassi Messaoud axis [10].

The Austrian phase is characterized by the following: These are compressive movements in an east-west direction.

Petroleum System of Hassi Messaoud area
A1-Cambro-Ordovician play

As with the Hassi Messaoud, El Agreb, and El Gassi oil-producing fields in the Cambrian reservoir, the majority of the structures drilled have revealed further, albeit relatively limited accumulations (as at OL and HGA). From the standpoint of surface area and closure, the Ordovician (Hamra quartzites) has demonstrated the presence of impregnated columns exceeding 100 m in length and surface areas exceeding 500 km² (HTF-HDZ zone). Test results indicate that the oil flow rate ranges from 6 to 14 m³/h (Fig. 5). The ring-shaped configuration of the Ordovician reservoir renders it of considerable interest [4].

A2-Cambrian play

The Cambrian play is productive in the Hassi Messaoud field and in surrounding areas, as well as in the Rhourde El Baguel, Mesdar, El Agreb, Zotti, and El Gassi fields.

The Ri unit represents a transition between the coarse facies of the Ra zone and the pelitic sandstone of the overlying alternating zone. The transition from the R2/Ra assemblage to Ri is characterized by an evident facies change, with the sandstones exhibiting medium to coarse grain sizes and bioturbation (Scolithus). The upper portion of the Ri reservoir is characterized by a shallow transgressive marine sandstone. The unit comprises a well-sorted fine to medium

clean sandstone with abundant bioturbation (Scolithus). The thickness of this unit is variable and may be unconformable with the reservoir Ra [4].

A3-Cambrian Ri/Ra lithology:

A thick sequence of detritic rocks, comprising sandstones, quartzites, and conglomerates, is situated between the basement and the Ordovician. The Cambrian is represented by a set of sandstone sediments, which have been divided into two members: a lower and an upper. The thickness of the lower member, Ra, is approximately 150 meters. It is represented by fine to coarse gray-white sandstones and by compact, indurated light-gray conglomerates, which are ferruginous in places. The upper member, designated as Ri (isotropic), is represented by pinkish gray sandstones of quartzite composition with a siliceous cement. Stylolitic joints and fracturing are present. The Cambrian reservoirs Ri and Ra appear to exhibit notable differences. The sandstone bodies and silts of reservoir Ra are discontinuous and of limited lateral extent, in contrast to sandstone Ri, which exhibits better continuity [4].
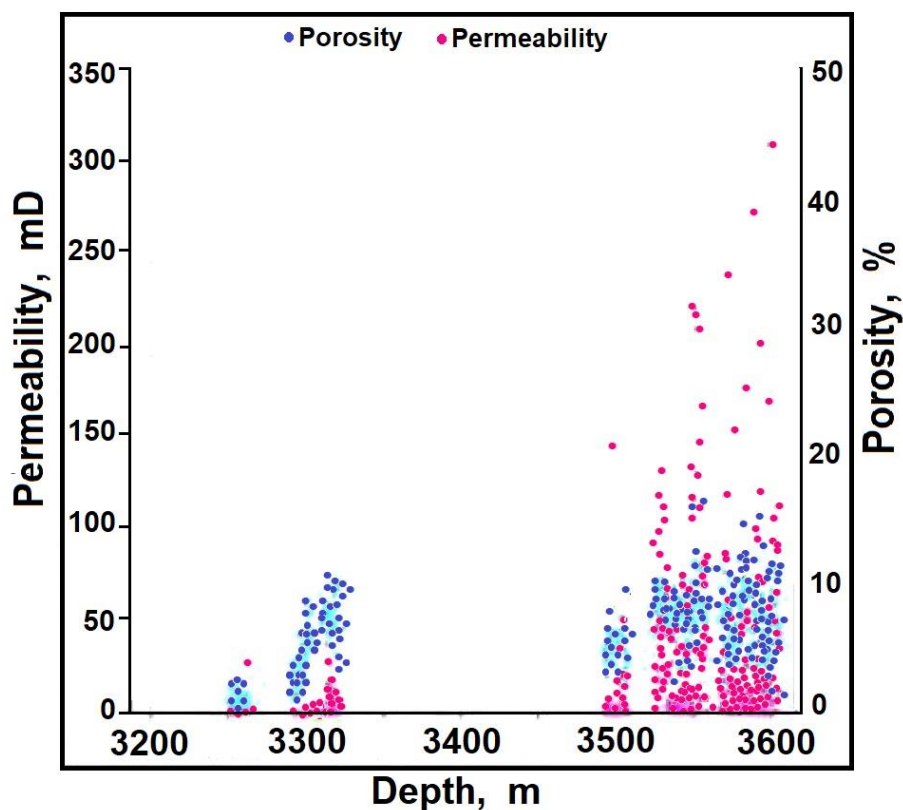
Fig. 10: Petrophysical results from the Cambrian reservoir[4] .

A4-Ri/Ra Reservoirs:

The Ri and Ra reservoirs discovered on the western border of the Hassi Messaoud field (OL and HGA) belong to the same category as those previously identified in the field. However,

there is considerable variation in the porosity and permeability values. This variability is directly related to the heterogeneous nature of the Cambrian sandstones. The characteristics of each member are contingent upon their lithology, clay content, and diagenetic history.

Core studies have demonstrated that the upper and middle portions of the reservoir Ri are generally less favorable, whereas the lower portion, corresponding to drain D5, exhibits more promising characteristics, with notable hydrocarbon production observed in the southern (HGA) and western (OL) regions. Ra is the primary reservoir for production in the Hassi Messaoud, El Gassi, Zotti, and El Agreb fields (Fig. 10) [4].

A5-Ordovician play Sedimentology:

The Taconian unconformity separates the basal Ordovician (Tremadocian) from the Upper Ordovician (upper Ashgill) and consists of fluvio-glacial and glacio-marine formations. In the western and eastern parts of the Messaoud dome, the Taconian unconformity takes the form of erosion, which is largely the result of glacial planing.

The unit from the Tremadocian to the Caradocian, that is, all the lower Ordovician, comprises two transgressive-regressive cycles:

The first of these is the Tremadocian-lower Arenigian cycle, during which the formations were deposited in a shallow to fluviatile marine environment.

The second is the Middle Arenigian-Caradocian cycle, which is truncated in places by the Taconian unconformity, includes the Hamra quartzites, Ouargla sandstones, Azzel marine clays, and the Oued Saret littoral deltaic sandstones [4].

The case of the El Gassi El-Agreb region

B1-Source rock

- **Silurien:** The Silurian clays constitute the source rock, generating source of hydrocarbons across the entire Saharan platform. This source is represented by black, carbonated and radioactive clays, very rich in organic matter, with a thickness varying from 20 to 70 m. Organic matter is amorphous in nature. The Silurian is preserved to the north of the Hassi Messaoud field, to the west (Bassin d'Oued Mya), to the southwest (Mouydir basin) and to the east of the Berkine basin (Perrodon, 1966) [16].

- **The argiles of El Gassi:** These black clays and organogenesis may have made the greatest contribution to the accumulation of Hassi Messaoud reserves; this 37 to 50 meter thick formation is presented in the grabens of the Hassi Messaoud structure (Sonahess, 2007) [10].

B2-Covers rock

The Gassi El-Agreb structural zone is characterized by the presence of a permeability barrier for Cambrian oil deposits, formed by clay-salt deposits from the Triassic and Jurassic (Sonahess, 2007) [10].

B3-Traps

Given the importance of the tectonic movements which have affected the region, the traps encountered are essentially linked to horsts (complex tectonics), but there are also Litho stratigraphic traps such as those which are in the Ordovician and which can be encountered on the western flank of the Gassi El-Agreb ridge (Sonahess, 2007) [10].

During different geological periods, this area played the role of a high zone and as a result, the Paleozoic sediments underwent intense erosion during the Hercynian phase, which generated traps under unconformity (Sonahess, 2007) [10].
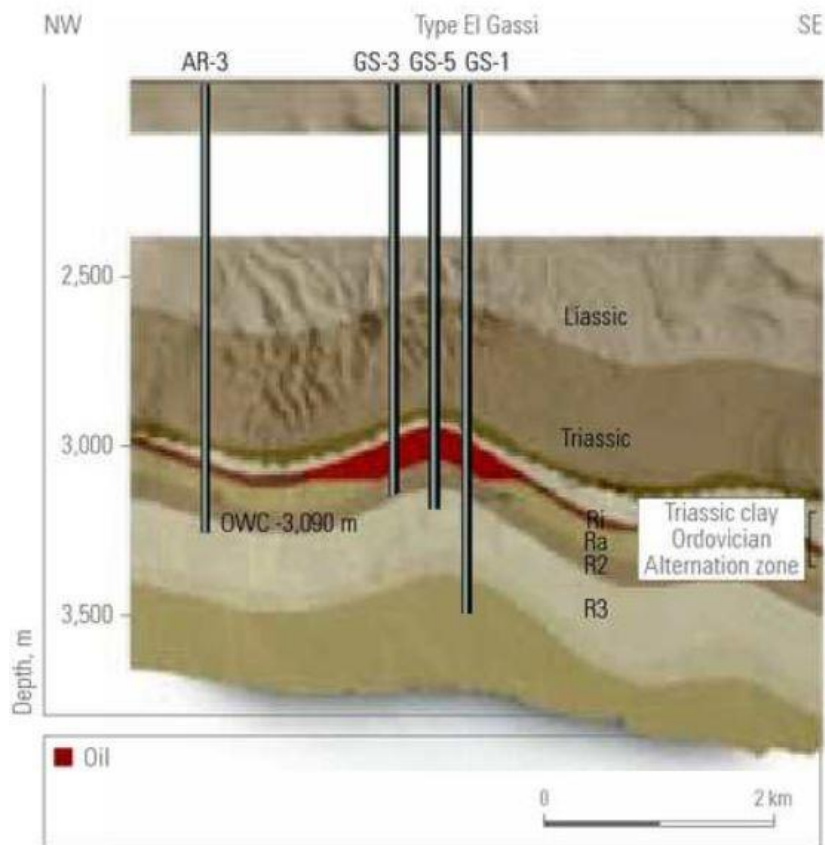
Fig. 11: Diagram characterizing the type of traps at Gassi El-Agreb [4].

Migration of hydrocarbons

The biomarker data and maturity parameters of aromatic hydrocarbons, as well as the data of pyrrolic nitrogen compounds, indicate that the source of the oil at Gassi El-Agreb is the Silurian source rocks of the Oued Mya basin. This also represents the source of filling of the reservoir rock of the large Hassi Messaoud anticlinal structure, which mainly comes from the West-Northwest and North-Northeast sectors of the region. The oil exhibited lateral migration over considerable distances, originating from the Silurian source rock in the Oued Mya basin and the Silurian source rock situated to the north-north-east of Hassi Messaoud.

The available evidence suggests that the oils originate from the Mokh-El-Kebch, N'goussa, Guellala, and Draa Temra fields, which exhibit short migration distances and are the primary agents responsible for the vertical filling of the reservoir from the underlying Silurian source rocks (Sonahess, 2007) [10].

The evidence indicates that the oil subsequently migrated southward, reaching Haoud Berkaoui and Benkahla. It then continued its southward migration, filling the Hassi Messaoud reservoir. Upon reaching the Hassi Messaoud reservoir, the oil migrated in a northerly direction towards the ridge situated in the center, before continuing in a westerly direction towards the northern, southern and western parts of the Gassi El Agreb field. It is evident that the filling of the Hassi-Guettar and Gassi-El-Agreb structure is derived from the northern region, with the oils of El Agreb having migrated through a petroleum system over considerable distances (120 to 140 km).

The data indicate a north-to-south migration of oil, with oil maturity decreasing from north to south across the El-Gassi, Zotti, and El-Agreb fields (Sonahess, 2007) [10].

Conclusion

The Hassi Messaoud field represents the largest hydrocarbon deposit in Algeria. The field is situated 650 km south-southeast of the capital city of Algiers. The Hassi Messaoud field is situated at the northern extension of the Amguid-El Biod mole, occupying the central part of the Triassic province. This structure appears to be a vast structural dome of nearly 1,600 km². The stratigraphic series of the Hassi Messaoud field is situated on the basement at a depth of approximately 4,393 meters. This series is notable for the absence of the Silurian, Devonian, Carboniferous, and Permian. The Hercynian discordance is more pronounced in the center of the structure, where the clay-sandstone and salt deposits of the Triassic rest directly on the Cambrian.

The Gassi El-Agreb field (GEA field) is a satellite deposit of the Hassi Messaoud deposit. It is located approximately 120 km southwest of Hassi Messaoud. The field was first discovered in 1956 and subsequently brought into production in 1959. The reservoir in this field is of Cambro-Ordovician age. The Gassi El-Agreb reservoir is situated within an Upper Cambrian sandstone formation, which was deposited in a fluvial and marine environment, with the addition of deltaic marine silica. The structural configuration of the Gassi El-Agreb reservoir is that of a large double-slope anticline. The structural style of this trend is characterized by a northwest-southeast orientation and reverse sub-vertical faults, which are indicative of a strike-slip tectonic regime.

The reservoir in the Gassi El-Agreb region is composed of Cambro-Ordovician rocks. The Cambrian series comprises the following zones from bottom to top: R3, R2, Ra, and Ri. The Ordovician series is represented by the zone of alternations, which is composed of sandstones, quarzitic sandstones, gravels, and conglomerates. At the roof, we observe improved grading and rounding of grains.

Chaptertwo:

Definition and measurement of petrophysical parameters

Chapter two
Definition and measurement of petrophysical parameters

1-Introdution

A reservoir is defined as a rock formation comprising voids, pores, and cracks that allow fluids to circulate and collect. The petrographic characterization of reservoirs is expressed in terms of porosity and permeability, which are two key parameters influencing the reservoir's overall performance. The relationship between porosity and permeability is often complex but essential for understanding the reservoir's behavior and optimizing its exploitation.

Petrophysical studies aim to accurately assess the reservoir's characteristics, which is crucial for calculating the hydrocarbon reserves of a deposit and for developing an economically viable exploitation strategy.

The primary objective of this segment of the study is to identify the evolution of porosity and permeability parameters and their distribution in the Ri and Ra reservoirs, as well as to assess the impact of fracking on these two parameters.

2-Objectives and study area

In this study we examined a number of wells located in the Gassi El Agreb field. The location of each well is shown on the map below (Fig. 10).

The aim of this petrophysical study is, on the one hand, to evaluate qualitatively and quantitatively the petrophysical parameters, namely porosity, permeability, grain density and degree of saturation; on the other hand, to study the spatial distribution of each of these parameters and to deduce the correlation between them.

White light macrophotographic analysis allows us to obtain a stratigraphic and lithographic description of the area under study. With this approach, the cores taken from the boreholes are photographed rigorously and with high resolution.

3- Methodology

The following format will be employed in presenting the study:

- The parameters and methods used for measurement will be defined.
- The classification and relationship between these parameters will be discussed.

4- Definitions of petrophysical parameters

In order to optimize the exploitation of a given hydrocarbon deposit, it is necessary to determine the quality of the reservoir at the productive levels. This is achieved by measuring a range of

parameters, including petrophysics (porosity, permeability, useful thickness, saturation, etc.), from samples (plugs) taken from the cores using a variety of logging techniques.
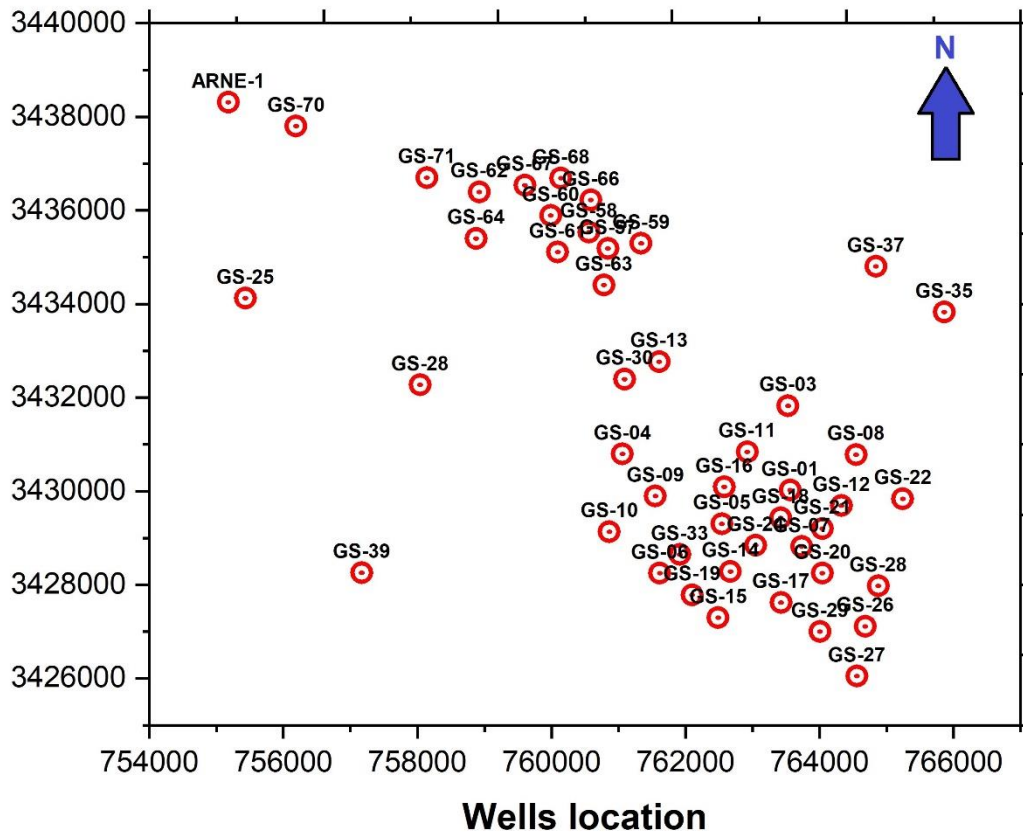
Fig.12: Location map of wells studied in the Gassi El-Agreb field.

4-1- Porosity:

Porosity of rocks refers to the amount of empty space within a rock. It is expressed as a percentage of the total volume of the rock that is occupied by voids or pores [17].

$$\phi = 1 - \frac{solid\ volume}{total\ volume} = \frac{Pores\ volume}{total\ volume} \quad (\%) \qquad Eq.2.1$$

Porosity is an important property of rocks because it influences how much water and other fluids a rock can hold. It also affects the ease with which fluids can flow through the rock, which is called permeability.

There are two main types of porosity:

- Primary porosity: This type of porosity is created when the rock is first formed. For example, the spaces between sand grains in sandstone are an example of primary porosity.

- Secondary porosity: This type of porosity is created after the rock has formed. It can be caused by weathering, fracturing, or the dissolution of minerals. An example of secondary

porosity is the cavities that can form in limestone when limestone is dissolved by acidic groundwater.

The porosity of a rock can vary depending on a number of factors, including [17]:

- The size and shape of the grains that make up the rock

- How well the grains are packed together

- The presence of cement that fills in the spaces between the grains

- Whether the rock has been weathered or fractured

(a) Porous media.

(b) Cubic packing.
(Equal grain size) $\phi = 47.6\%$.

(c) Rhombohedral packing.
(Equal grain size) $\phi \approx 26\%$.

(d) Cubic packing.
Two grain sizes $\phi \approx 12.5\%$.
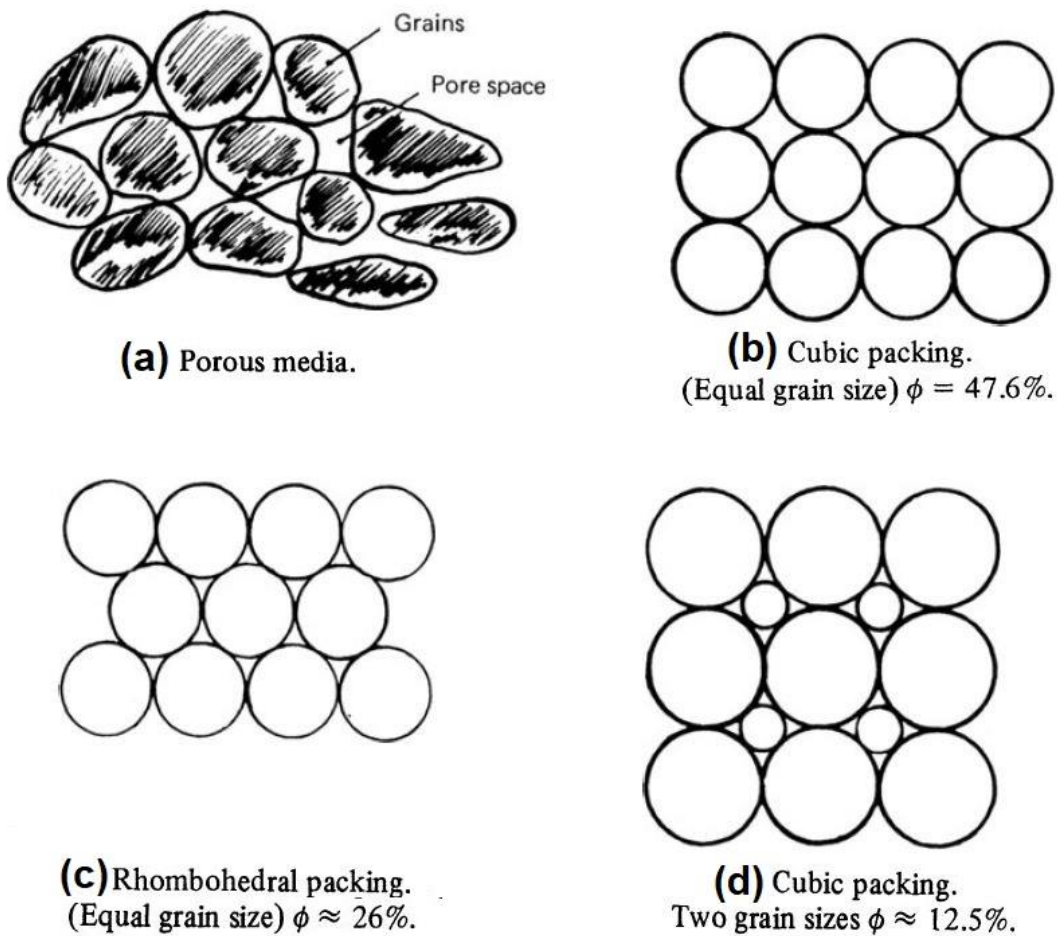
Fig.13: Different packing types of matter [17] .

Total porosity includes:

❖ On the one hand, the intergranular or inter-crystalline porosity constituting the porosity ϕ_1, which depends on the shape and size of the solid elements, as well as on their ranking,

❖ On the other hand, vacuolar porosity, acquired by dissolution, and fissure Porosity and fracture, mechanically acquired, constituting the secondary porosity ϕ_2 that we most commonly found in chemical or biochemical rocks (limestone).

The total porosity ϕ_t is given by:

$$\phi_t = \phi_1 + \phi_2 \quad (\%) \qquad\qquad\qquad Eq.2.2$$

❖ Connected porosity represents the percentage of pores connected to each other. It can be much lower than total porosity.

❖ Effective (or useful) porosity is the porosity accessible to free fluids. It is in20 to 25% lower than total porosity. This percentage is all the more that the grain size of the rock is finer, which accentuates the action of the capillary phenomena.

- The porosity of a rock is said to be low if it is less than 5%, mediocre by 5 to 10%, Medium 10-20%, good 20-30% and excellent if above 30%. Only porosity is of interest in determining the volume of "recoverable" hydrocarbons.

- The porosity of a rock is its property of presenting voids Pores and cracks. It is expressed quantitatively as the percentage of the volume Porous in relation to the total volume of the rock:

$$\phi_t = \frac{V_v}{V_t} \quad (\%) \qquad\qquad\qquad Eq.2.3$$

- The porosity is influenced by the size of the grains, their arrangement, their shapes, the cement and compaction.

- In addition to this total porosity Ø t, we define the useful porosity ϕu_u, which corresponds to the volume of voids likely to be occupied by fluids, is given by the formula:

$$\phi_u = \phi_t - S_w \quad (\%) \qquad\qquad\qquad Eq.2.4$$

S_w: Water saturation

4.2. Permeability

A porous medium allows the movement of fluids only to the extent that its pores are interlinked; it is then said to be permeable.

Permeability thus represents the ease with which a training allows fluid of given viscosity of the bushing. Darcy's law expresses permeability.

As being: the connectivity of a medium one centimeter long (dx), allowing a Volume of 1 cm^3 (Q) per unit of time (s), of a fluid with a viscosity of one centipoise (u) under the effect of a pressure gradient (Δ P) of an atmosphere through a section (s) one cm^2.

The formula is expressed as follows:

$$K = Q \cdot \frac{\mu}{S} \cdot \frac{\Delta x}{\Delta P}$$

Eq.2.5

Δp: Pressure difference between upstream and downstream.

Δx: Fluid path in cm.

S: Surface area exposed to the fluid in cm^2.

μ: Viscosity in centipoise.

4-3-Saturation: Water Saturation and Archie's Equation

The fraction of pores filled with water is called water saturation (Sw). Oil, gas, or other fluids can occupy the remaining pore space. The hydrocarbon saturation (Sh) represents the fraction of the pore volume filled with these hydrocarbons and can be calculated using the following equation:

$$S_h = 1 - S_w$$

Eq.2.6

It is generally accepted that reservoirs were initially filled with water. Over geological time, oil and gas, formed elsewhere, migrated through permeable layers and displaced some of the water, accumulating in the larger pores. However, this migration process does not remove all the water. Some water, called irreducible water saturation ($S_{w(irr)}$), remains trapped on the rock grain surfaces due to surface tension and within the smallest pore spaces [17] .

Archie's Equation and Resistivity

The presence of hydrocarbons, gases, or other fluids with different electrical properties compared to water will affect the electrical resistivity of the rock formation. Archie's equation is a widely used formula that relates the formation resistivity (Rt), water saturation (Sw), formation porosity (Φ), and several empirical constants[17] :

$$R_t = a \times \emptyset^m \times S_w^n$$

Eq.2.7

where:

Rt: Formation resistivity (ohm-meters)

Φ: Formation porosity (fractional value between 0 and 1)

Sw: Water saturation (fractional value between 0 and 1)

a: Tortuosity factor (usually a constant close to 1)

m: Cementation exponent (varies depending on rock type, typically between 1.8 and 2.6)

n: Saturation exponent (often assumed to be 2)

Note: The values of "a", "m", and "n" need to be determined or estimated based on the specific rock formation and fluid properties for accurate application of Archie's equation [17].

$$S_w = \sqrt{\frac{R_0}{R_t}}$$
Eq.2.8

R_0: resistivity of the rock in the water-saturated zone.

R_t: resistivity of the rock in the undersaturated zone.

$R_{xo}0$: resistivity of the rock in the water-saturated zone of the invaded zone,

R_{xo}: resistivity of The rock in the undersaturated zone of the invaded zone.

Formula that can also be written:

In general, n = 2 for most loose rocks, then for the virgin zone

And for the washed area:

WithS

S_{x0}= filter saturation.

S_w= water saturation.

For oil tanks, we also define.

S_{hc}= hydrocarbon saturation in the virgin zone.

S_{hr} = residual hydrocarbon saturation in the washed area.

$S_{xo}+ S_{hr}$= 1 in the washed area.

S_w+S_{hc} = 1 in the blank area.

The saturation of a fluid is a ratio of the volume occupied by this fluid to the volume Total pores. The letter S designates it,

If the fluid is the formation water, we have:

$$S_w = \frac{V_w}{V_p}$$
Eq.2.9

If the formation water is the only fluid present: S_w=1.
If hydrocarbons are also present:

$$V_{hy} = V_p - V_w \qquad\qquad\qquad\qquad\text{Eq.2.10}$$

Water saturation is:

$$\phi == \frac{V_p - V_{hy}}{V_p} = \frac{V_w}{V_p} \qquad\qquad\qquad\qquad\text{Eq.2.11}$$

5- *Classification of petrophysical parameters (according to Monicard)* [17]

5-1- *Porosity:* is classified as:

Table 1: Class of porosity according to Monicard.

Type	Interval value
Low :	$\phi < \ 5\%$
Poor :	$5\% \ < \phi < 10\%$
Average :	$10\% \ < \phi < 20\%$
Good :	$20\% \ < \phi < 30\%$
Very good :	$\phi > 30\%$

5-2- Permeability*:*

The range of permeability encountered is very wide, it varies from 0.1md to more than 10 Darcy

to better specify the values we accept [17]:

Table 2: Class of permeability according to Monicard.

Type	Interval value
Very low:	$K < 1 \ mD$
Low :	$1 \ mD \ < K < 10 \ \ mD$
Mediocre :	$10 \ mD \ < K < 50 \ \ mD$
Average :	$50 \ mD \ < K < 200 \ mD$
Good :	$200 \ mD \ < K < 500 \ mD$
Excellent :	$500 \ mD \ < K < 1000 \ mD$
High permeability	$K > 1000 \ mD$

6-Measurement Method:

6-1. Porosity measurement*:*

There are two methods of measurement:

Direct method:
Porosity measurements by this method are carried out in the laboratory on Extracted samples. The method consists of measuring the volume of the solid Vs, using porosimeter using helium gas.

Then the total volume V_t is measured using a positive displacement mercury pump by theArchimedes' Principle.

The porosity will be given by the following formula:

$$\phi = \frac{V_p}{V_t} \times 100 = \frac{V_t - V_S}{V_t} \times 100 \qquad \text{Eq.2.12}$$

V_P: Void Volume

Vs: Solid Volume

V_t: Volume

Indirect method: Combined Electrical and Nuclear Logging for Porosity Determination

This method utilizes both electrical and nuclear logging techniques to assess porosity in rock formations.

- Electrical Logging: Electrical resistivity measurements are obtained through logging tools. The Archie equation relates formation resistivity (Rt) to porosity (phi) and formation factor (F):

$$R_t = aF^n \qquad \text{Eq.2.13}$$

, where (a) and (n) are empirical constants that depend on the rock type and pore fluid salinity. By rearranging the equation and solving for porosity, we can estimate porosity based on the formation resistivity and formation factor obtained from electrical logging data.

- Nuclear Logging: Nuclear logging techniques, like density logging, measure the density of the formation. Porosity can be derived from the density data using appropriate models that account for the densities of the rock matrix and the fluids within the pores.

Advantages of Combining Methods:

- Combining electrical and nuclear logging methods can provide more accurate and reliable porosity determination compared to using a single method.
- Electrical logging may be ineffective in certain formations due to conductive clays or brines. Nuclear logging can provide valuable information in these cases.
- Conversely, nuclear logging may be affected by the presence of certain minerals. Electrical logging data can be used to compensate for these effects.

$$F = \frac{0.62}{\phi^2} \qquad \text{Eq.2.14}$$

$$F = \frac{R_0}{R_w}$$ <div align="right">Eq.2.15</div>

F: Formation factor.

Ø: Useful porosity in (%).

R_w , and R0: Respectively the resistivities of the water zone and the oil.

6.2. Permeability Measurement:

The analysis is conducted on samples with a diameter of 1" or 1.5" and a length of 1.5" using two measuring devices: a conventional permeameter and an ultrapermeameter. Both devices operate at a constant load. Nitrogen is employed as the crimping gas and for analysis. These devices are of Core Lab design and are manufactured based on Darcy's law, which states that:

$$Q = K \frac{S \Delta P}{\mu \Delta x}$$ <div align="right">Eq.2.16</div>

K: permeability in mD (millidarcy)

Δp: Pressure difference between upstream and downstream

Δx: Gas path in cm

S: Surface area exposed to gas in cm^2

μ: Viscosity in centipoises.

Chapter three

Analysis and interpretation of the results

Chapter three

Analysis and interpretation of the results

Section 1: Seismic analysis

Introduction

1-Introduction

The Gassi El-Agreb region is believed to contain significant hydrocarbon deposits. To identify these deposits and assess their viability, a seismic survey is essential. This non-intrusive method employs sound waves to image the subsurface, revealing geological structures and potential hydrocarbon reservoirs.

The results of this seismic exploration will have a profound impact on the entire process of finding, extracting, and evaluating these resources. To understand how this will occur, it is necessary to examine the various stages of the process in detail.

Prospecting: The survey will identify promising locations for drilling by pinpointing potential traps and formations favorable for hydrocarbon accumulation.

Drilling: Seismic data allows for informed well placement, optimizing drilling efficiency and reducing the risk of encountering unexpected geological formations.

Nevertheless, no exploration is without its challenges. Potential problems, such as complex geological structures or environmental considerations, may arise. Fortunately, advanced seismic techniques and mitigation strategies can address these issues, ensuring a successful and responsible exploration endeavor.

2-Vertical seismic profile (VSP)

In the field of geophysics, a vertical seismic profile (VSP) is a technique used for seismic measurements, which are then correlated with surface seismic data. The defining characteristic of a VSP is that either the energy source, or the detectors (or sometimes both) are situated within a borehole. In the most common type of VSP, hydrophones (or more often geophones or accelerometers) record reflected seismic energy originating from a seismic source at the surface, which is then analyzed [18]. A class of borehole seismic measurements is employed for correlation with surface seismic data, to obtain images of higher resolution than surface seismic

images, and to look ahead of the drill bit. This measurement technique is also referred to as a VSP. In its most basic form, a VSP is defined as a set of measurements taken in vertical wellbore using geophones positioned within the wellbore and a source located at the surface in proximity to the well. In a more general context, VSPs may vary in terms of the well configuration, the number and location of sources and geophones, and the manner in which they are deployed [18].
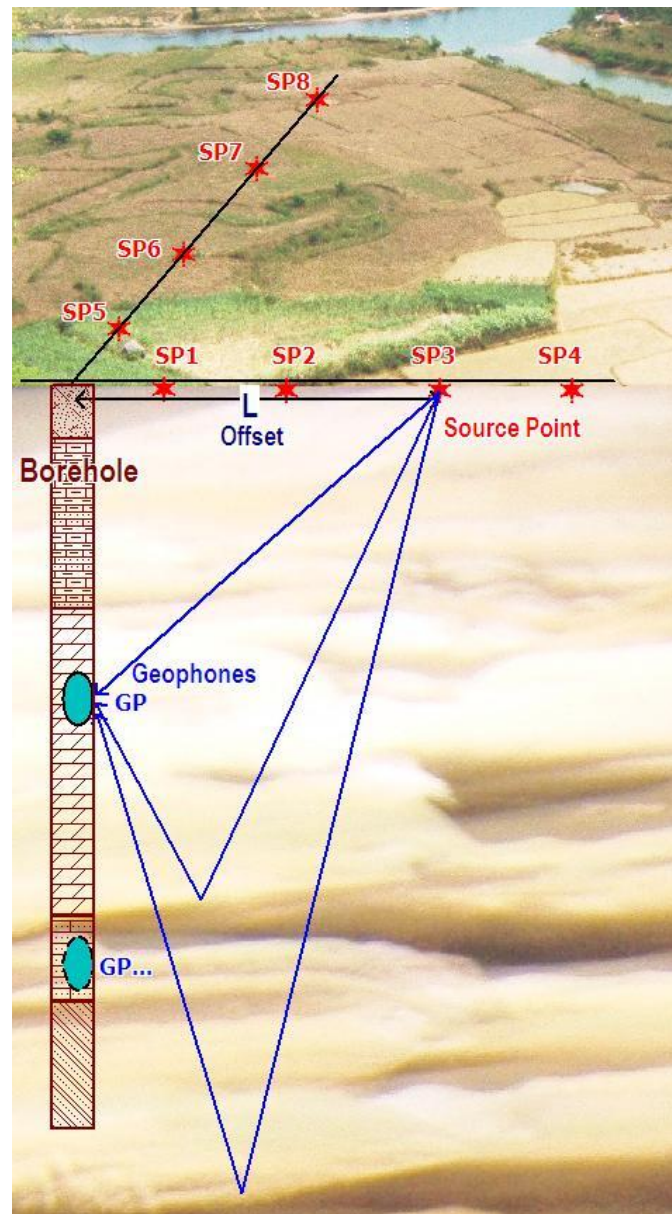

Fig.14: Typical layout of Vertical Seismic Profiling Survey [19].

The majority of VSPs employ a surface seismic source, which is typically a vibrator on land and an air gun in offshore or marine environments. VSPs encompass a variety of configurations, including zero-offset VSPs, offset VSPs, walkaway VSPs, walk-above VSPs, salt-proximity

VSPs, shear-wave VSPs, and drill-noise or seismic-while-drilling VSPs. A VSP is a more comprehensive survey than a check-shot survey due to the closer spacing of the geophones, typically approximately 25 m (82 ft), whereas a check-shot survey may encompass measurements of intervals that are hundreds of meters apart. Additionally, a VSP employs the reflected energy present in the recorded trace at each receiver position, in addition to the initial direct path from the source to the receiver. In contrast, the check-shot survey employs only the direct path travel time. In addition to linking well data to seismic data, the vertical seismic profile also enables the conversion of seismic data to zero-phase data and the differentiation of primary reflections from multiples [18].

3-Amplitude Versus Offset analysis (AVO)

In geology, AVO, which stands for Amplitude Versus Offset analysis, is a technique used in reflection seismology. It analyzes how the amplitude (strength) of reflected seismic waves changes with the offset, which is the distance between the source of the seismic waves and the receiver (i.e. geophone) [18].

The variation in seismic reflection amplitude with change in distance between the shot point and the receiver indicates differences in lithology and fluid content in the rocks above and below the reflector. AVO analysis is a technique employed by geophysicists to ascertain the thickness, porosity, density, velocity, lithology, and fluid content of rocks [18]. The successful implementation of AVO analysis necessitates the application of specialized processing techniques to seismic data and seismic modeling, which enables the determination of rock properties with a known fluid content. With this knowledge, it is possible to model other types of fluid content. A gas-filled sandstone may exhibit an increasing amplitude with offset, whereas a coal may exhibit a decreasing amplitude with offset. One limitation of AVO analysis using only P-energy is that it is unable to yield a unique solution, which can result in misinterpretation of the results. One common misinterpretation is the failure to distinguish between a gas-filled reservoir and a reservoir with only partial gas saturation, which is commonly referred to as "fizz water." Nevertheless, AVO analysis employing source-generated or mode-converted shear wave energy enables the differentiation of degrees of gas saturation. AVO analysis is more successful in young, poorly consolidated rocks, such as those found in the Gulf of Mexico, than in older, well-cemented sediments [18].

4-Diagram of the reservoir geophysics process

The following paragraphs will describe the reservoir geophysics workflow, as illustrated in Fig. 1. As illustrated in Fig.1, the initial point of departure for the workflow is the data itself. The

well data is displayed on the left side of the plot, while the seismic data is presented on the right. Ideally, the well data should include P-wave velocity, V_P, S-wave velocity, V_S, and density, ρ, in order to facilitate adequate rock physics and synthetic modeling. Nevertheless, should only P-wave velocity and density be available, Gassmann modeling can be employed to generate S-wave velocity. A plethora of rock physics models are available, ranging from simplified models of unconsolidated gas sand to complex fractured carbonate models. The following section will present an approach to modeling unconsolidated gas sands initially proposed by Ødegaard and Avseth (2003) [20-22].

The second step, synthetic seismic modeling, begins with the extraction of a wavelet from the seismic data and then the tying of the zero-offset synthetic seismogram to the stacked seismic data. Subsequently, pre-stack synthetics can be generated and compared to the pre-stack seismic data. This paper will not discuss synthetic tying and modeling; rather, it will assume that these steps have already been completed [21, 22].
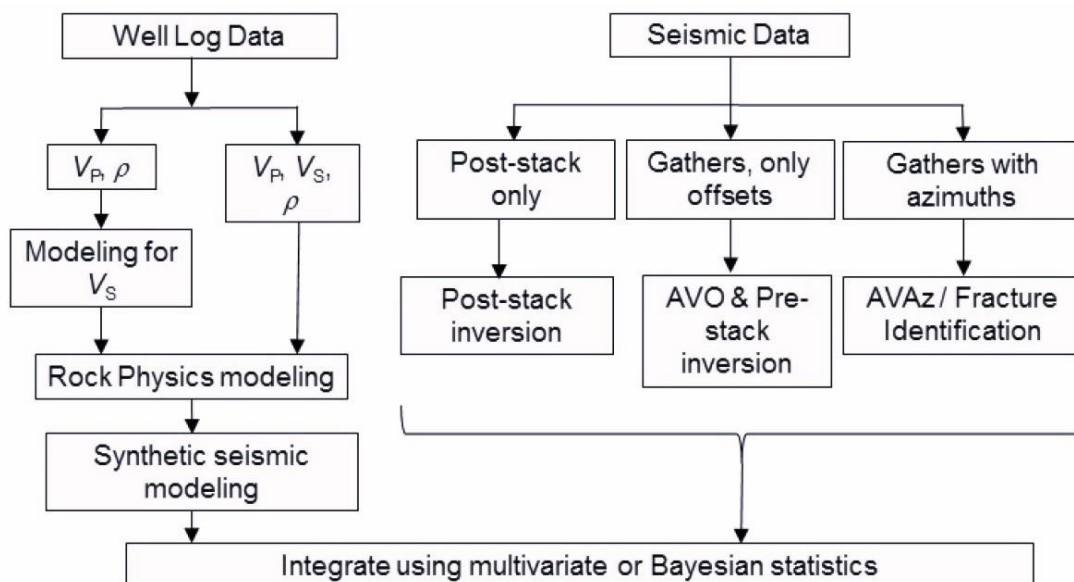
Fig. 15: A reservoir geophysics workflow. [21]

The next step is to consider the seismic data input stream, as illustrated in Fig. 15. A pivotal decision regarding the optimal course of action will be contingent upon the nature of the data available within the project. In the event that only post-stack data is available, the subsequent process will be limited to post-stack inversion, which results in the calculation of P-impedance, defined as the product of density and P-wave velocity. If pre-stack data with offset or angle information is available, and then full pre-stack inversion can be implemented, resulting in P-impedance, S-impedance, and density. From this, elastic volumes such as the V_P/V_S ratio, Poisson's ratio, Young's modulus, λ-μ, λ-ρ, and V_P and V_S can be generated. In this presentation,

we will demonstrate the application of pre-stack inversion to our gas sand example. We will illustrate how the results can be interactively selected from various lithological and fluid zones on the inverted dataset and displayed on a cross-plot, integrated with a rock physics template [21, 22].

As illustrated in Fig. 15, if the pre-stack data has been recorded with a comprehensive range of azimuths, AVAz analysis can be applied, enabling the identification of fractures. However, in the dataset utilized in this study, azimuth information was not available [21, 22].

In the final step depicted in Fig. 15, it should be noted that all of the rock physics and seismic attributes can be integrated using either multivariate or Bayesian statistics. The final section of this study will demonstrate how Bayesian statistics, utilizing both bivariate Gaussian and mixture Gaussian probability density functions, can be employed to assign a probability distribution to each lithological or fluid zone identified in the seismic data, in conjunction with the rock physics model. This enables the probability of identifying a hydrocarbon zone in other areas of the survey to be quantified [21, 22].

5-Seismic study of the El Gassi region

5.1. Geographical location of GEA (Gassi El-Agreb) region.

The GEA (Gassi El-Agreb) field is situated in the Ouargla wilaya, approximately 975 km southeast of the capital city of Algiers and 103 km from Hassi Messaoud. The field is comprised of three sections (see Fig.3). The Gassi, Zotti, and El Agreb fields are covered by a production-sharing contract (PSC) between SONATRACH and Amerada Hess.

The contract was initiated on October 21, 2000, with an initial term of twenty years. Its objective was to enhance the recovery rate of the three fields. The three fields are El Gassi, El Agreb, and Zotti.

The primary subsurface redevelopment of the existing project is represented by the gas compression and reinjection (GCR) project at El Gassi, augmented water injection at Agreb West, and gas lift on all fields.

5.2. Available database and its enhancement

Legacy data for the Production Sharing Contract (PSC) area was compiled into a digital database, but coverage was limited, especially for older wells and overburden sections. Seismic data was also sparse and of poor quality.

Since acquiring the PSC, significant data collection and processing efforts have been undertaken. A high-resolution 3D seismic survey was acquired and processed in 2001-2002, covering the entire area. This data was then inverted for acoustic impedance to improve

understanding of the subsurface. Additionally, modern well logs, VSP surveys, and overburden data were acquired in specific wells to further refine the seismic data and enable accurate well-to-seismic ties.
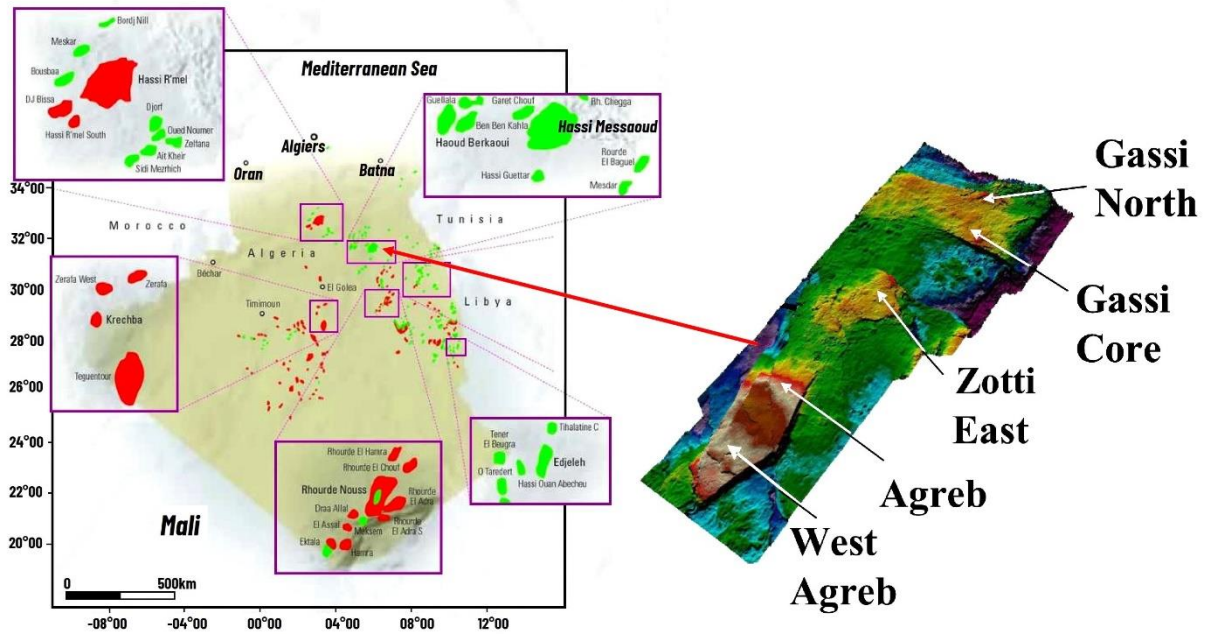
Fig.16 GEA's geographical location [4, 23].

As VSP data became available, the initial 3D seismic processing was revisited and a full reprocessing project was completed in 2005. This improved processing led to better noise suppression, clearer fault delineation, and ultimately the successful discovery of oil at the AR-71/71z well (See Figs.18 and 19).

Further inversion work was conducted to create additional datasets from the 3D seismic data, including a "pseudo-high frequency" volume for improved reservoir interpretation and an (partially successful) attempt at a density volume to differentiate between different rock layers. Gravity and magnetic data were also acquired alongside the 3D seismic survey and incorporated into the overall structural interpretation.

5.3. Well to Seismic Ties

While significant static corrections were necessary to align the borehole seismic data with the surface seismic data (a common procedure in land seismic studies), the resulting well-to-seismic ties for the Gassi El Agreb (GEA) area are well defined. Both processed seismic

volumes (2002 and 2005) were standardized to a zero-phase response, where increased acoustic impedance is represented by a trough in the seismic signal (Figure S5).

A number of key horizons were identified within the post-Hercynian section, which correspond to significant changes in rock velocity or structural features (Figure S6). These horizons were interpreted on a regional scale for use in studies analyzing depth conversion sensitivity and overall structural evaluation. For the purpose of reservoir characterization, the two most significant horizons are the Hercynian unconformity and a "Basement" reflector. The well GS-1 in the El Gassi field demonstrates that this reflector correlates with the infra-Cambrian basement or the base of the R3 lithozone. The mapped Hercynian unconformity peak is the result of a tuning effect between the Triassic Clayey and the top of the Cambrian section. Imaging the basement event is of great importance for structural interpretation, as it allows geologists to determine the pre-Hercynian structure (including dips) and estimate the thickness of the Cambrian section (amount of erosion). The Basement event is evident as a pronounced trough in both seismic data vintages. Both the Basement and Hercynian Unconformity horizons were mapped in detail in order to establish an accurate picture of the GEA reservoir's structural framework.
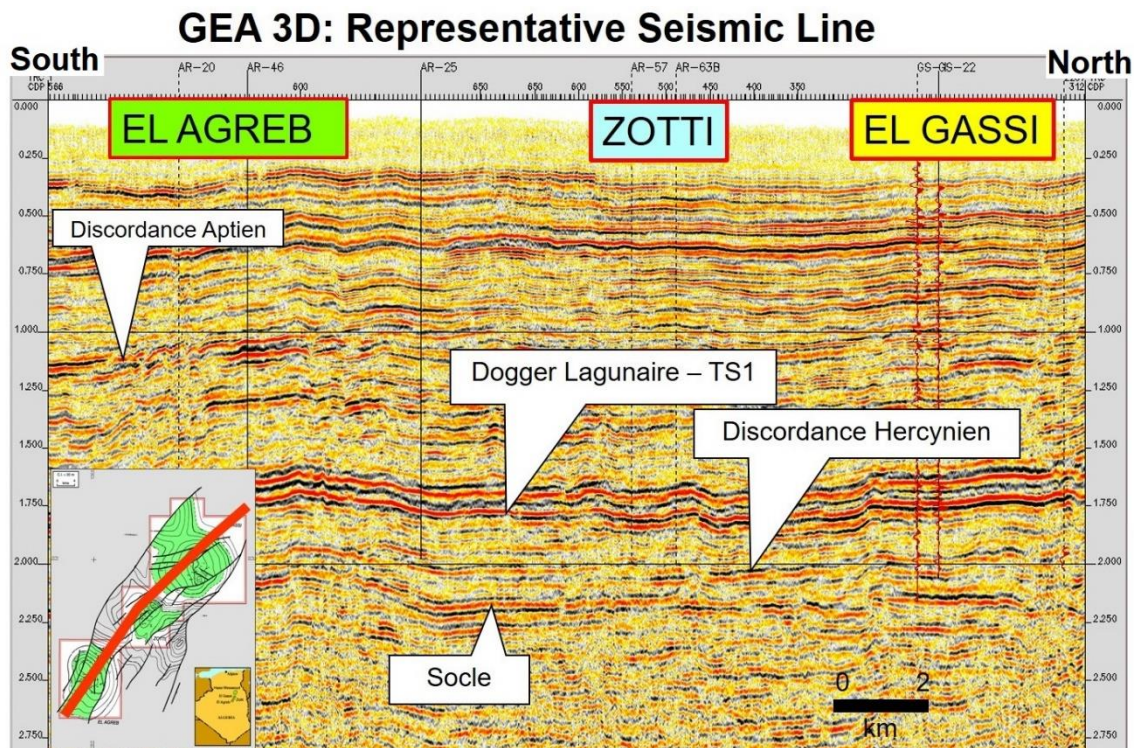
Fig.17: Gassi El-Agreb 3D: Representative seism line [10].

5.4. Seismic Structural Interpretation Strategy

The seismic interpretation strategy focused on building a two-part structural picture. First, it aimed to establish a regional understanding of the post-Hercynian overburden, focusing on key velocity breaks and unconformities. Second, it aimed to decipher the pre-Hercynian structure and its development in detail by meticulously interpreting the Hercynian Unconformity and Basement events.

To achieve this, extensive use was made of various data types, including reflectivity, impedance, coherency information, and dip/azimuth maps. This integrated approach led to the development of a comprehensive fault framework for all three fields. Notably, coherency data proved highly effective in defining the intricate fault pattern within the Cambrian section (Figure S7).
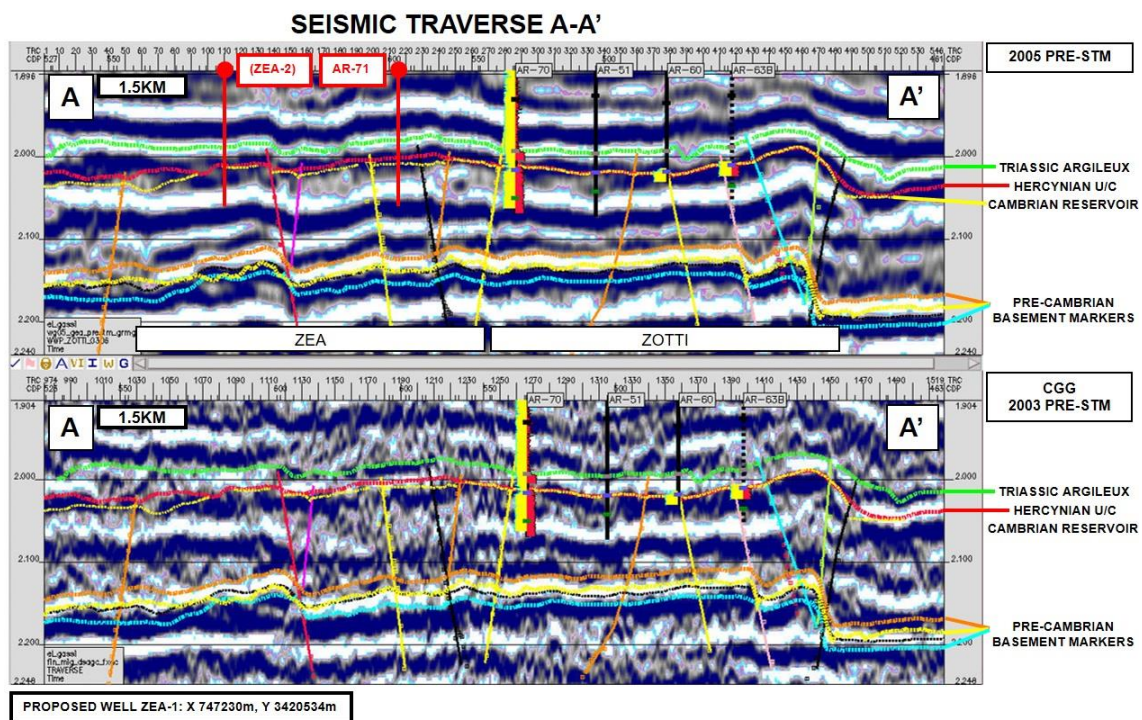
Fig.18: Noise reprocessing and multiple attenuation provide an image that facilitates the precise delineation of Cambrian faults [10].

5.5. Seismic Structural Interpretation of the Gassi El Agreb Area

The Gassi El Agreb Area (GEA) boasts a rich and complex geological history spanning from the Pre-Cambrian era to the present day. This long and dynamic timeline has resulted in an intricate structural framework that significantly influences the region's hydrocarbon reservoirs.

▪ **Early Stages: A Peneplained Basement and Cambrian Deposition**

The story begins with a Pre-Cambrian basement that was extensively eroded, creating a relatively flat surface. The Cambrian period witnessed the deposition of sediments on this

peneplained surface, likely in a conformable manner (meaning the layers lie relatively flat on top of each other). Seismic data supports this notion, although direct evidence is scarce.
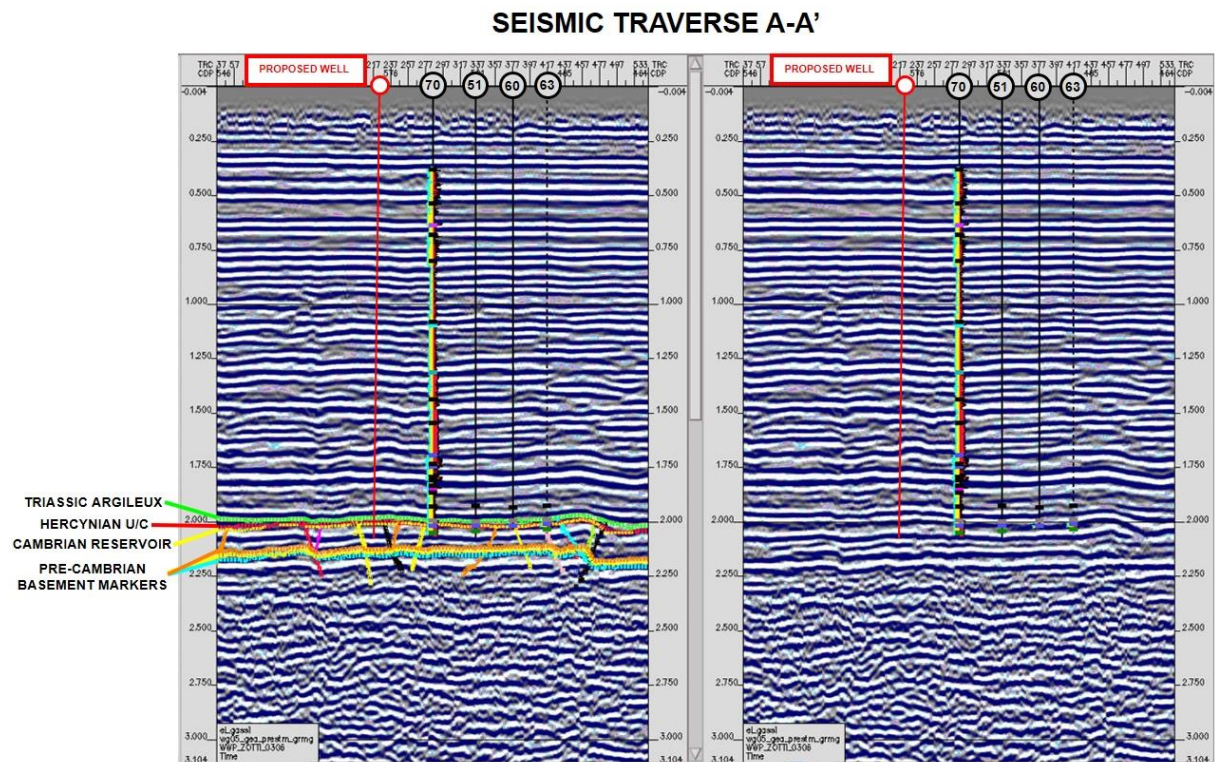
Fig.19: Proposed wells that led to AR71/71z wells' location [10].

- **Pre-Hercynian Faulting and Uplift**

A period of extensional tectonics, most likely during the Ordovician and Frasnian eras, is inferred based on regional geological knowledge. However, due to subsequent events, direct evidence of these faults on the seismic data is absent. The Hercynian Orogeny brought about a regional uplift, leading to erosion of most of the post-Cambrian and pre-Hercynian sediments.

- **Hercynian Orogeny: Reshaping the Landscape**

This mountain-building event significantly affected the GEA. Many earlier faults were reactivated, and the overall structure was reshaped. Notably, El Agreb and Zotti were dominated by North-South and North-Northwest-South-Southeast trending structures and faults. Additionally, the Hercynian unconformity (boundary) serves as a key reference point for understanding the Cambrian structure.

- **Austrian Compression and Continued Fault Reactivation**

The Austrian compression phase further modified the reservoir morphology. Some Hercynian faults were reactivated, particularly the north Zotti bounding fault (Fig.9). New Austrian faults

were also formed, with El Agreb acquiring its present-day shape due to the influence of NNE-WSW and NE-SW bounding faults.

- **The Remaining Story: Alpine Uplift and Modern Structure**

The most recent Alpine tectonic phase left its mark on the shallowest mappable horizon (Senonian Lagunaire). This indicates that some structural trends remained active. The NNE-WSW Agreb bounding faults are a prime example, demonstrating the ongoing influence of these structures.
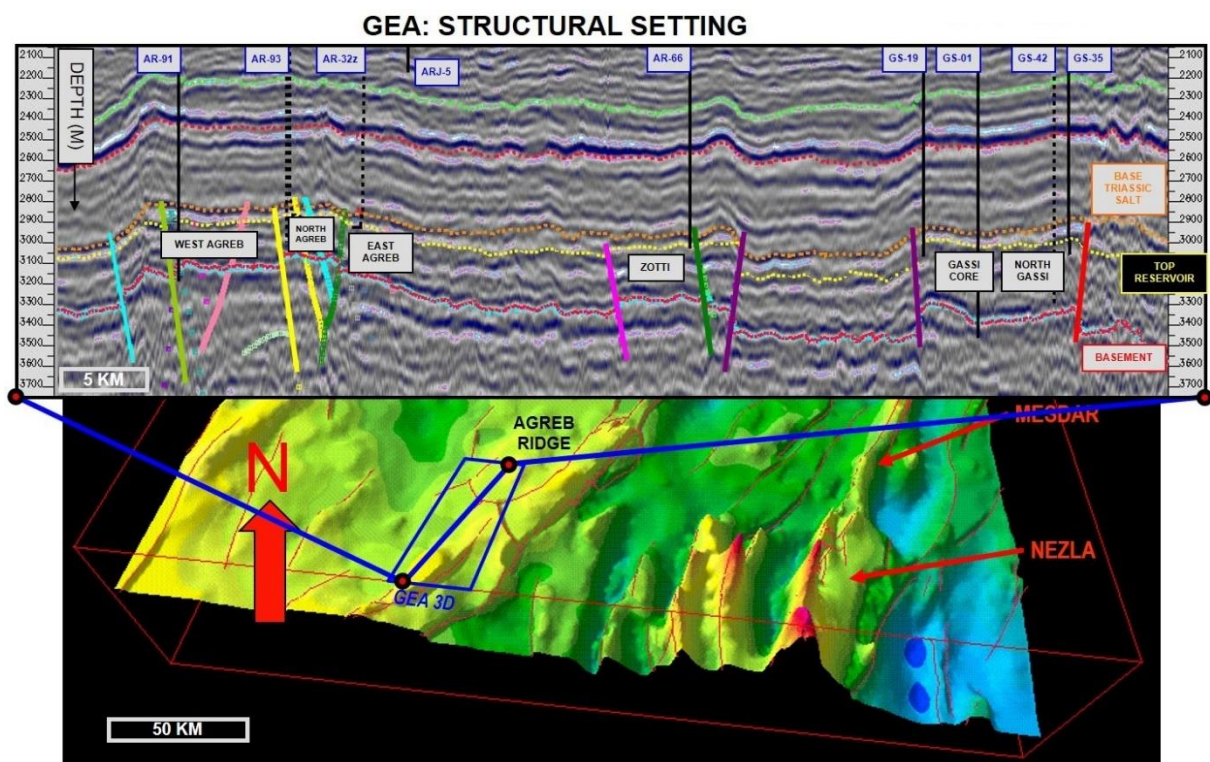
Fig.20: Gassi El-Agreb structural setting [10].

- **Challenges and Assumptions in Reservoir Characterization**

The lack of clear seismic reflection at the Top Reservoir level presents a challenge. Therefore, the assumption is made that the reservoir roughly follows the Basement morphology, with local variations based on well data. Additionally, the Basement is assumed to be largely peneplaned, with potential isolated hills ("monadnocks") existing in some areas.

- **Reservoir Morphology through Time**

Maps depicting the Basement morphology at different tectonic phases offer valuable insights into the corresponding reservoir morphology. The thickness of Cambrian and Ordovician sediments can be estimated based on these maps. Notably, El Gassi wells encountered both

Cambrian and Ordovician, with thicker Ordovician sections in Gassi North compared to the Core area.

- **Limitations of Isopach Mapping**

The isopach map, generated by extending upwards from the Basement, serves as an approximation of the Top Reservoir. However, discrepancies may arise due to the influence of faulting on the isopach measurements.

In conclusion, the GEA's complex geological history, characterized by multiple tectonic phases and fault reactivation events, has shaped the current reservoir structure. While challenges exist in directly mapping the Top Reservoir, a combination of seismic data, well information, and assumptions about the Basement morphology allows for a comprehensive understanding of the reservoir characteristics.

5.6. Seismic Structural Similarities in El Gassi and El Agreb Fields

The 3D seismic data reveals a striking similarity between the structural features influencing the Cambrian strata in both El Gassi and El Agreb fields. The complex fault pattern observed within the Cambrian Ri/Ra sandstones of these fields, estimated to be 550 million years old, is a testament to their extensive structural history.

5.7. El Gassi Fault Analysis

The seismic interpretation of El Gassi (Fig. 21) identifies several significant fault trends that correlate with regional occurrences. These faults primarily follow a dominant North-South (N-S), Northwest Southeast (NW-SE), Northeast Southwest (NE-SW), and East West (E-W) orientation.

EL GASSI TOP RESERVOIR DEPTH STRUCTURE

Left lateral strike slip along a Riedel shear leading to the creation of secondary Riedel and conjugate Riedel Shears at Gassi North
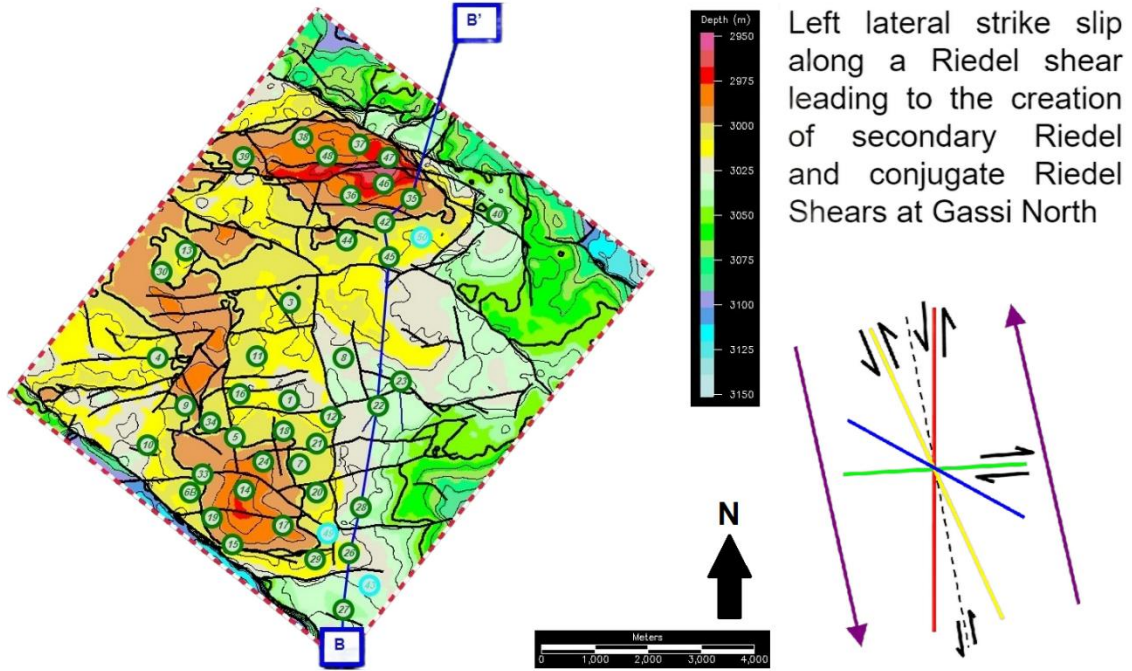
Fig.21: El Gassi top reservoir depth structure and Main faults.

ZOTTI TOP RESERVOIR DEPTH STRUCTURE
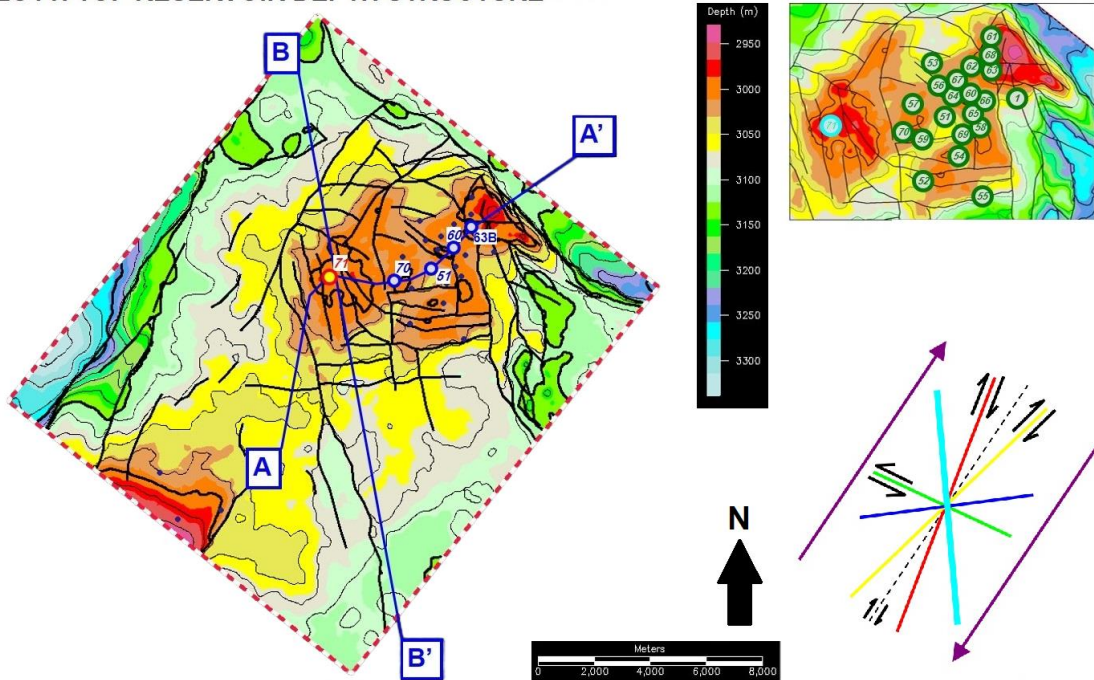
Fig.22: Zotti top reservoir depth structure and Main faults.

Fig.23: El Agreb top reservoir depth structure and Main faults.

The N-S trending faults exhibit a multi-phase reactivation history, possibly originating from the Pre-Cambrian Pan-African continental collision. In contrast, the NW-SE and NE-SW trending faults are concentrated within the El Gassi core area and define the structural boundaries of the underlying, much larger El Gassi horst. Their orientation aligns with the Paleozoic NW-SE extensional event followed by the Hercynian NW-SE compression. Notably, these faults experienced significant post-Hercynian reactivation, primarily through reversal, which also affected the overlying strata. This reactivation is likely linked to the Early Cretaceous "Austrian" W-E compressional phase. The mapped faults in El Gassi are generally sub-vertical, with dips ranging from 60° to 80°.

5.8. Conclusions: El Gassi and El Agreb Structural Interpretation

5.8.1. Enhanced Reservoir Characterization through Coherency and AI

The integration of coherency analysis and AI data has revealed a more nuanced understanding of the structural features within the fields. This has allowed a more detailed picture to be developed, facilitating optimal well placement and the identification of key faults crucial for reservoir modeling. The recent drilling of wells in El Agreb has demonstrated the accuracy now achievable in well prognosis thanks to these advancements.

5.8.2. Complex Deformation History Impacts Reservoirs

The deformation history of the fields is complex, characterized by two main trends: a North-South (pre-Cambrian) trend and an East-West trend that persisted from the Jurassic to the Aptian period. Evidence suggests that the major North-South trends may diminish reservoir quality by acting as seals. Additionally, the possibility exists that East-West faults, like GS-15, may function as pressure baffles within the reservoir.

El Gassi: The field is bounded by Northwest-Southeast and Southwest-Northeast faults. These faults were initially formed through normal faulting, but have undergone significant reversal and reactivation. The subtle Southwest-Northeast trending faults may act as seals within the reservoir (Fig.8).

El Agreb: Similar to El Gassi, the field is bounded by South-Southwest-North-Northeast faults that were initially formed through normal faulting but have since undergone substantial reversal and reactivation (Fig.10).

5.8.3. Interpretation Validated by Well and Dynamic Data

The interpretations derived from the structural analysis are well supported by well data and dynamic data. For instance, a North-South trending fault in El Agreb appears to compartmentalize the reservoir. In El Gassi's core area, there is good agreement between the mapped faults and the independently derived reservoir model areas. Furthermore, the observed Northwest-Southeast trending faults in El Gassi correlate with the water cut seen in the wells, suggesting a connection between these faults and water influx.

Influence of Basement Fabric and Fault Reactivation on Reservoir Quality

The pre-Cambrian basement fabric heavily influences the present-day structure of the Gassi El Agreb (GEA) area. The overall structural configuration of the three fields is a consequence of:

- The reactivation of this basement fabric during the Hercynian (Caledonian) and Austrian/Alpine Orogenies (Fig.10).
- The creation of secondary fractures oriented in echelon (not directly parallel) to the regional stress direction.
- The interplay between reactivation of existing fractures and the formation of new fractures.
- The influence of pre-existing fractures on the development of later fractures.

All the faults within the fields have been subjected to both extensional and compressional forces (in a strike-slip setting). This implies that all faults likely possess some degree of "damage" in the form of cataclastic seal, mineralization, or fault smear, which can decrease permeability (Kh) over an unknown distance. This "radius of disturbance" is a significant source of

uncertainty, as it weakens the confidence in straightforward predictions about drilling near specific fault orientations, given the possibility that these faults may still be open. Unfortunately, due to limitations in identifying the amount and stress conditions of fault movement, precisely determining the extent of this damage is extremely challenging.

A more logical assumption is that recent fault reactivations may have generated small fractures within the rock (outside of the main fault zones as identified by seismic data) adjacent to the fault trends following the Hercynian event. Since these fractures are relatively recent, the absence of any significant fluid flow events after this orogenic episode suggests that they are more likely to remain open. This would enhance permeability (Kv) and promote fluid flow and reservoir drainage.

Section 2: sediment and stratigraphy

Well GS-36

Descriptions, observations and comments

Interval 3200 m to 3228 m

Core #1

The core was composed of bioturbated sandstone, which was interbedded with abundant thin silty claystone and claystone beds and lenses. Stylolites, which were observed to be filled with clay (possibly illite or chlorite), were also noted. No evidence of large fractures, either open or closed, was observed in the core at any point. The core exhibited cross-bedding characteristics at depths as great as 3226 meters. After this depth, only minimal evidence of cross-bedding was observed.

The rock itself (fresh breaks) exhibited a wide range of colors, from gray to light gray, light yellowish brown to brownish gray, and occasionally light grayish white. The degree of silicification and clay content in the matrix significantly influenced the color, with quartzitic rocks exhibiting lighter colors. The principal component was quartz, colorless, rarely pale yellow, light brown, transparent to translucent, in places opaque, off to milky white, occasionally smoky gray, predominantly well sorted, but with very variable grain sizes from fine to coarse. The dominant grain size changed very rapidly, in some cases within centimeters, grains chiefly subrounded, in places rounded, with depth also subangular. The rock is very hard with an excellent siliceous cement and common quartz overgrowths, which often fuse grains together. There are rare instances of microcavities that are filled with crystalline (hexagonal)

quartz. The rock is predominantly clean, but there are local areas with a gray, brown, or yellowish green argillaceous matrix. The visible porosity is fair to moderate, and there are occasional areas with very good visible porosity. In other areas, the porosity is zero, which is typical of the most heavily silicified areas. The first eight meters (3200m to 3207m inclusive) exhibited a high degree of silicification, which corresponded to a markedly poor porosity. This was in contrast to the 3203m to 3204m interval, which exhibited excellent visible porosity and was not heavily silicified.

The porosity was not heavily silicified.

Beyond 2208 m, the visible porosity was generally better, although there were isolated samples where it dropped to zero. It should be noted that the porosity in this and the other cores exhibited occasional rapid changes (over centimeters) from poor or zero to good. In general, the core exhibited minimal mineralization, with sporadic instances of disseminated pyrite (mostly microscopic), iron, chlorite, and other minerals. The silty claystone and claystones were predominantly greenish gray, occasionally light brown, and exhibited high argillaceous content. They were locally graded to clay and were firm to moderately hard, subfissile, and platey.

The majority of the core exhibited yellow fluorescence, which was occasionally bright yellowish gold and rarely pale yellow. This fluorescence was observed across the entire sample, although in some instances, only the center fluoresced, suggesting that the margins may have been flushed by the coring process. Additionally, moderate to slow, occasionally fast, bright bluish white streaming cut was observed. In some cases, the cut fluorescence was reduced to diffusion only. All the samples displayed some form of cut fluorescence. In some instances, a trace brown residue (ring) was observed.

It should be noted that the core was cut at an angle of 9 degrees.

3201.7 meters of Banded Bioturbated Sandstone. The lighter the color, the more silicified the sandstone tends to be. It is notable that bioturbation is present in the lighter bands (3201.7B and D), which may facilitate the communication of zones with superior porosity in the vertical plane. Toward the base of the section, cross-bedding is observed.

The 3203.5-meter section comprises coarse-grained gray sandstone. Even in a photograph, the porosity can be discerned. It is noteworthy that the lower left region exhibits a greenish yellow argillaceous matrix. Samples from this depth exhibited a bright yellow gold direct fluorescence and a fast streaming cut fluorescence.

3206.2 m Banded Sandstone with variable visible porosity. While not readily apparent in the photograph, the darker bands exhibit significantly higher porosity than the lighter bands. In

certain instances, the pore spaces have been filled with sand grains that were blown over the core. These can be discerned as light brown specks within the darker brown bands.

The 3209.5-meter Banded Sandstone exhibited a considerable degree of variability in grain size. The grain size is observed to be coarser in the darker bands, with the presence of some very coarse milky white "floaters." The coarser sections exhibited excellent visible porosity, with numerous large pore spaces discernible in the photograph. A stylolite can be observed directly below the number "#" on the box lid.

The stratum in question is 3211.5 meters of cross-bedded sandstone. This is an exemplary illustration of the cross-bedding observed in the core sample. It is noteworthy that some of the grains are of considerable size.

3214.5 meters: Greenish gray silty claystone. A well-developed zone of silicification is visible in the lower portion of the section, to the left of the silty clay. The zone of silicification above the clay is relatively poorly developed. Further to the left, a thin clay-filled stylolite can be observed, accompanied by an unusually large silicified zone above and below it.

At a depth of 3219.5 meters, the rock formation comprises cross-bedded and partially silicified sandstone. It is evident that the lighter-colored bands are more tightly packed as a result of silicification. Additionally, a stylolite is visible on the left.

At a depth of 3224.8 meters, the rock formation comprises greenish gray silty claystone. A silicified zone is evident above and below the bed. It is notable that the bed angle exceeds the 9-degree angle of the core sample, suggesting that the reservoir may be tilted. Unfortunately, the photograph does not clearly illustrate the bioturbation at this depth.

At a depth of 3225.5 meters, the rock formation is composed of cross-bedded sandstone. It is evident that the cross-bedding extends in all directions. It is noteworthy that the grain size undergoes a rapid change. Of particular interest is the coarse "diamond" (with the large milky white grains) which is clearly defined, especially on the right-hand side, from the top to the bottom.

At a depth of 3226.5 meters, the rock is silicified sandstone. The high degree of silicification is evident. This section is only one meter below the previous shot and displays the rapid changes in lithology that can be observed in a reservoir that is not homogeneous.

In conclusion, the core analysis revealed a banded bioturbated sandstone formation with significant variations in porosity, grain size, and silicification. While highly silicified zones exhibited minimal porosity, other sections displayed excellent visible porosity. Cross-bedding features were prominent throughout most of the core, except at deeper sections. Clay-filled

stylolites were observed at various depths. Fluorescence analysis indicated potential fluid flow paths. The presence of bioturbation in lighter-colored bands suggests possible vertical connectivity within the reservoir. The core exhibited a rapid change in properties over short distances, highlighting the reservoir's heterogeneity. The tilted nature of some claystone beds at deeper depths suggests a potential reservoir tilt. Overall, the core analysis provides valuable data for understanding the reservoir's characteristics and potential hydrocarbon flow.

Interval 3228 m to 3251 m

Core #2

The core was composed of bioturbated sandstone, which exhibited abundant thin silty claystone and claystone beds and lenses. Clay-filled stylolites, which were observed to contain illite and chlorite, were also present. No large fractures were observed at any point in the core, whether open or otherwise.

The rock itself (fresh breaks) exhibited a color range from brownish gray to light gray, with the degree of silicification and clay content in the matrix influencing the hue. The color was lighter in quartzite. The principal component was quartz, colorless, rarely pale yellow, light brown, transparent to translucent, in places opaque, off to milky white, occasionally smoky gray, predominantly well sorted, but with very variable grain sizes from fine to coarse.

Fig. 24:Core #1 taken during drilling of well GS-36

The dominant grain size changed very rapidly, in some cases within centimeters, grains chiefly subrounded, in places rounded, with depth also subangular. The rock is very hard with an excellent siliceous cement and common quartz overgrowths, which often fuse grains together. There are rare instances of microcavities that are filled with crystalline (hexagonal) quartz. The rock is predominantly clean, with a grey, brown, and intermittent argillaceous matrix. It has fair to moderate visible porosity, with instances of zero visible porosity (in areas of the rock that are

most heavily silicified). In general, the core exhibited minimal mineralization, with sporadic instances of pyrite (mostly microscopic), iron, chlorite, and other minerals. The silty claystone and claystone were predominantly greenish gray, occasionally light brown, and exhibited high argillaceous content. Local variations in composition led to gradations in hardness, ranging from firm to moderately hard, with a subfissile texture and platey structure.

The majority of the core exhibited bright gold direct fluorescence, which was observed across the entire sample. However, in certain areas, the fluorescence was limited to the center, while the margins were flushed by the coring process. The cut was characterized by slow to moderate bright bluish white streaming, which was occasionally absent. Additionally, a trace of brown residue (ring) was observed. It is noteworthy that the core was cut at an angle of 9 degrees.

3233.75 m Sandstone with green clay lens situated beneath a greenish gray silty claystone. It is notable that the degree of silicification is particularly high in close proximity to the clays. The lens is absent on the other side of the sample.

The angle of the silty claystone is greater than 9 degrees, which suggests that it is not a horizontal feature.

The other photos of this section show the piece in situ with the rest of the core in the box. It is notable that the abundant "biscuit" fractures are all perpendicular to the core.

The 3234.75-meter Banded Sandstone displays excellent visible porosity in the darker (brown) bands. These bands are less silicified and are associated with improved porosity. Horizontal and subhorizontal biscuit fractures can be observed once more.

At 3236.5 meters, the sandstone displays clear evidence of bioturbation. This is evident in the angled orientation of the bioturbation marks, which likely resulted from the core being cut at an angle. The worms and rudimentary roots that created these marks were vertical in orientation. It is important to note that the original sediments that were burrowed into were also not horizontal, as the burrows curled at an oblique angle. Once again, abundant biscuit fractures can be observed running perpendicular to the length of the core. In the past, the origin of these fractures was not clear. Russell made a point in the field that they could well be stress relief fractures formed as the core comes to the surface. This may well be the case, as if they are always observed perpendicular to the core, whether it is vertical or deviated.

Additionally, they are typically confined to the heavily silicified (lighter) sections of the core, which are the least compressive and therefore the least expansive or elastic/plastic, i.e., more susceptible to splitting.

The 3238-meter section of bioturbated brown sandstone is characterized by the presence of bioturbation.

3241.5 m: Angled thin green clay with bioturbation (above). It is notable that the silicification is particularly pronounced below the green clay. Furthermore, abundant horizontal microfractures can be observed once more running perpendicular to the length of the core, particularly in the lighter-colored areas.

At 3248 meters, The discrepancy between the color of the core on the exterior and when it is freshly fractured.

Interval 3251 m to 3280 m

Core #3

In general, the core consisted of sandstone with abundant thin silty claystone and claystone beds and lenses. The evidence of bioturbation decreased with depth. Abundant clay-filled (illite, chlorite?) stylolites (see previous reports) and other solution features were also observed. There was evidence of one large open fracture (3269.6-3270.0), and no other large fractures were seen, open or otherwise, at any point in the core.

During the processing of the core (cutting), which was conducted as soon as the core was on the surface, gas was observed desorbing from specific areas. This phenomenon predominantly coincided with highly silicified (tight) sections. Additionally, oil was observed bubbling out in a single small section (3277.75). Two small zones were observed that were highly silicified and exhibited the emergence of small beads of salt water from horizontal "biscuit" fractures (3252.5 to 3255.0 and 3262.5 to 3263.0). These beads rapidly precipitated orange salt. It is noteworthy that these observations were made in fractures that are now believed to have been formed as a result of stress relief as the core was brought to the surface. Consequently, it can be reasonably assumed that the "biscuit" fractures do not exist in any form within the reservoir.

Fig. 25:Core #2 taken during drilling of well GS-36

The rock in question (fresh breaks) was identified as sandstone, exhibiting a light gray to grayish white coloration, particularly in deeper sections, with some exhibiting a light brownish gray hue. Once again, the degree of silicification exerts a significant influence on the coloration. The greater the quartzitic content, the lighter the color. The principal component was quartz, colorless, transparent to translucent, with opacity varying from milky white to smoky gray. Individual isolated dark rounded grains were occasionally observed at depth. The grain size

exhibited considerable variability, ranging from fine to coarse and predominantly exhibiting well-sorted characteristics. The dominant grain size underwent a significant change, with some instances exhibiting a shift of up to one centimeter. The grains were primarily subrounded to subangular, with some rounded grains present. The depth of the grains varied, becoming rounded to subrounded in some instances. The rock was predominantly very hard with an excellent siliceous cement and common quartz overgrowths, which often fused grains together. There were rare instances of microcavities that were filled with crystalline (hexagonal) quartz. The rock was predominantly clean, with a grey, brown, and yellowish green intermittent argillaceous matrix. This matrix diminished with depth. Some sections exhibited moderate hardness (3274 m) with a relatively poor siliceous cement, which was a notable observation. Visible porosity was moderate to high, with occasional instances of excellent porosity, and in some areas, notably the most heavily silicified, it was nearly absent. These observations are detailed in the visible porosity note below. Once again, the porosity in this and the other cores was observed to undergo rapid changes in quality, with the porosity varying from very poor or even zero to very good over centimetre distances. In general, the core exhibited minimal mineralization, with isolated instances of disseminated pyrite (mostly microscopic), iron, and illite. (In association with the solution features and other minerals). A single vertical microfracture at a depth of 3262 meters was filled with pyrite.

The silty claystone and claystones were predominantly greenish grey, occasionally yellowish green, and exhibited high argillaceous content. In some areas, they graded locally to clay, were firm to moderately hard, fissile in the horizontal plane, and platey. Many of the solution features, including stylolites, were also filled with clay. This clay was predominantly light greenish grey, silvery grey, or occasionally yellowish green. It had a pearly lustre and was fissile in the horizontal plane. It could be split into extremely thin disks across the core.

It should be noted that a feature of very hard siliceous sandstones is that when they are broken, they tend to split cleanly, with the grains remaining intact. The assessment of visible porosity in instances where the grains have split rather than separated from one another frequently results in an underestimation of the porosity. The opportunity to observe between the grains is significantly diminished, and the extent of open gaps between the grains is challenging to ascertain, particularly when the grains themselves are transparent. This is exemplified by the ability to shine a light through a piece of quartzite up to 1.5 cm thick. An effective method for assessing porosity in what initially appear to be tight formations is to examine the depth of

invasion of the drilling fluids, the presence of flushed zones that should fluoresce but do not, and the presence of tiny particles of baryte between the quartz grains.

All of the cores exhibited bright yellowish gold fluorescence, with occasional yellow direct fluorescence and rare pale yellow fluorescence. This fluorescence was commonly observed across the entire sample, although in some instances, only the center fluoresced, suggesting that the margins may have been flushed by the coring process. In some cases, the flushing penetrated deeply into the interior of the core. The majority of the cut exhibited moderate to good fluorescence, with occasional instances of fast, bright bluish white streaming fluorescence. In select instances, the cut fluorescence was diminished to diffusion only (in samples with a high degree of silicification). All of the samples exhibited some degree of cut fluorescence. No evidence of cut coloration was observed.

The core was sectioned at an angle of 9 degrees.

At 3,251.2 meters and 3,251.8 meters. The sandstone exhibited a high degree of variability in porosity. The areas of good visible porosity can be discerned on the photographs as the darker, flat or matt areas, as the surface of the core reflects light in a manner that differs from the surrounding material.

At a depth of 3252 meters, the rock is characterized by a light grayish brown color. The rock is very coarse and exhibits good visible porosity.

At 3254.75 meters, a series of photographs was taken before and after a rub down. The sandstone is highly silicified and exhibits numerous "biscuit" fractures, which are predominantly horizontal but exhibit a slight sub-angled inclination. The precipitation of orange salt on the surface of the core was the result of the dissolution of saltwater that had seeped through the fractures. The zone in question extended from approximately 3252.5 to 3255.0 meters.

At a depth of 3255 meters, a yellowish green clast of silty claystone is observed within a light gray sandstone matrix. I am uncertain as to what interpretation should be made of this observation. The clay exhibited homogeneity and did not affect the adjacent sandstone, with distinct boundaries.

3255.05m Light grayish white silicified sandstone. The quartzite is extremely hard, colorless, transparent, fine-grained, well sorted, subrounded, well sorted, grains tightly interlocked, highly silicified with quartz overgrowths, and exhibits poor to no visible porosity. It exhibits bright yellow direct fluorescence and bright bluish white diffused cut.

3257m An illustration of the phenomenon whereby the core assumes the color of the surrounding mud. The observed coloration is brown, but the actual color is light grayish white. It is noteworthy that cores with darker colors tend to exhibit higher porosity, as drilling fluids can penetrate more deeply into the core, resulting in darker brown hues. At a depth of 3261.5 meters, the invasion is observed in a fresh break. It is noteworthy that the darker brown stains have penetrated a few millimeters into the light gray sandstone.

At 3262 m, a fine, near-vertical microfracture is observed cutting through a banded sandstone. The fracture was filled with pyrite, which is visible in the second shot as a small, dark spot at the center of the core.

At 3262.5 meters, the second zone where salt was observed precipitating on the surface of the core. This zone extended from 3262.5 to 3263.0 meters. It is noteworthy that the sandstone is highly silicified, and that the salt has emerged from horizontal "biscuit" fractures.

At 3263 meters, a thin disk of clay was observed, exhibiting a light greenish gray to silvery gray coloration with a pearly lustre. The clay was identified as containing illite and chlorite.

At 3264.9 meters, a bed of greenish gray silty claystone is observed to be several centimeters thick. It is noteworthy that the bed is inclined at a slight angle. It is likely that the core was oriented, which would result in the bed being horizontal in the reservoir. Additionally, there is a dearth of a substantial, well-developed silicified zone in close proximity to the clay. This observation differs from those made on the previous two cores.

The stratum of sandstone is located just above the silty claystone at a depth of 3264.9 meters. The sandstone is characterized by a grayish white coloration, with fine to medium grain size. It exhibits bright yellowish gold direct fluorescence, with the exception of a flushed zone measuring 0.5 cm around the edge. The cut is bright bluish white and fast-flowing.

At 3266.75 meters, an extremely thin clay layer is observed cutting across the sandstone. This may be indicative of a solution feature. Upon splitting the sample, a layer of pearly, silvery greenish gray clay was revealed.

At a depth of 3269.5 meters, the rock is composed of very coarse-grained sandstone. The sandstone appears to be light brownish gray, although microscopic examination revealed that samples from this depth consisted of colorless, transparent, and occasionally milky white, translucent, coarse to very coarse, well-sorted quartz grains. A notable quantity of baryte was observed within the sample. Although the sample was exceedingly hard and exhibited an excellent siliceous cement, it was only partially silicified. Some sections exhibited high degrees of silicification, with minimal to no visible porosity. In contrast, other sections exhibited

minimal silicification, yet displayed high degrees of visible porosity, as the silicification effectively bonded the grains together. The sample exhibited a high degree of visible porosity. The sample exhibited bright yellowish gold to yellow direct fluorescence and a fast bright bluish white streaming cut.

3269.6m: Probable near vertical open fracture. The photograph is not of optimal quality, but a section of the core was sheared off. This continued down to 3270m. Unfortunately, the lower piece has moved (the scribe lines are not aligned) and it appears that the sheared section suddenly stops. On the larger image, it can just be made out that it doesn't stop. The continuation of it is in shadow on the right. It is possible that this is a fracture, but it is also possible that it is not.

3273.5m There are three shots before and after a rub. It should be noted that shot B is taken from the opposite end of the box when compared to the other two shots to allow the light to catch the good visible porosity in the coarser grained darker areas. Hence, it has been oriented upside down.

3274.2m There are close-up shots of porosity on the core surface. The rock is coarse-grained sandstone with only moderate siliceous cement. The quartz is colorless, rounded, and moderately well sorted, with moderate to good visible porosity. Baryte is present in pore spaces throughout the sample. Speckled bright gold direct fluorescence, slow diffuse bluish white cut. The rock is medium to coarse-grained, well sorted, subrounded sandstone with a surface texture that suggests porosity. Under the microscope, moderate to fair visible porosity is observed. The sample exhibited bright yellowish gold direct fluorescence and bluish white streaming cut.

3277.5m Oil was observed to be associated with pore spaces. While it is generally not advisable to observe oil bubbling out of a core when it is on the surface, this phenomenon is indicative of the presence of oil at depth rather than salty water. This section was the only piece to display this phenomenon. After a brief rub, the light revealed a texture on the surface, which further demonstrated the presence of porosity. It should be noted that the oil only bubbled slightly, and that the majority of the oil may have been present on the surface for an extended period, desorbing at depth.

3279.0 m: The sandstone is highly silicified, exhibiting darker bands that are not as silicified, which display signs of porosity. This once again demonstrates the complete lack of homogeneity within the reservoir. Small-scale contrasting features seem to prevail.

3280 m: The TD for GS-36 was unfortunately determined to be a box of rubble.

Fig. 26: Core #3 taken during drilling of well GS-36

In summary of the Core Analysis (3251.2m - 3280m):

This section of the core consisted primarily of sandstone with varying degrees of porosity, grain size, and silicification. Here are the key observations:

Porosity: Visible porosity ranged from poor to excellent, with darker colored sections generally exhibiting higher porosity. The core displayed rapid changes in porosity over short distances.

Grain Size: Grain size varied from fine to very coarse, with some sections showing significant variation within a short distance.

Silicification: The degree of silicification significantly impacted the rock's properties. Highly silicified zones displayed minimal porosity, while less silicified sections exhibited good porosity.

Claystone: Greenish gray silty claystone beds were present throughout the core. These beds were sometimes tilted, suggesting a potential reservoir tilt.

Fluids: Gas desorption was observed from highly silicified zones during core processing. Oil was observed bubbling from a single zone, indicating the presence of oil at depth.

Fractures: One large open fracture was identified, and some "biscuit" fractures were observed, which were likely created during core retrieval and not representative of the reservoir.

Solution Features: Clay-filled stylolites were common throughout the core, indicating past fluid movement.

Diagenetic Minerals: Pyrite and illite were observed within the core, indicating diagenetic processes.

Core Handling Effects: The core color could be affected by drilling mud invasion, with darker colors indicating deeper invasion and potentially higher porosity. Additionally, some "biscuit" fractures were likely artifacts of core handling.

Overall, the core analysis revealed a highly heterogeneous reservoir with significant variations in properties over short distances. The presence of oil and gas indicates the potential for hydrocarbons within the reservoir.

Core log for different depth of GS-36 well.

Well GS-38

Descriptions, observations and comments

Interval 3184.7 m to 3212.3 m, Ri

Core #1

Cambrian Ri: Depth 3184.7 to 3201 meters. The stratigraphic unit in question is composed of sandstone. The rock is predominantly greyish brown to brown, with occasional light yellowish brown bands and stripes, occasional small open fractures, stylolitic (stylolites filled with green clay and pearly grey illite and disseminated pyrite), and no greenish grey siltstone beds. In some areas, slight bioturbation is observed, accompanied by local silicification and evenly distributed horizontal stress relief "biscuit" fractures. Quartzite grains are colorless, transparent, and occasionally milky white, pale brown, or translucent. The rock is very hard and predominantly

composed of very fine to fine grains, with occasional medium grains. The grains are tightly interlocked and subrounded to subangular, spherical to subspherical. The rock is predominantly well sorted, with moderate to poorly sorted grains. It has excellent siliceous cement, common quartz overgrowths, poor to fair visible porosity, pale yellow to bright gold direct fluorescence, and an OBM flushed margin of 3-5mm. It occasionally has very deep flushing and very slow to no bluish white cut.

The depth of the stratum is 3184.8 meters, and it is located in the Cambrian River. The stylolite is filled with a greenish gray clay.

At a depth of 3187.75 meters, the sandstone is composed of fine-grained brownish gray and yellowish brown particles. It should be noted that bioturbation is present. At the lowest point, a small, crescent-shaped fracture can be observed just above the greenish gray stylolite.

At a depth of 3,189 meters, the Cambrian Ri was observed. The rock is composed of fine-grained, silicified, light yellowish brown sandstone, exhibiting abundant horizontal biscuit fractures.

At a depth of 3193 meters, the Cambrian Ri is characterized by an open fracture that runs across a stylolite. It should be noted that the fracture does not traverse the stylolite. The fracture can be observed above the stylolite, running in a northeast-southwest direction before dropping to a vertical position.

At a depth of 3198.7 meters, the Cambrian Ri is composed of yellowish brown, medium-grained sandstone. While the images do not fully capture the characteristics of this section of core, it does exhibit a reasonable degree of visible porosity. This observation was made without the use of a lens or microscope.

At a depth of 3201 meters, the Cambrian Ri/Ra exhibits a less than optimal image quality. However, it is hypothesized that this is the interface between the Ri and Ra. The images show a wide range of grain sizes between 3201.5 and 3201.75 meters.

Cambrian Ra: Depth 3201.3 to 3211.9 meters. Sandstone: greyish brown, light grey, light yellowish brown, banded, striped, bioturbated, stylolitic (stylolites filled with green clay, pearly grey illite and disseminated pyrite), occasional greenish grey siltstone/claystone bands, occasional partially The rock contains mineralized fracture complexes and microfractures, which are locally crossbedded and heavily silicified in places. The matrix is partially pyritized in some areas, and the grains are predominantly colorless, transparent, or occasionally milky white, translucent, very fine to fine, or occasionally medium to coarse, subangular to subrounded, spherical, with well to moderate sorting. In some areas, the rock displays rapid

transitions from fine to medium to coarse grain sizes. The grain size ranges from fine to medium to coarse. The fine-grained fractions are tightly interlocked with excellent siliceous cement and quartz overgrowths. The coarser fractions are often cemented on the grain contact interface only. The visible porosity is highly variable, especially where the grain size changes rapidly. Tightness is observed where the grain size is siliceous and the porosity is evenly distributed, horizontal, and stress relief "biscuit" fractures are abundant. Moderate to good visible porosity with distinct oily fluorescence is observed in silica-free zones. The core exhibited an odor and oil on its surface. The coarser fractions exhibited good to occasionally excellent visible porosity (where not silicified). Pore spaces were rarely pyritized, and their fluorescence was dull yellow to bright gold. The direct fluorescence of the 3-5mm OBM flushed zone was bright, and it occasionally exhibited complete flushing. The bluish white streaming cut improved with depth, and it occasionally exhibited no cut (Ra baffle).

The claystone and siltstone are greenish gray in color, with local silvery gray variations. They are firm to moderately hard, with a high argillaceous content and a silty texture. Rare disseminated pyrite is observed in the silvery gray areas.

At a depth of 3202.5 meters, the Cambrian Ra formation is observed to exhibit a partially open fracture in a fine-grained sandstone with a relatively high degree of pyritization. The break in the core is not readily apparent as a fracture, and may instead be a break in a section where the matrix is actually pyritized.

At a depth of 3202.75 meters, the Cambrian Ra formation is observed to be slightly deeper than the previous photos. A complex of pyritised fractures is observed in a highly silicified poorly sorted sandstone. At a depth of 3204.75m, Cambrian Ra (baffle?), a silicified bioturbated sandstone is noted. The angle of the bedding is also observed. At a depth of 3206m, Cambrian Ra (baffle?), a more silicified sandstone with abundant horizontal "biscuit" fractures is observed. At a depth of 3208.1 meters, the rock is identified as Cambrian Ra. It is a fine to medium-grained, light gray (along the break) silicified sandstone with a partially pyritized matrix (NW corner).

At a depth of 3208.5 meters, the rock is identified as Cambrian Ra. It is a banded light brownish yellow, light brown, fine to medium-grained sandstone. It is notable that the darker areas exhibit visible porosity. These areas had oil on them when the core was first viewed. The oil had already desorbed, with only a few areas exhibiting slight signs of pinpoint bubbling on the surface. The core can be divided into two sections, above and below this depth. The core below this depth appeared to be much more oil-rich. At depth 3208.7m, Cambrian Ra, the core comprises

greenish grey siltstone and claystone. At depth 3209m, Cambrian Ra. The rock contains more porous material interbedded with sections that have undergone partial silicification. At a depth of 3209.1 meters, the rock is Cambrian Ra. The same characteristics are observed. At a depth of 3210.5 meters, the rock is Cambrian Ra. It contains partially mineralized material (pyrite) near a vertical microfracture cutting silicified, cross-bedded, and variable-sized grain sandstone. At a depth of 3210.9 meters, the rock is Cambrian Ra. A close-up of the porosity in poorly sorted, partially silicified sandstone.

At depth 3211.7m, Cambrian Ra. The last meter of core #1. Banded, poorly sorted sandstone with some very good visible porosity.

In summary of Cambrian Ri and Ra Formations (3184.7m - 3211.9m)

Cambrian Ri (3184.7m - 3201.3m)

- This formation consists mainly of brownish gray to yellowish brown sandstone with occasional bioturbation and stylolites.
- Grain size is very fine to fine with some medium grains, generally well-sorted.
- Visible porosity is poor to fair.
- The presence of oil was not observed.

Cambrian Ra (3201.3m - 3211.9m)

- This formation is more varied than Ri, containing sandstone, siltstone, and claystone.
- Sandstone ranges from greyish brown to light colored, with banding, bioturbation, stylolites, and occasional fractures.
- Grain size varies from very fine to coarse, with some areas exhibiting rapid changes.
- Visible porosity is highly variable, with tighter zones in silicified areas and good to excellent porosity in coarser, less silicified zones.
- Oil fluorescence was observed in some sections, and oil was present on the core surface in some areas.
- Pyrite mineralization is more frequent in Ra compared to Ri.

Overall Observations:

- The Cambrian Ri/Ra boundary is transitional, with a significant increase in grain size and variability within Ra.
- Visible porosity is generally better in Ra compared to Ri.
- The presence of oil staining and fluorescence suggests potential hydrocarbon flow within the Ra formation.
- Both formations contain stylolites, indicating past fluid movement.

- **Interval 3212.3 m to 3240.3 m, Cambrian Ra**
- Core #2
- Cambrian Ra
- At a depth of 3212.3m to 3240.3m
- The sandstone is characterized by a variety of colors and textures. It is greyish brown, light grey, light yellowish brown, banded, striped, bioturbated, and occasionally stylolitic. Stylolites are filled with green clay, pearly grey illite, and disseminated pyrite. Greenish grey siltstone/clay is also common. The rock contains stone bands, occasional partially mineralized fracture complexes and microfractures, with pyritization levels decreasing with depth (appearing to have reached 3232m). The rock is locally crossbedded and heavily silicified in places, with quartzite grains that are predominantly colorless, transparent, or occasionally milky white, translucent, very fine to fine, or medium to coarse. The grains are subangular to subrounded, spherical, and well to moderately sorted. Localized areas exhibit poor sorting, with rapid transitions from fine to medium to coarse grains. The grains are tightly interlocked with excellent siliceous cement and quartz overgrowths. Pyrite cement is rare and sporadic, and it diminishes with depth. The visible porosity is highly variable, particularly in areas where grain size changes rapidly. It is tight where siliceous and exhibits occasional horizontal stress relief, commonly referred to as "biscuits." The rock displays "uit" fractures, where silica-free moderate to good visible porosity is observed. A rare oily odor is present, and oil is occasionally observed on the surface of the core. Coarser fractions display good to occasionally excellent visible porosity, where not silicified. The direct fluorescence is dull yellow to bright gold, with a bright fluorescence observed in the tightest zones. The 3-5mm OBM flushed zone is occasionally completely flushed, and the streaming cut displays moderate to poor bluish white fluorescence. At depths exceeding 3220 meters, the brightness of the gold fluorescence tends to increase, while the fluorescence of the cut tends to deteriorate with depth.

Claystone/Siltstone: greenish grey, locally silvery grey, firm to moderately hard, very argillaceous, silty, where silvery grey is rare and disseminated pyrite is present.

Color Note: The core tends to take on a lot of color from the mud. As a general rule of thumb, the better the porosity, the darker the brown the core appears, as the mud is able to penetrate further into the pore spaces. The lighter the color of the core, the tighter it tends to be, as the mud is unable to penetrate and stain the rock. In general, freshly broken sections of core tend to be light brownish gray or light gray to almost white. The light brownish gray sections tend

to correspond to the brown areas on the outside of the core, while the light gray to white sections correspond to the light yellowish brown (silicified) sections.

Fig. 27: Core #1 taken during drilling of well GS-38

At a depth of 3213 meters, the rock formation is identified as Cambrian Ra. It is a fine to medium-grained, poorly sorted sandstone, exhibiting brown and light yellowish brown colors (see color notes). Moderate silicification is observed. A black fine vertical fracture is noted, which is attributed to the presence of pyrite.

At a depth of 3214 meters, the rock formation is identified as Cambrian Ra. It exhibits partial pyritization near a vertical microfracture in a tight silicified sandstone. The fracture can be seen cutting across the core. In the cross-section view, drilling fluids are observed to be weeping from the fracture, despite the partial pyritization. The fracture terminates at the top of the side-view section photo. It is notable that the color of the fresh break on the cross-section (light grey to white) differs from that of the side of the core (light yellowish brown).

At depths of 3214.5 and 3214.75 m, Cambrian Ra. The rock is cross-bedded and partially silicified sandstone. The brown sections exhibit greater visible porosity than the light yellowish brown (silicified) sections.

At a depth of 3215-16m, Cambrian Ra, the rock is cross-bedded sandstone. While not evident in the photograph, there are rapid changes in grain size. Once again, there is a relationship between the apparent color of the core and the porosity.

At a depth of 3216.5 meters, the Cambrian Ra formation is characterized by a relatively heavy silicification of cross-bedded sandstone. At a depth of 3217.75 meters, the Cambrian Ra formation is observed to exhibit a close-up view of sandstone with notable variability. The light highlights the visible porosity in the brown area, while the light yellowish brown section lacks a discernible texture and is tightly silicified. It is noteworthy that the silicification does not appear to be influenced by grain size in this instance. Milky white coarse grains can be observed in both the brown and yellowish sections.

At a depth of 3220-21m, Cambrian Ra, the silicified sandstone is interbedded with abundant greenish grey claystone/siltstone beds. Four thin beds of claystone within this metre have attracted a great deal of silicification.

At depth 3223.25m, Cambrian Ra, another photograph is provided to illustrate the contrast between the silicified sections and non-silicified sections. The brown areas display poor to very good visible porosity, whereas the yellowish brown areas are tight. The crossbedded sandstone exhibits a considerable degree of grain size variability. Despite the considerable grain size variability, the degree of sorting on a small scale remains good. The porosity in the darker areas is noteworthy.

At depth 3226.5m, Cambrian Ra, the fractures are primarily pyritised but still partially open in fine-grained sandstone. The fracture can be observed in both the vertical and horizontal orientations.

At a depth of 3229.5 meters, the Cambrian Ra formation exhibited good to excellent visible porosity in the sandstone. At a depth of 3230.5 meters, the Cambrian Ra formation displayed

an open fracture in the sandstone. This fracture did not appear to be associated with any mineralization. Directly below the fracture, there was evidence of friable sand, which is thought to be largely missing. The fracture is open and partially pyritized. While this is not immediately apparent in the photographs, a significant portion of the core is actually missing. There is slight mineralization on the fracture plane in the top left corner. Additionally, on 3231.75A, a near-vertical pyritized (black) microfracture can be observed.

At depth 3231-32m, Cambrian Ra, as above, showing the missing section profile.

At a depth of 3233.8 meters, the Cambrian Ra formation is observed to consist of a greenish gray siltstone and claystone bed, accompanied by an associated silicified aureole. Of note is the presence of a small green clay clast within the aureole, situated above the main clay bed.

At a depth of 3237.25 meters, the Cambrian Ra formation is observed to consist of cross-bedded sandstone. This is a notable example of cross-bedding, taken from both the top and bottom (photo A is oriented "up" the core). It is notable that the brown areas immediately adjacent to the silicified (yellowish) section exhibit high porosity.

At depth 3238.5m, Cambrian Ra. Greenish grey Claystone/Siltstone bounded by silicified aureole, which itself is bounded by an area of low silicification. This was taken looking up the core. Consequently, the greatest level of silicification associated with the clay is on the top. Of note are the brown stripes cutting into the silicified section. These are likely worm burrows.

At depth 3239-40m, Cambrian Ra. Rubble recovered from near the base of the core. The yellow clay was initially observed in the lowermost 2 meters of Core #2. The lighter circles represent cross sections of burrows.

In summary of Cambrian Ra (3212.3m - 3240.3m)

Rock Characteristics:

- Sandstone is the dominant rock type, with colors ranging from greyish brown (more porous) to light yellowish brown (silicified and tighter).
- Banding, striping, bioturbation, and stylolites are common.
- Grain size varies from very fine to coarse, with some rapid transitions.
- Sorting is generally good, but some poorly sorted zones exist.
- Pyrite mineralization is present, decreasing with depth.

Porosity:

- Highly variable, with better visibility in coarser and less silicified zones.
- Brown colored areas (on core exterior) tend to be more porous than light yellowish brown areas.

Other Observations:

- Greenish grey siltstone/claystone is interbedded with sandstone.
- Fractures are present, sometimes pyritized and occasionally open.
- A possible missing section is noted around 3230.5 meters.
- Clay clasts and potential worm burrows are observed within the siltstone/claystone.
- The core may be stained by drilling mud, affecting its color.

Overall:

The Cambrian Ra in this section shows significant variability in grain size, porosity, and silicification. Brown colored areas are indicative of higher porosity, while yellowish brown areas are more silicified and tighter. The presence of fractures, pyrite mineralization, and potential burrows suggests a complex geological history.

Interval 3240.3 m to 3259.0 m, Cambrian Ra

Core #3

Cambrian Ra

3240.8 m – 3259.0 m The stratigraphic section is composed of sandstone. The rock is characterized by a variety of colors and textures. It ranges from greyish brown to light grey, light yellowish brown, off white, banded, striped, bioturbated, and occasionally stylolitic. Stylolites are filled with green clay, pearly grey illite, and rarely disseminated pyrite. Greenish grey siltstone/claystone beds and layers are common, and some are extremely thin. Occasionally, partially open microfractures with only light to moderate mineralization (pyrite) are present. Pyritization levels increase after 3258m. Locally, crossbedding is observed. The rock is heavily silicified in certain areas, with quartzite grains that are predominantly colorless, transparent, or occasionally smoky gray, milky white, or translucent. The grains are very fine to fine, with some medium to coarse grains present. The grains are subangular to subrounded and spherical.

The sorting is well to moderately good, with locally poor sorting. There are rapid transitions from fine to medium to coarse grains, especially where crossbedded. The grains are tightly interlocked with excellent siliceous cement and quartz overgrowths. Rare, isolated disseminated pyrite cement was observed at a depth of 3247m. It was white, firm to crumbly, non-reactive, and unidentifiable (properties similar to talc).

Occasional isolated yellowish green clay clasts were observed, and the visible porosity varied considerably, especially where the grain size changed rapidly. Tightness was observed where the cement was siliceous, with occasional horizontal stress relief "biscuit" fractures. Where

silica was absent, moderate to good visible porosity was observed, and the core occasionally emitted an oily odor. Occasional oil was observed on the surface of the core, below 3240m. Salt was observed along many "biscuit" fracture planes. Coarser fractions exhibited good to occasionally excellent visible porosity where not silicified. Uniform dull yellow to bright gold direct fluorescence was observed (bright where tight). With depth, fluorescence became patchy, 3-5mm OBM flushed zone, occasionally completely flushed, moderate to very poor bluish white streaming cut, occasionally diminishing to diffused cut only.

Fig. 28: Core #2 taken during drilling of well GS-38

The claystone/siltstone is greenish grey in colour, with localised silvery grey patches. It is firm to moderately hard, with a high argillaceous content and a silty texture. The silvery grey patches are rare and occur in disseminated pyrite.

Color Note: The core tends to exhibit a high degree of coloration derived from the mud. In general, the greater the porosity, the darker the brown color of the core, as the mud is able to penetrate more deeply into the pore spaces. The lighter the color of the core, the tighter it tends to be, as the mud is unable to penetrate and stain the rock.

In general, freshly broken sections of core tend to be light brownish grey or light grey, with some exhibiting a near-white coloration. The light brownish gray sections are indicative of the brown areas on the exterior of the core, while the light gray to white sections correspond to the light yellowish brown (silicified) sections.

At depths of 3242.5m and 3242.4m, Cambrian Ra. Partially silicified, bioturbated banded sandstone. Note the very thin green clay (photo GS38-3242.5) associated with the silicification. A partially open, nearly vertical fracture can be seen running down the core. The end photo (GS38-3242.4) illustrates bioturbation. The dark circles are a cross-sectional profile of the caves. (Russ, is this the correct interpretation?)

At depth 3243.6m, Cambrian Ra. Silicified sandstone with "biscuit" fractures. Orange salt has been precipitated from fluids seeping out of the fractures.

At depth 3244.4m, Cambrian Ra. Stylolite in silicified sandstone. The left part is completely covered by greenish-gray clay. It is likely that the stylolite develops first, then the clay acts as a barrier to fluid movement. As compaction occurs, silica-saturated fluids concentrate near the barriers and the sandstone becomes silicified.

At depth 3245.7m, Cambrian Ra. Greenish-gray siltstone/claystone. Note the relatively high dip angle. The core was cut vertically. A small open fracture can be seen at the bottom of the photo.

At depth 3246.5-47m, Cambrian Ra. One meter further down the core and everything is horizontal. Note the clay bed at the bottom of the photo. The core itself is only partially silicified.

At depth 3246.7m, Cambrian Ra. A closer look at the previous meter from the opposite end (looking uphole). Note the bioturbation. There are also some open cavities.

At depth 3248-49m, Cambrian Ra. A section of relatively silica-free brown (from mud stains) sandstone.

At depth 3249.25m, Cambrian Ra. Cross-bedded partially silicified sandstone. Grain size varies rapidly. The banding is a result of differential silicification. The darker bands have moderate to

good visible porosity (the texture can be seen on the photo). The lighter yellowish areas are dense.

At depth 3249.4m, Cambrian Ra. Coarse-grained sandstone with very good porosity. This small section was very poorly cemented compared to the rest of the core. Loose quartz grains may stick to the side of the core.

At depth 3252.9m, Cambrian Ra. Silicified sandstone with associated mudstone. Note the sudden change from silicified sandstone to relatively silica free.

At depth 3253.5m, Cambrian Ra. Partially open near vertical fracture. There were no outward signs of mineralization in the fracture plane. The fractured formation is partially silicified cross bedded sandstone.

At depth 3254.5m, Cambrian Ra. Cross bedded sandstone. Note the rapid change in grain size with the coarser fractions showing good visible porosity. 3254.5A Running through the beds is a bioturbation feature, quiet unlike those seen higher up in the section, which appears to terminate in a coarse section. 3254.5B This is the other side of the core. A vertical micro-fracture can be seen at the top that does not extend to the other side of the core.

At depth 3254.5m, Cambrian Ra. Cross-bedded sandstone. Note the rapid change in grain size, with the coarser fractions showing good visible porosity. 3254.5A Running through the beds is a bioturbation feature, quiet unlike those seen higher up in the section, which appears to terminate in a coarse section. 3254.5B This is the other side of the core. A vertical micro-fracture can be seen at the top that does not extend to the other side of the core.

At depths 3255.25m and 3255.15m, Cambrian Ra. Heavily silicified sandstone. Despite being almost completely silicified and altered to quartzite, small areas still show visible porosity. 3255.15 shows the end of the piece. In the center, 1/3 of the way down from the top, a small yellowish-green clay clast is just visible. Note the color difference between the outside of the core and the fresh fracture.

At depth 3256.5-57m, Cambrian Ra. Variable sandstone. Some sections are silicified, others not. There is a considerable amount with good visible porosity. This is again seen in the coarser fractions. A thin horizontal fracture (probably stress relief) can be seen with orange salt precipitate along it.

At depth 3257-58m, Cambrian Ra. General view of good quality, silica-free, brown-stained sandstone.

At depth 3258.25m, Cambrian Ra. A small horizontal feature was noticed in a section of brown-stained sandstone. After splitting the core, the feature was found to be a very thin layer of

greenish-gray clay. Note the extremely small vertical "fracturette" that cuts through the clay layer.

At depth 3258.5m, Cambrian Ra. Fractured, cross-bedded sandstone with varying degrees of silicification. It can be seen that the fractures are predominantly pyritized. However, there are sections where they are partially open. The main vertical fracture is seen on both sides of the core. It tapers off towards the top of the meter length. Grain size is variable and again the coarser fractions, even in highly silicified zones, show very good porosity.

At depth 3258.9m, the Cambrian Ra. Banded sandstone with greenish-gray claystone clasts.

In summary of Cambrian Ra (3240.8m - 3259.0m)

Rock Characteristics:

- Similar to the previous section, the rock is mainly sandstone with variable colors (greyish brown, light grey, yellowish brown) reflecting the degree of silicification.
- Banding, striping, bioturbation, and stylolites are observed.
- Grain size varies significantly, with occasional rapid transitions.
- Sorting is generally good to moderate, with some poorly sorted zones.
- Pyrite mineralization increases with depth.

Porosity:

- Visible porosity is highly variable, with better porosity in coarser and less silicified zones.
- Brown colored areas (on core exterior) tend to be more porous than light yellowish brown areas.

Other Observations:

- Greenish grey siltstone/claystone beds are present.
- Microfractures with light to moderate mineralization (pyrite) are occasionally observed.
- "Biscuit" fractures and salt precipitation are noted along some fractures.
- Clay clasts and bioturbation features are present.
- The core may be stained by drilling mud, affecting its color.

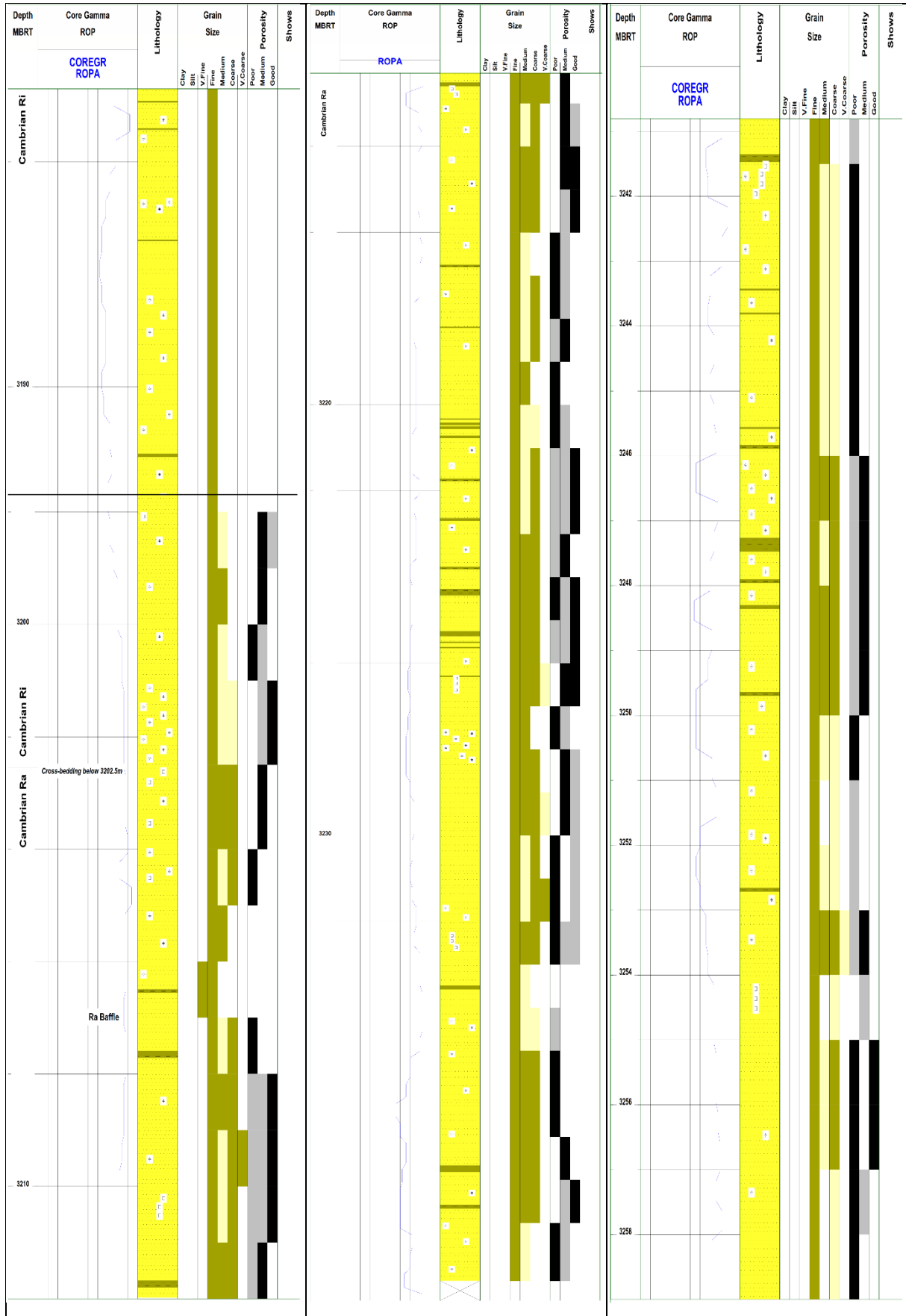Fig. 29: Core #3 taken during drilling of well GS-38

Fig. 30: Core log for different depth of GS-38 well.

Section 3: Permeability and porosity evolution in term of depth

1. Distribution of the petrophysical parameters according to the depth

1.1 well GS 36:

By observing the difference in the physical parameters relative to the depth :

permeability :

We record between the interval 3204 m to 3208 m an average permeability value of K>200 mdand between the interval 3208 m to 3212 m the permeability was good k>400 md B but between 3218 m and 3280 m it was fluctuating and low.

Porosity :

At a depth of 3236 m the lowest porosity value is Φ<5%. Between the interval 3272 m and 3274 mthe porosity is good Φ>15%, where it fluctuates at other depths.
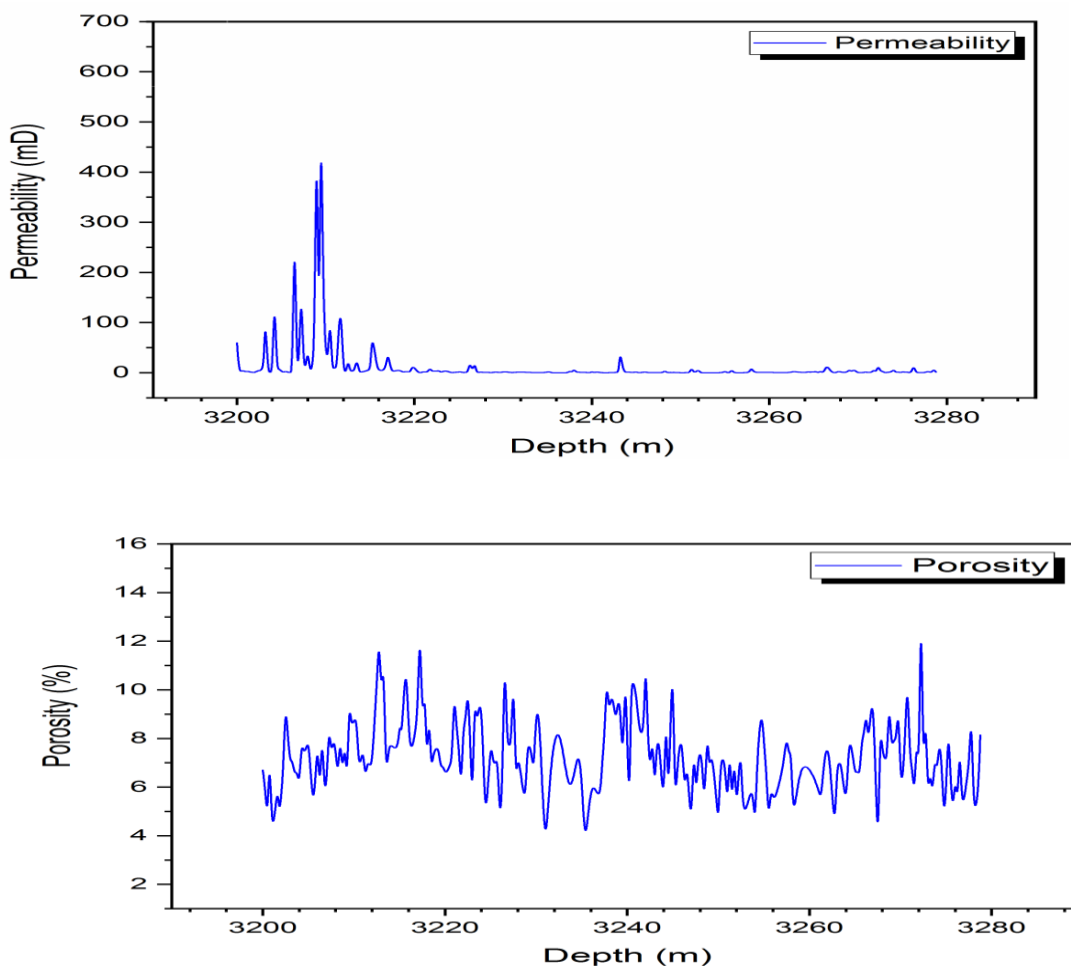

Fig 31: Permeability and porosity evolution curves in term of depth in GS36.

1.2 Well GS 38 :

Permeability :

Through the curve, we note that the permeability at depth 3214 m was good where k<100, and at depth 3222 m it ranges between 40 md<k< 50md.

Porosity :

at depth 3239 m we have porosityΦ = 11% and the lowest score is recorded at depth 3221 m and fluctuates at other depths**.**
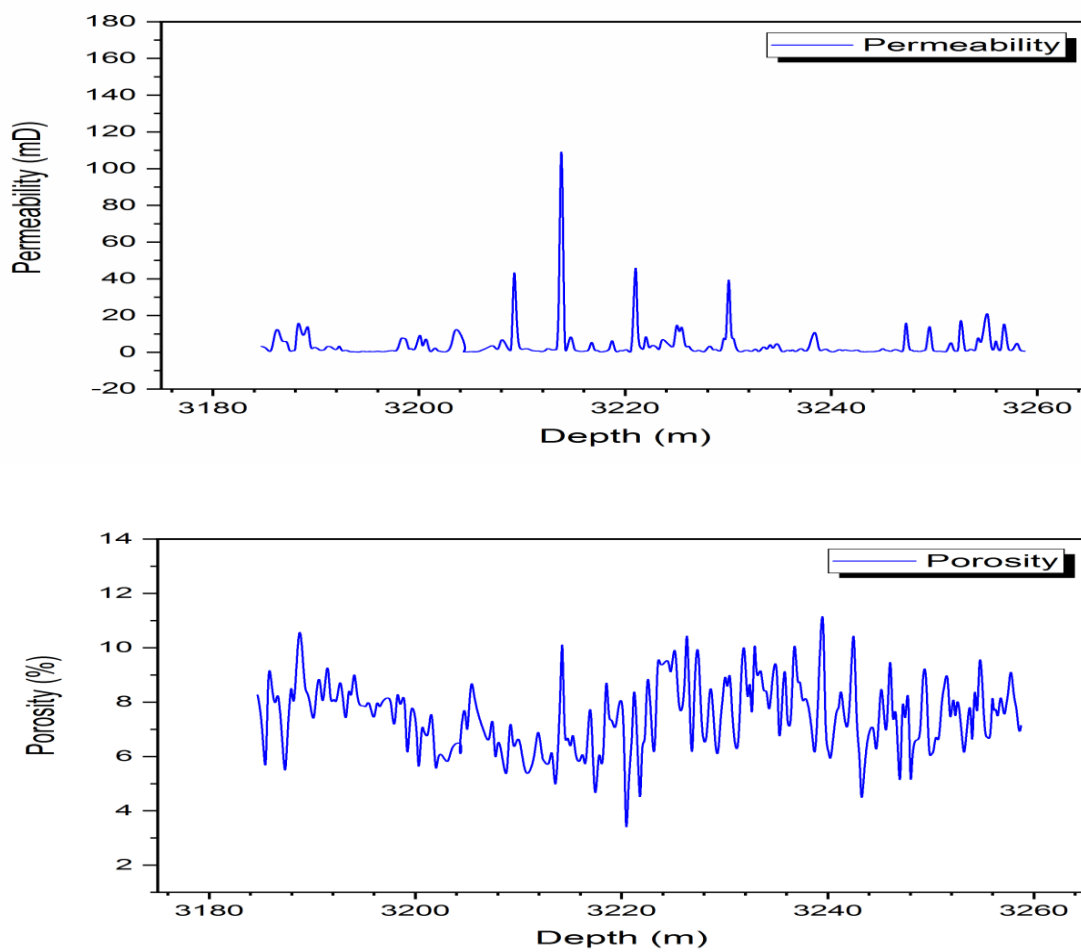

Fig 32: Permeability and porosity evolution curves in term of depth in GS38

1.3 Well GS 41 :

Permeability :

Through the given curve we have the permeability ratio between the interval 3223 m and 3224m where k>200 md, but at the depth 3212 m is very low and fluctuates in the rest.

Porosity :

between the interval 3228 m and 3232 m recorded good porosity where it was low before at the depth 3206m2 %>Φ>1 %.
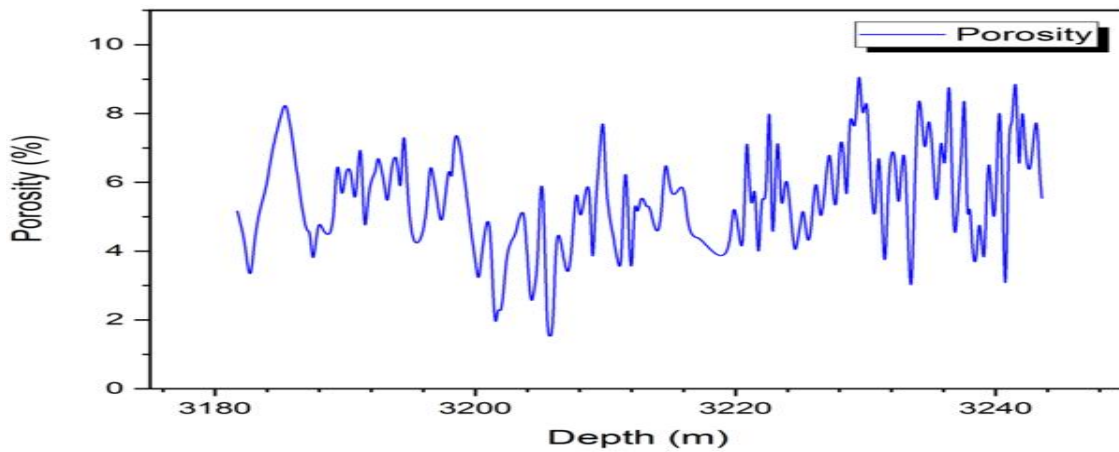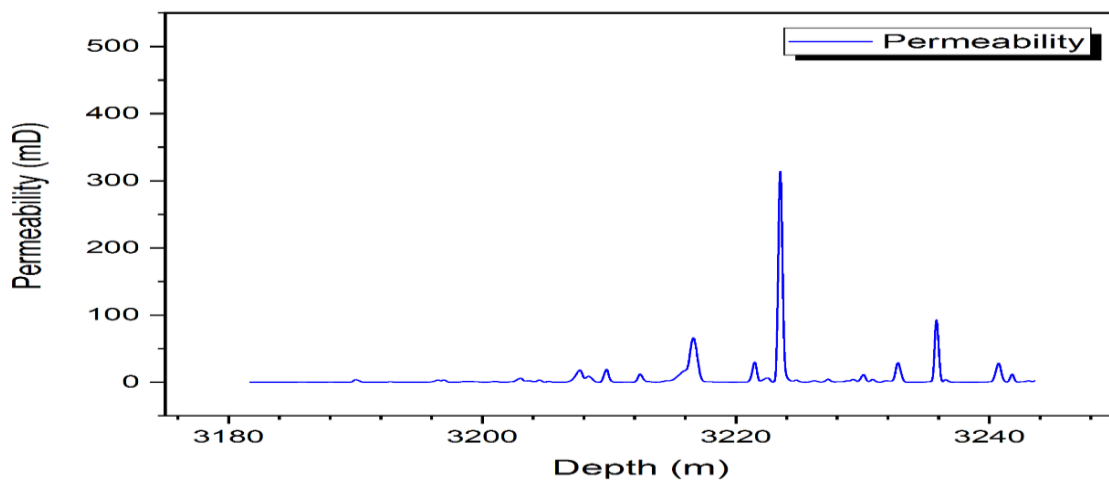

Fig. 33: Permeability and porosity evolution curves in term of depth in GS 4

1.4 Well GS 44 :

Permeability:

At depth 3223 m the permeability is relatively high at k=36, but it decreases significantly at depth 3258 m to k<16md.

Porosity:

The maximum degree of porosity is recorded at depth 3255 m Φ> 11%, while at depth 3227 m the porosity Φ=3%. This data shows variations in permeability and porosity at different depths, which is important for understanding the subsurface characteristics.
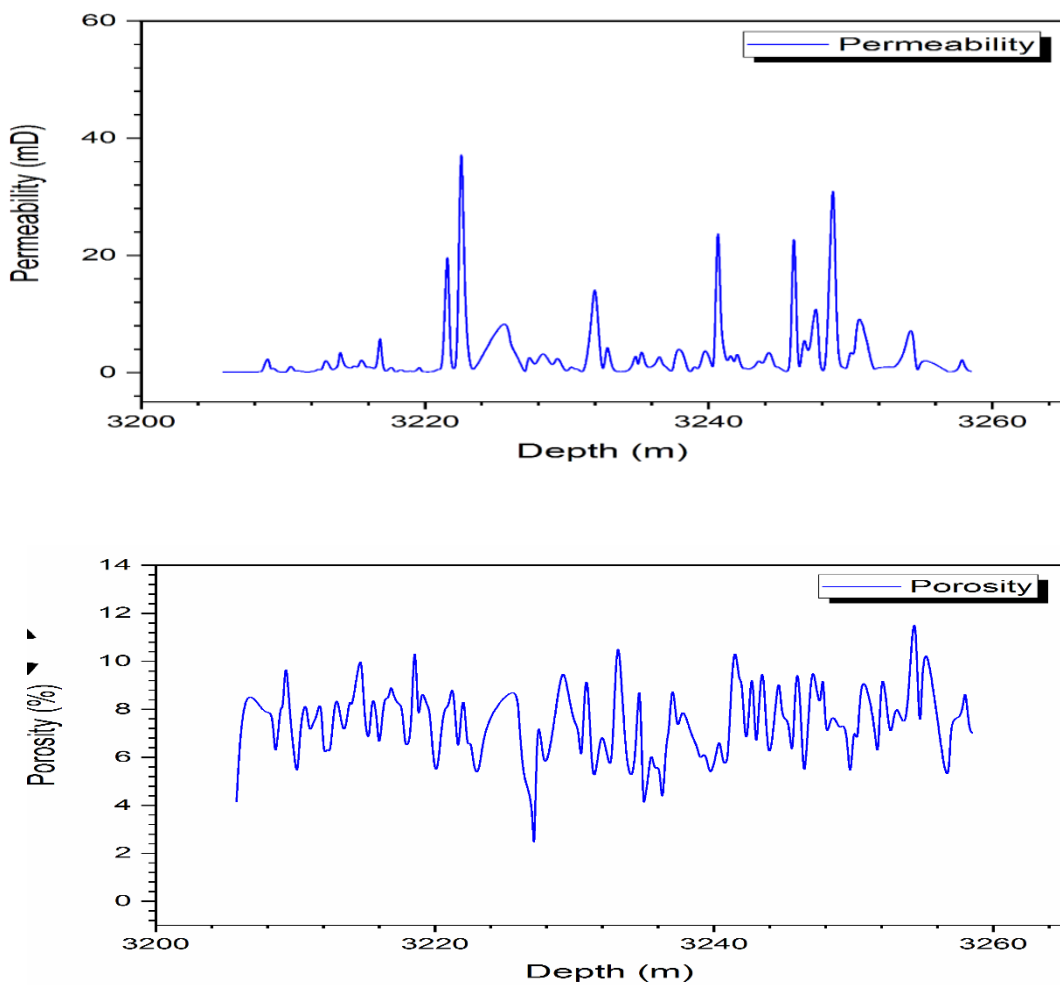
Fig. 34: Permeability and porosity evolution curves in term of depth in GS 44.

1.5 well GS 50 :

Permeability:

From the curve, we note that the permeability at depth 3243 m was good K>150 md and was recorded before it was lower at depth 3240 m and fluctuated at other depths.

Porosity:

it was good at depth 3218 m where it exceeded Φ>10 % and at depth 3202 m it was very low where Φ = 2 % and medium to fluctuate in the rest depths.
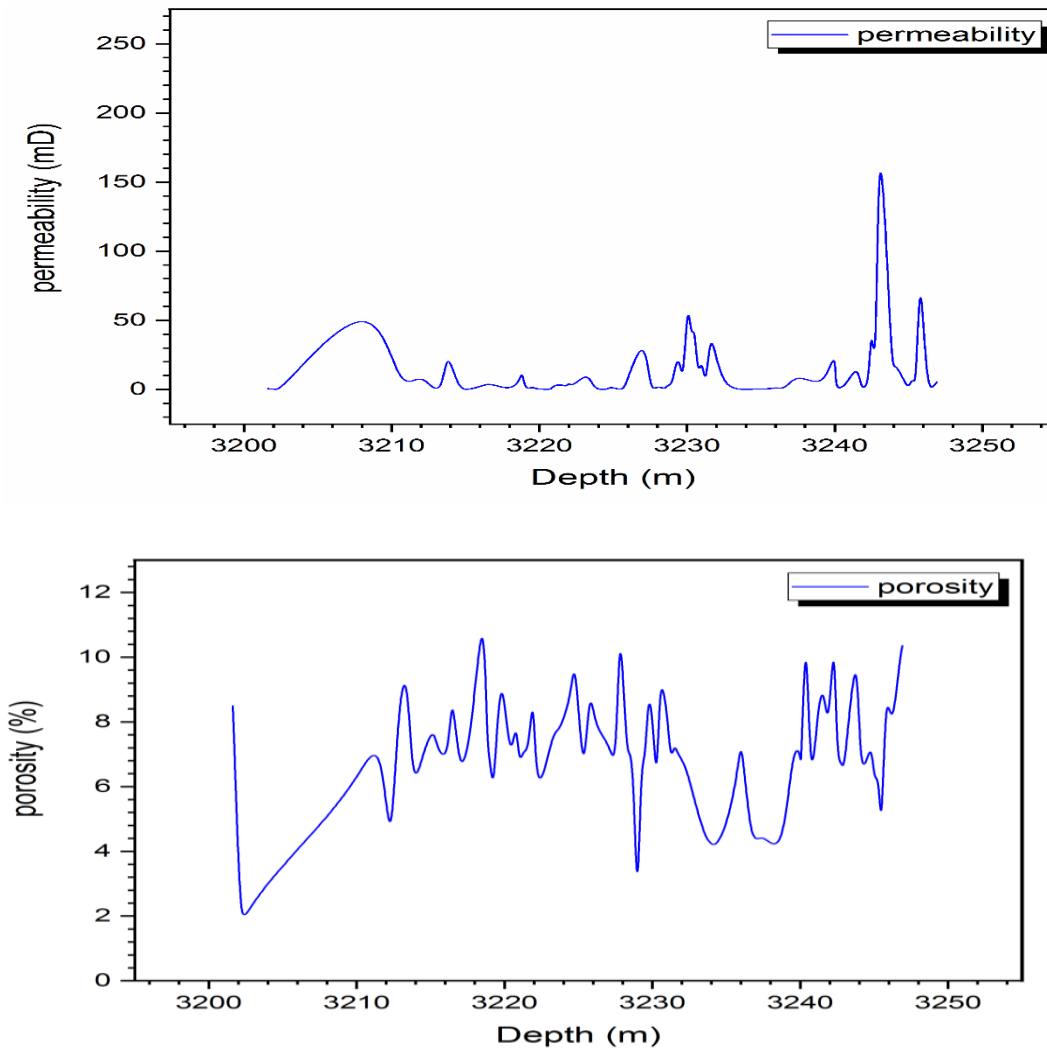

Fig. 35: Permeability and porosity evolution curves in term of depth in GS50

Analysis of petrophysical parameters

Interpretation of petrophysical data

Iso-quantity maps

Isoporosity and isopermeability maps are indispensable tools for geologists and petroleum engineers engaged in the study of oil and gas reservoirs. These maps illustrate the spatial distribution of porosity and permeability, two fundamental petrophysical properties that influence a reservoir's capacity to store and produce hydrocarbons [24-27].

These maps have a multitude of applications in the exploration, development, and management of oil and gas reservoirs, as well as in geological research and environmental risk assessment. The applications of isoporosity and isopermeability maps include:

1. Identification of potential reservoir zones: Isoporosity maps can be utilized to identify regions of rock formation with sufficient porosity to accommodate hydrocarbon storage. In contrast, isopermeability maps identify areas of the rock formation with sufficiently high permeability to allow hydrocarbons to flow to production wells [24-27].

2. Assessment of reservoir quality: By analyzing isoporosity and isopermeability maps in conjunction, geologists can assess the overall quality of a reservoir. Areas with high porosity and permeability are generally considered to be higher quality reservoirs, as they have the potential to store and produce hydrocarbons more efficiently [24-27].

3. Oilfield Development Planning: Isoporosity and isopermeability maps are indispensable tools for oilfield development planning. Such maps enable engineers to strategically position production wells and optimize hydrocarbon recovery techniques.

An understanding of geological processes is essential for the interpretation of isoporosity and isopermeability maps. Furthermore, isoporosity and isopermeability maps can be employed to investigate the geological processes that have shaped the formation and evolution of oil and gas reservoirs [24-27].

Spatial distribution of isopermeability: Isopermeability map

The isopermeability map provided represents the distribution of permeability (the ability of a rock to allow fluids to pass through it) in the El Gassi El-Agreb (GEA) zone, Algeria. The permeability is expressed in millidarcys (mD), which is a unit for measuring the permeability of reservoir rocks. The isopermeability values are represented by colored curves, with darker areas indicating higher permeability and lighter areas indicating lower permeability.

General observations:

The distribution of permeability within the GEA zone is heterogeneous, exhibiting both high and low permeability areas.

Zones of high permeability (greater than 10 mD) are primarily situated in the central region of the zone, in proximity to the wells GS-39, GS-38, and GS-37.

Zones of low permeability (below 5 mD) are primarily situated at the northern and southern extremities of the zone, as well as in the region between wells GS-57 and GS-41.

The location of wells GS-39, GS-38, and GS-37 within high permeability zones suggests that they were drilled in reservoirs of good quality.

Well GS-57 is situated within a zone of low permeability, which may account for the lower oil production observed.

In-depth commentary:

Well GS-57 is situated in an area of relatively low permeability (approximately 2.5 mD), which may account for its comparatively lower oil production in comparison to other wells in the same zone. The low permeability observed in this zone may be attributed to the presence of faults or other geological structures that impede fluid flow.

Wells GS-39, GS-38, and GS-37, these wells are situated in zones of high permeability (greater than 10 mD), indicating that they were drilled in reservoirs of optimal quality. The high permeability observed in this zone may be attributed to the presence of fractures or other geological structures that facilitate fluid flow.

Well GS-41: The well is situated in a zone of variable permeability, with values ranging from 5 to 10 mD. The heterogeneous permeability observed in this zone may be attributed to the presence of faults or other geological structures that act as barriers to fluid flow.

Well GS-44 is situated in a zone of relatively high permeability, with values estimated at approximately 7.5 mD. The permeability in this zone may be attributed to the presence of fractures or other geological structures that facilitate fluid flow.

Well GS-50: The well is situated in a zone of variable permeability, with values ranging from 5 to 10 mD. The heterogeneous permeability observed in this zone may be attributed to the presence of faults or other geological structures that act as barriers to fluid flow.

Well GS-36: The well is situated in a zone of relatively low permeability, with values estimated at approximately 5 mD. The low permeability observed in this zone may be attributed to the presence of faults or other geological structures that impede fluid flow.

In conclusion, it can be stated that:

The isopermeability map of the GEA zone provides valuable insight into the distribution of permeability in the region's oil-bearing reservoirs. This information can be utilized to identify the most prospective areas for oil production and to devise oilfield development plans.

It is crucial to acknowledge that the isopermeability map represents a mere estimation of the actual reservoir permeability. It is important to note that permeability can vary considerably within the same reservoir due to the presence of faults, fractures, and other geological structures. Additional well data, such as well logs and permeability tests, are necessary to obtain a more accurate estimate of reservoir permeability.
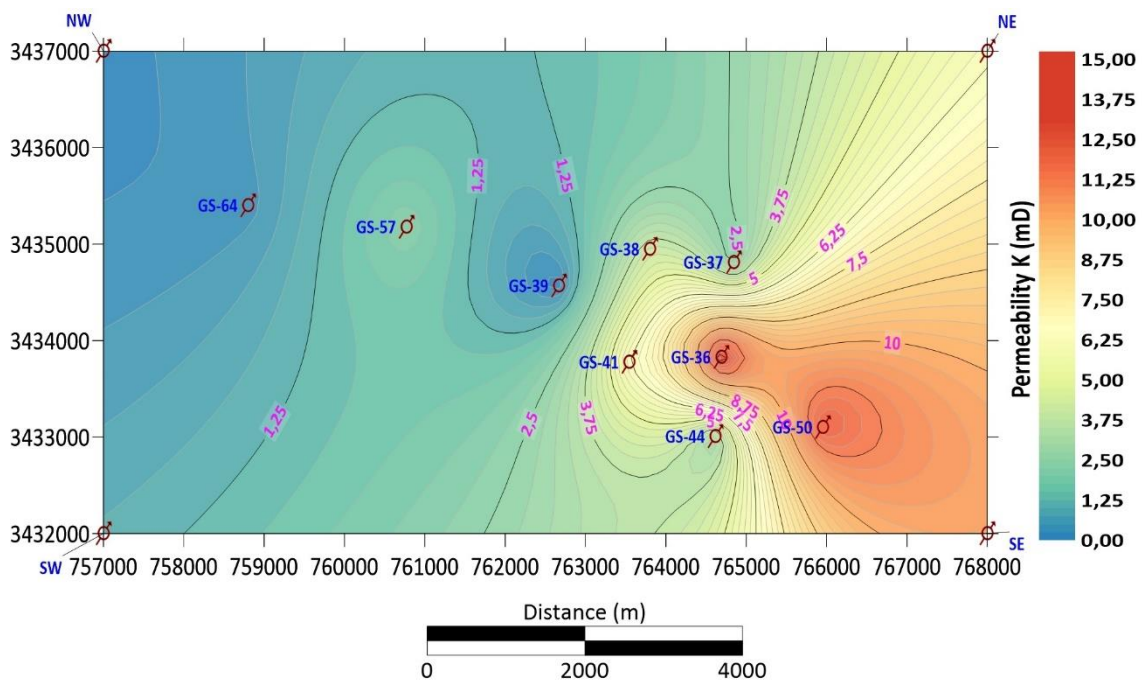

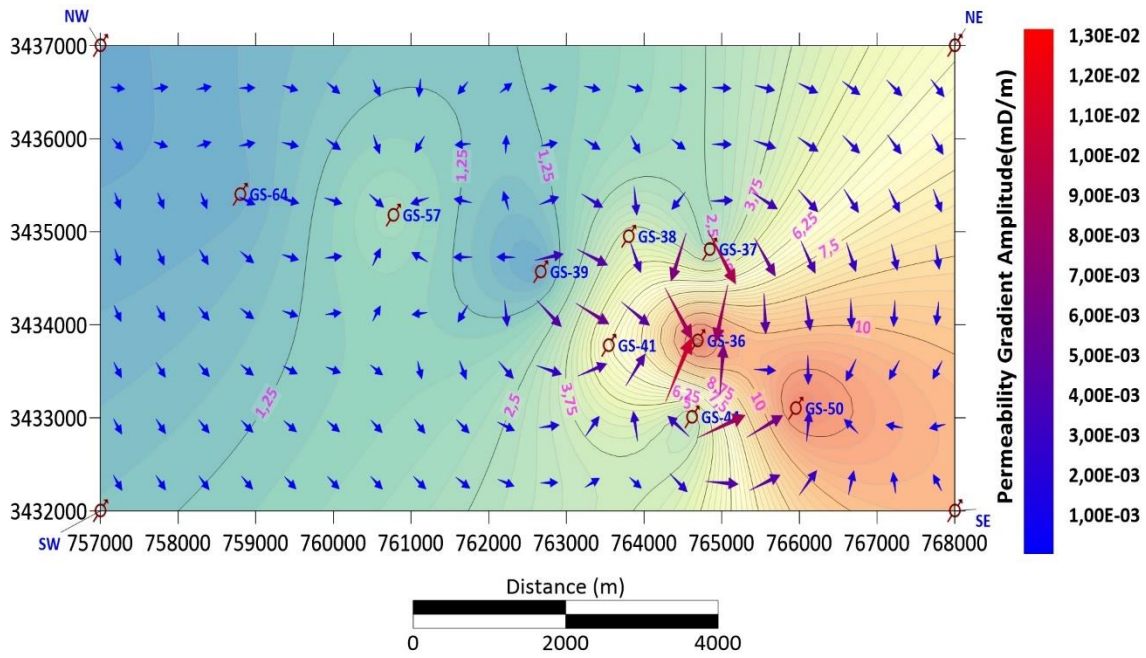Fig36: Isopermeability map of the El Gassi El-Agreb region.

Fig.37: Permeability gradient map of El Gassi El-Agreb area.

Spatial distribution of porosity: Isoporosity map

The isoporosity map depicts the distribution of porosity (void volume in a rock) within the El Gassi El-Agreb (GEA) area, Algeria. Porosity is expressed as a percentage. The isoporosity values are represented by colored curves, with darker areas indicating higher porosity and lighter areas indicating lower porosity.

General observations:

The distribution of porosity in the GEA zone is heterogeneous, exhibiting both high and low porosity areas.

Zones of high porosity (above 20%) are primarily situated in the central region of the zone, in the vicinity of wells GS-39, GS-38, and GS-37.

Low-porosity zones (below 10%) are situated primarily in the northern and southern extremities of the zone, as well as in the region between wells GS-57 and GS-41.

The location of wells GS-39, GS-38, and GS-37 within high-porosity zones suggests that they were drilled in reservoirs of good quality.

Well GS-57 is situated within a low-porosity zone, which may account for the observed decline in oil production.

Detailed Comments:

Well GS-57: This well is located in a zone of relatively low porosity (approximately 12%), which may explain its lower oil production compared with other wells in the zone. The low porosity in this zone could be due to the presence of cementing or other factors that reduce the void volume in the rock.

Wells GS-39, GS-38, and GS-37: These wells are situated in zones of high porosity (greater than 25%), indicating that they were drilled in reservoirs of optimal quality. The high porosity in this zone may be attributed to the presence of coarse rock grains or fractures that augment the void volume in the rock.

Well GS-41: This well is situated in a zone of variable porosity, with values ranging from 15% to 20%. The heterogeneous porosity in this zone may be attributed to the presence of cementing or fractures that affect void volume in the rock non-uniformly.

Well GS-44: This well is located in a zone of relatively high porosity (approximately 22%). The porosity in this zone may be due to the presence of coarse rock grains or fractures that increase void volume in the rock. This well is situated in a zone of variable porosity, with values ranging from 15% to 20%. The heterogeneous porosity in this zone may be attributed to the presence of cementing or fractures that affect void volume in the rock non-uniformly.

Well GS-36: This well is located in a zone of relatively low porosity (approximately 15%). The low porosity observed in this zone may be attributed to the presence of cementation or other factors that reduce void volume in the rock.

In conclusion, it can be stated that

The isoporosity map of the GEA zone provides valuable insight into the distribution of porosity in the region's oil-bearing reservoirs. This information can be utilized to identify the most prospective areas for oil production and to devise oilfield development plans.

It is crucial to acknowledge that the isoporosity map provides a mere estimation of the actual reservoir porosity. It is important to note that porosity can vary considerably within the same reservoir due to the presence of cementation, fractures, and other geological structures. Further data from wells, such as well logs and core analyses, is necessary to obtain a more precise estimation of reservoir porosity.

Moreover, it is crucial to consider reservoir permeability in conjunction with porosity. Permeability is defined as the capacity of a rock to permit the passage of fluids. A reservoir may exhibit high porosity but low permeability if it is heavily cemented or if the pores are not well connected.
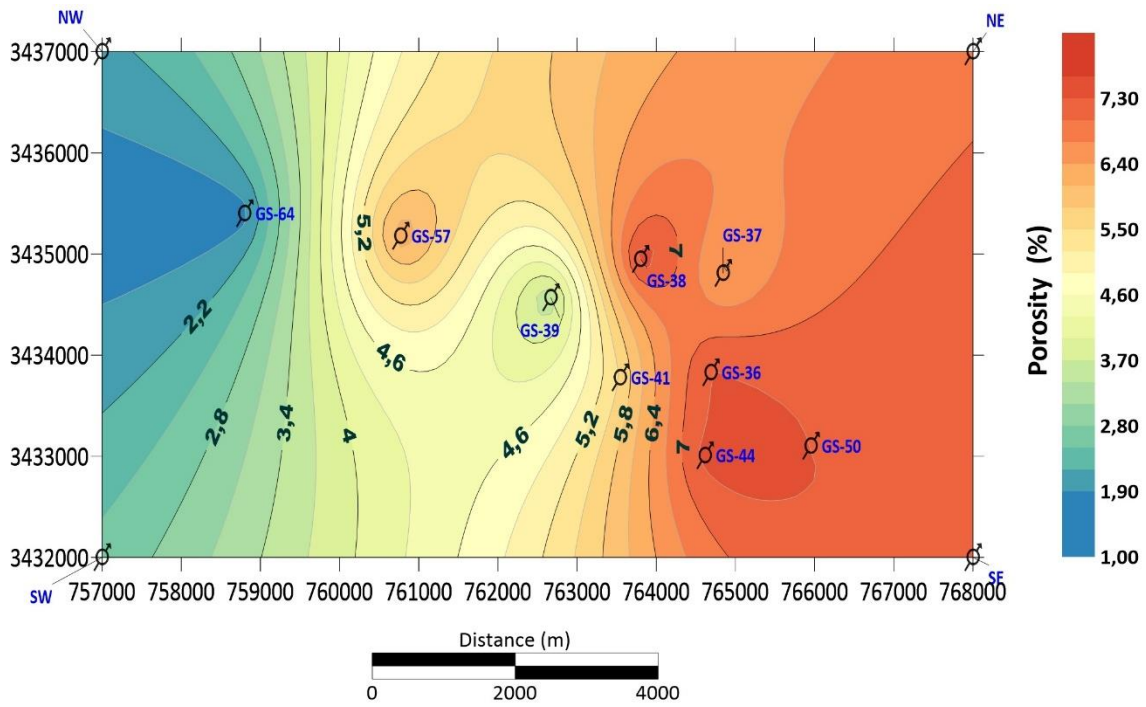
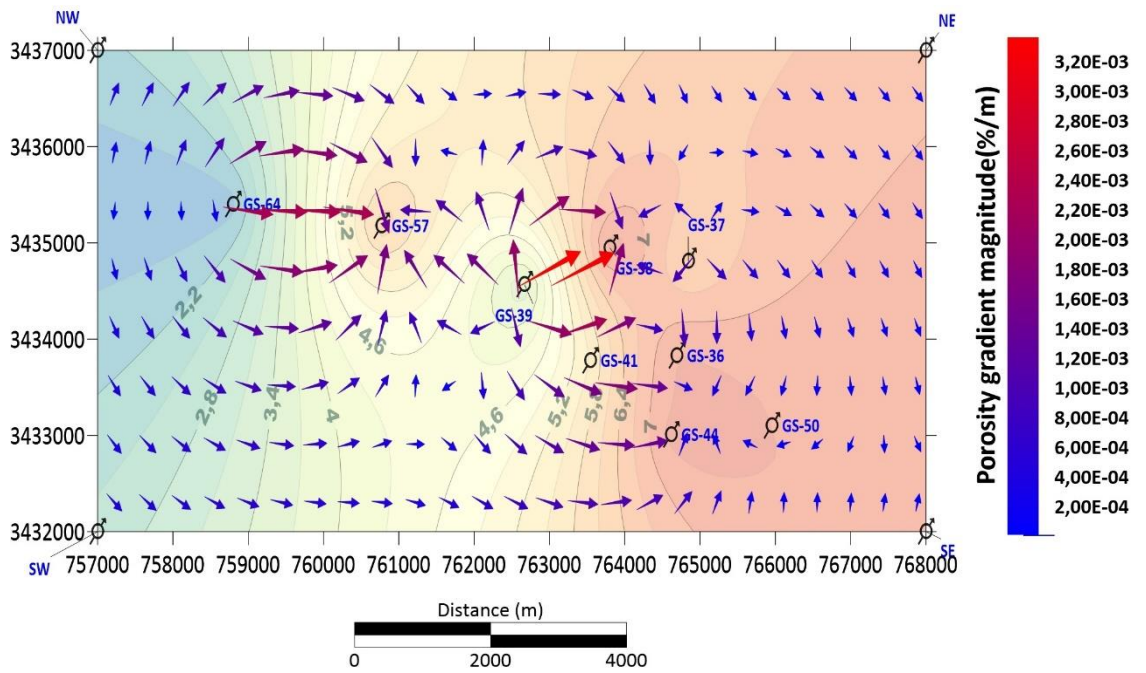Fig.38: Isoporosity map of El Gassi El-Agreb area.

Fig. 39: Porosity gradient map of El Gassi El-Agreb area.

General conclusion

The Hassi Messaoud field represents the largest known hydrocarbon deposit in Algeria. The field is situated 650 km south-southeast of the capital city of Algiers. The Hassi Messaoud field is situated at the northern extension of the Amguid-El Biod mole, occupying the central part of the Triassic province. This structure appears to be a vast structural dome of nearly 1,600 km². The stratigraphic series of the Hassi Messaoud field is situated on the basement at a depth of approximately 4,393 meters. It is noteworthy that this series is devoid of the Silurian, Devonian, Carboniferous, and Permian. The Hercynian discordance is more pronounced in the center of the structure, where the clay-sandstone and salt deposits of the Triassic rest directly on the Cambrian.

The Gassi El-Agreb field (GEA field) is a satellite deposit of the Hassi Messaoud deposit. The field is situated approximately 120 km southwest of Hassi Messaoud. The field was initially identified in 1956 and subsequently brought into production in 1959. The reservoir in this field is of Cambro-Ordovician age. The Gassi El-Agreb reservoir is situated within an Upper Cambrian sandstone formation, which was deposited in a fluvial and marine environment, with the addition of deltaic marine silica. The structural configuration of the Gassi El-Agreb reservoir is that of a large double-slope anticline. The structural style of this trend is characterized by a northwest-southeast orientation and reverse sub-vertical faults, which are indicative of a strike-slip tectonic regime.

The reservoir in the Gassi El-Agreb region is composed of Cambro-Ordovician rocks. The Cambrian series is comprised of the following zones, from the bottom to the top: The following rock units are present: R3, R2, Ra, and Ri. The Ordovician series is represented by the zone of alternations, which is composed of sandstones, quartzitic sandstones, gravels, and conglomerates. At the roof, we observe an improvement in the grading and rounding of grains. Seismic exploration played a pivotal role in the analysis of the El Gassi El Agreb (GEA) region's potential for hydrocarbon deposits. By employing techniques such as Vertical Seismic Profiling (VSP) and Amplitude Versus Offset (AVO) analysis, researchers were able to obtain comprehensive images of the subsurface geology and the faults that influence potential reservoirs. The complex geological history of the region resulted in a challenging structural framework, yet the seismic data revealed valuable insights. These insights include the possibility that north-south trending faults may act as seals and east-west faults might influence pressure within the reservoir. Nevertheless, there remain uncertainties in fully mapping the top reservoir and definitively understanding the impact of faults on fluid flow.

The core analysis of wells GS-36 and GS-38 in the El Gassi El Agreb region has revealed the presence of a complex and potentially hydrocarbon-rich reservoir. While the core is primarily composed of sandstone, with some claystone layers, the degree of silicification significantly impacts the porosity. In particular, highly silicified zones exhibit minimal porosity. Visible porosity variations are considerable, with darker-colored sections exhibiting a greater degree of porosity. The analysis of the Cambrian Ri and Ra formations encountered in Well GS-38 indicates a higher porosity and potential for hydrocarbon flow within the deeper Ra formation compared to Ri. The presence of oil staining, fluorescence, and gas desorption provides further evidence of the potential for hydrocarbons to be present. Nevertheless, the core also reveals rapid variations in properties and the presence of fractures, indicating the necessity for further evaluation in order to fully comprehend the reservoir's potential.

A comprehensive analysis of permeability and porosity data in the El Gassi El-Agreb (GEA) zone has revealed significant variations across the region. The high permeability and porosity zones, which are more favorable for oil and gas production, are concentrated around the wells GS-39, GS-38, and GS-37. Conversely, lower values are found at the zone's edges and between specific wells, which may explain the lower production observed in well GS-57. The newly created isopermeability and isoporosity maps are valuable tools for strategic well placement and optimizing recovery techniques in future oilfield development endeavors. Nevertheless, as estimations rather than absolute values, these maps require integration with geological understanding and additional well data for more precise assessments.

References

[1]   Tenaille M, Burger J, Perrodon A. Algeria. In: Owen EW, editor Trek of the Oil Finders: A History of Exploration for Petroleum Semicentennial Commemorative. American Association of Petroleum Geologists; 1975, p. 1450-71.

[2]   Beicip-Franlab. Zone périphérique du champ de Hassi Messaoud; réservoir cambro-ordovicien. Internal report CRD-SONATRACH; 1979.

[3]   Lasmi R. Caractérisation des Quartzites de Hamra dans les gisements de Hassi Terfa, Hassi D'zabat et Hassi Guettar : Pétrophysique, Fracturation et Modélisation. Faculté des Hydrocarbures et de la Chimie. Mémoire de Magister. Université M'hamed Bougara, Boumerdès, Algerie; 2013:151.

[4]   Zerroug S, Bounoua, N., Lounissi, R., Zeghouani, R., Djellas, N., Kartobi, K., Etchecopar, A., Tchambaz, M., Abadir, S., Simon, P., Fuller, J., Well Evaluation Conference Algeria. In: Schlumberger, ed. Lynx Consulting, Inc. Houston, TX, USA ed.: Schlumberger; 2007:489.

[5]   Aït-Salem H. Le Trias détritique de l'Oued Mya (Sahara algérien) : sédimentation estuarienne, diagenèse et porogenèse, potentialités pétrolières. Doctorat. Université Lyon-1, France; 1990:1 vol. (162 p.- [10] p. de pl.- [2] dépl.).

[6]   Traut MW, Boote DRD, Clark-Lowes DD. Exploration history of the Palaeozoic petroleum systems of North Africa. Geological Society, London, Special Publications 1998; 132(1):69-78.

[7]   Boote DRD, Clark-Lowes DD, Traut MW. Palaeozoic petroleum systems of North Africa. Geological Society, London, Special Publications 1998;132(1):7-68.

[8]   Bouchon R., Ortynski H.I., Lappaent C. de, Pommier G. Le développement de la sismique réfraction dans l'interprétation géologique du Sahara nord. Son role dans la découverte et l'étude du champ de Hassi Messaoud. 5ème Congrès Mondial du Pétrole (5th WPC). Sect. I. New York, USA; 1959:729-46.

[9]   Baadi F, Boughebache H. Etude et Analyse des Paramètres Pétrophysiques de la Zone 14 (Hassi Messaoud). Département des Sciences de la Terre et de l'Univers. Master. Université de Kasdi Merbah, Ouargla, Algérie; 2023:101.

[10]   SonaHess. GEA prospection and Drilling works. Internal report SonaHess, Hassi Messaoud; 2007.

[11]   Touag Kermani, MenanaThinhinane. Etudes des caractéristiques pétro-physiques d'un réservoir cambro-ordovicien du champ de H.M.D Master. Département des Mines et géologie Université Abderrahmane Mira de Bejaia; 2018:76.

[12]   Yahiaoui L. Analyse complexe et évaluation des programmes des puits en short radius et horizontaux a hassi messaoud aspect géologique et application dans la partie sud. Faculté des hydrocarbures et de la chimie. Mémoire de magister. Université m'Hamed bougara boumerdes; 2010:36.

[13]   Touag Kermani, MenanaThinhinane. Etudes des caractéristiques pétro-physiques d'un réservoir cambro-ordovicien du champ de H.M.D Département des Mines et géologie Master. Université Abderrahmane Mira de Bejaia 2018:76.

[14]   Report S. Internal report Division Production-SONATRACH, Hassi Messaoud; 2012.

[15]   Beicip-Franlab. Caractérisation et évaluation des réservoirs ordoviciens de pourtours de Hassi Massaoud Internal report DEP-SONATRACH; 2007.

[16]   Perrodon A. Géodynamique pétrolière: genèse et répartition des gisements d'hydrocarbures. Ed. Masson, Elf Aquitaine, Paris, France; 1980.

[17]   Monicard RP. Properties of Reservoir Rocks: Core Analysis. EDITIONS TECHNIP, Paris, France; 1980.

[18]   Schlumberger. "Diagram of VSP configurations". 2014.

[19]   BacLuong. "Vertical Seismic Profiling Survey", from Hanoi, Vietnam https://vi.wikipedia.org/wiki. 2014.

[20]   Ødegaard E, Avseth P. Interpretation of Elastic Inversion Results Using Rock Physics Templates, Extended Abstract, E17. 2003.

[21]   Russell B. Visualizing inversion results with rock physics templates. Inversion and Rock Physics Templates, CREWES Research Report — Volume 27. 2015.

[22]   Castagna JP, Backus M. AVO analysis-tutorial and review. Offset-dependent reflectivity: theory and practice of AVO analysis 1993:3-36.

[23]   Eddine OD. Traitement au reformat d'un puits producteur d'huile, cas de puits d'El Agreb AR 36 Superior production technician in the oil industry. Ecole de Hassi Messaoud, Algeria; 2015:59.

[24]   Donald P. H. Fundamentals of Formation Evaluation. Oil & Gas Consultants Intl; 1st US - 1st Printing edition; 1983.

[25]   Martini RF, Schiozer DJ, Nakajima L. Use of quality maps in reservoir management. Journal of the Brazilian Society of Mechanical Sciences and Engineering 2005; 27.

[26]   Djebbar Tiab, Donaldson EC. Petrophysics: Theory and Practice of Measuring Reservoir Rock and Fluid Transport Properties. 3rd edition ed.: Gulf Professional Publishing; 2011.

[27]   Tarek A. Reservoir Engineering Handbook. 5th edition ed.: Gulf Professional Publishing; 2019.

Abstract:

In the El Gassi field, the Cambrian reservoirs Ri and Ra are considered to be among the most important primary reservoirs, characterized by high heterogeneity resulting from the sandstone structure and tectonic phenomena that have impacted the reservoir quality through the faults and fractures they have caused.

Petrophysical studies in Ri and Ra show significant heterogeneity between porosity and permeability, reflecting challenges in understanding and managing these reservoirs.

Integration of sedimentological and petrophysical studies is considered essential to achieve a comprehensive reservoir description and improve reservoir management practices and production.

Keywords: Hassi Messaoud, Gassi El Agreb, Porosity, Permeability, Cambrian, Petrology.

خلاصة:

في حقل الجاسي، تُعتبر مكامن Ri و Ra الكمبريين من بين أهم المكامن الأولية في حقل الجاسي، حيث تتميز بعدم التجانس القوي الناتج عن بنية الحجر الرملي والظواهر التكتونية التي أثرت على جودة المكامن من خلال الصدوع والكسور التي أحدثتها.

تُظهر الدراسات البتروفيزيائية في مكامن ري ورع عدم تجانس كبير بين المسامية والنفاذية، مما يعكس الصعوبات في فهم وإدارة هذه المكامن.

ويعتبر تكامل الدراسات الرسوبية والبتروفيزيائية البترولية ضرورياً للحصول على وصف كامل للمكامن وتحسين ممارسات إدارة المكامن والإنتاج.

الكلمات المفتاحية: حاسي مسعود، قاسي العقرب، المسامية، النفاذية، الكمبري، علم البترول

Résumé :

Dans le champ d'El Gassi, les réservoirs cambriens Ri et Ra sont considérés comme parmi les réservoirs primaires les plus importants, caractérisés par une forte hétérogénéité résultant de la structure gréseuse et des phénomènes tectoniques qui ont impacté la qualité du réservoir par les failles et fractures qu'ils ont provoquées.

Les études pétrophysiques en Ri et Ra montrent une hétérogénéité significative entre la porosité et la perméabilité, reflétant les difficultés de compréhension et de gestion de ces réservoirs.

L'intégration des études sédimentologiques et pétrophysiques est considérée comme essentielle pour obtenir une description complète des réservoirs et améliorer les pratiques de gestion et la production des réservoirs.

Mots-clés : Hassi Messaoud, Gassi El Agreb, Porosité, Perméabilité, Cambrien, Pétrologie.